Impact of Anaerobic Biofilm Formation on Sorption Characteristics of Powdered Activated Carbon

by

Griselda Raquel Rocha Díaz de León

A thesis
presented to the University of Waterloo
in fulfillment of the
thesis requirement for the degree of
Master of Applied Science
in
Civil Engineering – Water

Waterloo, Ontario, Canada, 2021

AUTHOR'S DECLARATION

I hereby declare that I am the sole author of this thesis. This is a true copy of the thesis, including any required final revisions, as accepted by my examiners.

I understand that my thesis may be made electronically available to the public.

ABSTRACT

Subsurface contamination by petroleum hydrocarbons (PHCs) results from the leakage of petroleum products during extraction, processing or transport. It has been documented that activated carbon (AC) can effectively sorb organic compounds present in water. As a result, the use of carbon-based injectates (CBI) has gained popularity for use to treat groundwater impacted with PHCs in situ. CBI relies on the dynamic equilibrium between sorption, desorption and biodegradation of contaminants, leading to long-term treatment.

The aim of this study was to investigate the influence of biofilm formation on the sorption characteristics of PHCs to powdered activated carbon (PAC). Specifically, the sorption performance of PAC for toluene was evaluated before and after an anaerobic methanogenic toluene-degrading microbial biofilm was developed on the PAC. Batch microcosm experiments were used to grow a biofilm on PAC surfaces (bio-coated PAC). The microbial culture used in the microcosm experiments actively degraded toluene as demonstrated by toluene reduction and the methane production. Confocal microscopy was conducted for qualitative visualization and quantitative analysis of the biofilms. The biofilm continually developed on the PAC surfaces and increased its mass and thickness over the 180-day long experimental period.

The sorption characteristics of PAC without biofilm formation (fresh PAC) were compared to PAC samples removed from microcosms at Day 80 and Day 180. The change of sorption characteristics of PAC was evaluated based on best fit Freundlich isotherm parameters (K_f and n_f). The value of K_f was reduced from 79.8 for fresh PAC to 50.2 and 47.7 for Day 80 and Day 180 bio-coated PAC, respectively. An increase in n_f from 0.35 for fresh PAC to 0.42 for bio-coated PAC at Day 80 and 180 was also observed. These results show that the sorption performance of PAC was reduced when a microbial biofilm was developed. Although the biofilm growth was significant between Day 80 and Day 180, and a slight decrease in K_f was obtained for the bio-coated PAC at Day 180 compared to Day 80, the observed growth did not yield a statistically significant difference in the loss of sorption capacity between both time points. A simulated PAC barrier was used to demonstrate the

impact that biofilm formation could have on potential performance deterioration. The bio-coated PAC barrier performance was evaluated based on the percent reduction of breakthrough time as a function of incoming contaminant concentration. The breakthrough performance was found to deteriorate with the biofilm formation, with a greater impact at lower incoming concentrations (e.g., 60% reduction in breakthrough time for a concentration of 10 μg/L).

The results of this study revealed that the sorption performance of PAC could be hampered by biofilm formation leading to fouling the AC pores (by biomass production and/or sorption of microbial by-products) which may affect its long-term effectiveness.

ACKNOWLEDGEMENTS

First, I would like to acknowledge and express my greatest gratitude to my supervisor Professor Neil R. Thomson, for accepting me in his research group and giving me the opportunity to pursue this research. Thank you, Professor Thomson, for your patience, time and continuous support, supervision and advice over the past few years.

I want to extent my gratitude to my thesis readers, Dr. Anh Pham and Dr. Mark Knight, who took the time to review my work and provided valuable feedback.

Thanks to Shirley Chatten and Andrea Marrocco who provided me with training and guidance for the experimental part of my work. Thanks, Shirley, for the nice times during lab workdays. To Marianne Vandergriendt for the use of the anaerobic chamber. To the laboratory assistance from Mark Merlau and Mark Sobon. To Professor Elizabeth Edwards and Courtney Toth from University of Toronto for their suggestions on my research.

I am grateful to all the friends I made here at University of Waterloo with whom I shared great life experiences. To the friends of the lunch group and office mates for the joyful road trips. Specially to Ekin and Cristobal for being there during these times. My warmest thanks to Edit for the enormous support and kindness since the day I arrived to Canada.

For the financial support I would like to thank the Mexican National Council of Science and Technology (CONACyT), the Ministry of Energy (SENER) and the National Bank of Public Works and Services (BANOBRAS). To Professor Neil. R. Thomson for proving financial support (NSERC Discovery Grant) through a Graduate Research Scholarship (GRs). Likewise, I would like to thank Mitacs through the Mitacs Research Training Award.

DEDICATION

To my family. Especially to my mom for her love, support and encouragement through every step of my life. To Antonio for always being around no matter the circumstances. To Tiff for being the joy in my life. To my two rays of sunshine, that will live forever in my heart.

TABLE OF CONTENTS

LIST OF FIGURES

LIST OF TABLES

CHAPTER 1

INTRODUCTION

1.1 BACKGROUND

Energy resources have been fundamental in the development of human civilizations and are the basic component of a country's economic growth. It involves any type of energy that can be used to produce heat, electricity, or other forms of energy conversion processes (Rashid, 2015). Energy consumption has constantly increased throughout human history, and since the Industrial Revolution, fossil fuels (mainly coal, oil, and natural gas) have facilitated industrial expansion, and are the primary energy source in many countries (Black, 2014; Rashid, 2015).

However, fossil fuels (e.g., petroleum products) have harmed the environment, producing greenhouse gases, solid by-products, and accidental releases to the surface, subsurface, and aquatic ecosystems. In 2018, The Conservation of Clean Air and Water in Europe reported 741 fuel spills from pipelines and pump stations since 1971, releasing about 80-000 m^3 of petroleum derivatives (Balseiro-Romero et al., 2018). Petroleum spills on land can infiltrate to the subsurface and reach underlying aquifers giving rise to environmental impacts due to their toxic chemical components (e.g., petroleum hydrocarbons (PHCs)). In groundwater, dissolved fractions of these PHCs, such as benzene, toluene, ethylbenzene and xylene isomers (so-called BTEX), can be transported large distances far away from the source, impacting ecosystems and polluting sources of drinking water (Corapcioglu & Baehr, 2011; Cunningham et al., 2001; Lueders, 2017; Phelps & Young, 1999).

Several studies have shown that exposure to BTEX compounds is toxic to animals as they can be absorbed through the body. Long-term exposure has shown to alter the nervous system, liver enzymes, blood cells and have shown to be related on the development of some types of cancer (Agency for Toxic Substances and Disease Registry (ATSDR), 2004; Aksoy, 1989; Fayemiwo et al., 2017; Onwurah et al., 2007; Snyder, 2000, 2012). Due to the identified health risks associated with BTEX compounds, drinking water guidelines have been implemented in different countries establishing maximum acceptable concentrations of 1 µg/L for benzene, 25-60 µg/L for toluene, 3-140 µg/L for ethylbenzene and 20-90 µg/L for xylenes (Health Canada (HC), 2006; NHMRC & NRMMC, 2011).

Reported concentrations of BTEX in groundwater range from ~ 0.1 to 1.8 µg/L for BEX and <1-100 µg/L for toluene, and in contaminated groundwater it has been found up to 330, 3500, 2000 and 1340 µg/L respectively for each BTEX compound (Fayemiwo et al., 2017; Leusch & Bartkow, 2010). The persistence of BTEX in groundwater represents an imminent hazard to drinking water sources. These compounds have been found in drinking water across the world (Alquwaizany et al., 2019; Goss et al., 1998; Schmidt et al., 2004; Serrano et al., 2007), and in some cases exceeding the maximum acceptable concentrations.

With more than 80% of the total populace depending on groundwater as their source of drinking water, defilement of groundwater by petroleum contamination requires evaluation and remediation (Logeshwaran et al., 2018). Activated carbon (AC) has shown good performance in adsorbing aromatic compounds, rapidly decreasing dissolved phase contaminant concentrations in the bulk water and is commonly used in water treatment.

Carbon-based injectates (CBI) is a recent technological approach for in situ treatment of groundwater contaminated with organic contaminants (e.g., PHCs). It is based on the injection of AC supplemented with different additives (i.e., nutrients, bacteria) into the subsurface (Harp, 2009; Lewis, 2012). The underlying conceptual model involves sorption of contaminants to AC due to its high adsorption capacity and enhanced biodegradation of

contaminants in the AC zone by allowing prolonged contact time between microbes (indigenous or inoculated) and contaminants. Once contaminants are biodegraded, sorption sites are regenerated allowing long-term treatment (Fan et al., 2017; Lewis, 2012; USEPA, 2018). As a result of its increasing popularity, different commercial products have been developed and applied in field with claims of rapid contaminant removal and long-term effectiveness (Fan et al., 2017).

To account for the long-term performance of this technology, adsorption/biodegradation processes must be maintained over time. During AC aging in the field, microbial communities are expected to form biofilms surrounding AC particles. Therefore, it is hypothesized that a decrease of sorption sites may occur as AC ages. This can occur due to fouling of AC pores by biofilm formation and competitive sorption of microbial degradation byproducts or microbial metabolites. In addition, competitive adsorption between strong and weakly sorbed compounds may result in the desorption of contaminants from the AC matrix where maintenance of biodegradation becomes a critical factor. To date, investigations regarding the influence of microbial biofilm formation on the sorption of PHCs during AC aging have not been widely studied, and thus additional research is required on this topic.

1.2 RESEARCH HYPOTHESIS

The presence of biofilm formation on powdered activated carbon will negatively impact petroleum hydrocarbon sorption characteristics.

1.3 RESEARCH OBJECTIVE

The overall objective of this research is to investigate the influence of biofilm formation on the sorption characteristics of PHCs to powdered activated carbon (PAC) under anaerobic conditions.

1.4 RESEARCH SCOPE

To generate the data to satisfy the research objective, three phases of experimentation were adopted.

1. baseline evaluation of sorption/desorption isotherms for the selected model PHC,
2. establish microbial biofilm on PAC, and
3. posterior evaluation of sorption/desorption isotherms for the selected model PHC.

This thesis consists of five chapters. Chapter 1 provides the motivation for this thesis, objective, and scope. Chapter 2 presents a literature review with the background knowledge that serves as a baseline for this work. Chapter 3 describes the experimental design and methods used during the experimental work. Chapter 4 provides the results and discussion from the experimental data. Finally, Chapter 5 gives a conclusion containing the general findings from this work as well as some recommendations. In addition, appendixes with protocols followed during the experimental work and supplementary material are provided.

CHAPTER 2

LITERATURE REVIEW

2.1 INTRODUCTION

Petroleum-based products are the main energy source in many countries (Logeshwaran et al., 2018). In 2019, the total world petroleum consumption was 100.75 million barrels per day (MMbbl)(EIA, 2020) with U.S.A., China, Japan, India, and Russia as the top 5 consumers (Praveen, 2013). Petroleum, including crude oil and petroleum products, are used almost in every sector of our lives (transportation fuels, manufacturing industry, heating, and many other intermediate and end-user goods) (EIA, 2019).

The increase in production and consumption of petroleum has caused corresponding increment in pollution of soil, surface water and groundwater threatening ecosystems and human health (Balseiro-Romero et al., 2018; EPA, 1999; M. Yang et al., 2013). Emissions from the petroleum industry occur in every chain of the oil-producing process; from the extraction to the final user. Petroleum releases to the environment may be from routine activities in the oil extraction like oil well drilling operations due to improper waste management practices or accidental rupture of storage tanks or pipelines (Adams et al., 2015; Duffy et al., 1980; Gong et al., 2014; Logeshwaran et al., 2018).

It has been documented that most oil spills occur quite frequently on land (Vanloocke et al., 1975) as a result of the intensive use of rail tankers to transport oil on a daily basis and the more than 300,000 kilometers of pipelines in use (Ivshina et al., 2015). This has generated the implementation of strict legislation for operation and maintenance of underground storage tanks; and some industry associations such as CONCAWE, have established technical guidelines to prevent pipeline accidents and spills (Balseiro-Romero et al., 2018).

Despite the improvements in the storage and transportation of petroleum products, many incidents regarding fuel spills have been reported. A sampling of underground fuel storage tanks in the United States showed that about 35% of the tanks were leaking (Joel & Amajuoyi, 2010; Onwurah et al., 2007). In 2018, The Conservation of Clean Air and Water in Europe reported 741 fuel spills from pipelines and pump stations since 1971 releasing about 80,000 m^3 of fuel polluting around 1,200,000 m^2 of land (Balseiro-Romero et al., 2018).

In 2013, a pipeline rupture in Arkansas spilled 507 m^3 of crude oil, the oil reached Lake Conway impacting wetland vegetation, wildlife, water, and soil (Belvederesi et al., 2018). In 2016, the Colonial Pipeline 1, which supplies up to 50% of gasoline sold on the East Coast of the U.S.A., spilled around 954 m^3 of gasoline in Alabama (U.S.EPA, 2016). In Nigeria, 1527 oil spill incidents were recorded between 2012 and 2015; the high frequency of spill incidents had posed challenges in terms of clean-up, remediation, and rehabilitation of land (Albert et al., 2018).

An investigation of pipeline accidents by Belvederesi et al. in 2018 using data provided by PHMSA (Pipeline and Hazardous Material Safety Administration) found that 8.7% of incidents that occurred between 2010 to 2017 caused water contamination; 68% of this lead to surface water contamination, followed by groundwater contamination in 29% of the cases. Compared to the oil spills from the break-up of platforms and super-tankers in the sea, the majority of oils spills that occur on land are of moderate scale (100-1000 m^3), and remain unreported to the general population resulting in less public concern; however, they can cause subtle long-term ecological perturbations (Duffy et al., 1980; Ivshina et al., 2015).

Oil pollution continues to be a problem around the world due to the complexity of petroleum composition. Petroleum is comprised of a mixture of a broad range of hydrocarbons, with a variety of molecular weights, solubility, volatility, and toxicity. The

major hydrocarbon groups found in petroleum are chain alkanes and cycloalkanes which constitute more than 65% of the volume of gasoline products and include isoprenoids, sulphur, oxygen, or nitrogen-containing polar compounds and aromatic hydrocarbons (Onwurah et al., 2007).

2.2 BTEX CONTAMINANTS

A group of priority contaminants frequently found in petroleum products are the so-called BTEX group (benzene, toluene, ethylbenzene, and xylene isomers), they fall in the category of the aromatic hydrocarbons group and constitute up to 20% volume fraction in gasoline (Balseiro-Romero et al., 2018; Do Rego & Pereira Netto, 2007; Logeshwaran et al., 2018; E. López et al., 2008). In addition, BTEX is extensively produced in the chemical industry, with a worldwide annual production of up to 10 million tons for each BTEX compound (Leusch & Bartkow, 2010).

Benzene is used in the fabrication of nitrobenzene, cyclohexane, and ethylbenzene. It can be found in acetones for resins, rubbers, lubricants, and pesticides. Toluene is used in the production of polyurethane foam, as a solvent in paints, silicones, rubbers, and glues. In the fuel industry, it is used as an octane booster in gasoline blends. Ethylbenzene is used in the production of polymers such as polystyrene and can also be used as a solvent for paints and adhesives. Xylene is used as a precursor to terephthalic acid which is used in the production of polyethylene terephthalate plastics and polyester clothing. As with the rest of the BTEX compounds, it can also be found in rubbers, paints, and adhesives (Clark, 2016; Thongplang, 2016).

Because of the widespread industrial use of BTEX and its natural occurrence in petroleum, BTEX are ubiquitous compounds. Releases of petroleum products are one of the main sources of BTEX contamination in the environment, specifically in groundwater.

Noteworthy, the BTEX group is one of the most representative environmental contaminants due to its well-studied toxicity (Do Rego & Pereira Netto, 2007).

2.2.1 BTEX IN THE ENVIRONMENT: GROUNDWATER

When petroleum hydrocarbons are released into the soil, each compound will separate from the mixture depending on its physicochemical properties (Table 2.1). Generally, the oil will spread over the soil layer, and depending on the soil permeability the compounds will migrate downward due to gravity until exhausted to immobilization, or until it reaches the water table (Duffy et al., 1980; Vanloocke et al., 1975).

As a result of the relatively high solubility and low molecular weight, BTEX molecules often partition to soil pore water, leading to increased mobility with water and are commonly found moving towards contaminated groundwater plumes (Balseiro-Romero et al., 2018; Logeshwaran et al., 2018). Despite comprising up to 20% of volume fraction in gasoline, BTEX accounts for at least 98% of the dissolved compounds that partition from gasoline to groundwater (Logeshwaran et al., 2018; Wiedemeier et al., 1996). In groundwater, BTEX may be attenuated by dilution, dispersion, sorption, volatilization, and biodegradation. Biological degradation is deemed to be a major process influencing the fate petroleum hydrocarbons in groundwater; however, contaminant availability, concentration, temperature, nutrients, and dissolved O_2 influence biodegradation rates (Zamfirescu & Grathwohl, 2001).

Table 1 lists the physical-chemical properties of each BTEX compound, some key properties included are molecular volume that can be used to determine the volume that each molecule occupies in a sorbent material; the octanol/water partition coefficient which estimates hydrophobicity or the tendency of a compound to partition from water to organic media; and the water solubility that controls BTEX concentrations in aqueous solutions.

Table 2.1. Physical-chemical properties for BTEX compounds (Kershaw, 1996).

Compound	Benzene	Toluene	Ethylbenzene	*m*-Xylene	*o*-Xylene	*p*-Xylene
Molecular formula	C_6H_6	$C_6H_5CH_3$	$C_2H_5C_6H_5$	$C_6H_4(CH_3)_2$	$C_6H_4(CH_3)_2$	$C_6H_4(CH_3)_2$
Molecular weight (g/mol)	78.11	92.13	106.2	106.2	106.2	106.2
Boiling point (ºC)	80.1	110.6	136.2	139.3	144.0	138.0
Density (g/cm^3 @ 20ºC)	0.877	0.867	0.867	0.884	0.880	0.861
Molar Volume (cm^3/mol)	89.41	106.3	122.4	123.2	121.2	123.3
Molecular volume (A^3)	83.95	99.98	116.21	116.00	115.97	116.00
Water solubility (mg/L)	1770	530	160	160	176	185
Vapor Pressure (Pa @ 25ºC)	12690	3800	1268	1120	882	1170
Henry's Law Constant ($Pa\ m^3/mol$)	557	647	854	700	542	760
Octanol/water Partition Coeficient ($\log K_{ow}$)	2.13	2.69	3.13	3.20	3.12	3.15
Sorption Partition Coeficient ($\log K_{oc}$)	1.81	2.25	2.41	2.26	2.37	2.31

2.2.2 BTEX IN THE ENVIRONMENT: TOXICITY

BTEX toxicity and adverse health effects have been widely studied (Do Rego & Pereira Netto, 2007). Laboratory scale experiments in animals have shown that BTEX compounds are well absorbed by the body and can be extensively metabolized. Human exposure over a long period resulted in skin and sensory irritation, and detrimental respiratory health effects (Mitra & Roy, 2011). In addition, BTEX can cause toxicity in the nervous system affecting the nerve membranes and proteins resulting in altered neurotransmitter receptor functions and ion transport, affecting nerve impulses and regeneration of action potentials (ATSDR, 2004).

Hematotoxicity of benzene is well known, with chronic exposure to benzene causing damage to the bone marrow thus decreasing the number of blood cells, which leads to aplastic anemia, and in severe cases to the development of leukemia (ATSDR, 2004; Aksoy, 1989; Snyder, 2000, 2012). The carcinogenic effect of benzene is well established and is classified as a human carcinogen (IRIS, 2017; ATSDR, 2004; IARC, 2012; NIOSH, 2016). WHO international standards for drinking water proposed a health-based guideline values concentration < 0.01 mg/L (WHO, 2003a).

Ethylbenzene is also associated with carcinogenic effects in experimental animals, thus classified as a possible carcinogen to humans (ATSDR, 2004; Huff et al., 2010). Kim et al. (2015) investigated the gene expression and genomic methylation patterns in the blood of workers exposed to ethylbenzene, finding that ethylbenzene exposure altered DNA methylation patterns in 1506 genes which demonstrated DNA damage in humans. WHO international standards for drinking water proposed a health-based guideline values concentration < 0.3 mg/L; however, the reported odor threshold in water ranges from 0.002 to 0.13 mg/L (WHO, 2003b).

Toluene has not been confirmed as a human carcinogen based on insufficient or limited evidence in experimental animals (ATSDR, 2015; CEPA, 1992). However, studies with humans in various occupational settings have shown that it primarily affects the central nervous system causing effects such as confusion and loss of cognitive function after prolonged inhalation (Filley et al., 2004; Health Canada, 2006). WHO international standards for drinking water proposed a health-based guideline values concentration < 0.7 mg/L; however, this value exceeds the lowest reported odor threshold of 0.02 mg/L (WHO, 2003c).

Xylenes are rapidly absorbed by inhalation and are widely metabolized in the liver (Niaz et al., 2015). Acute exposure to xylenes results in cardiovascular, hepatic, and neurological effects (CEPA, 1993). Chronic exposure has been associated with leukopenia, anemia, dyspnea, and with negative impacts to the central nervous system and cardiovascular system (Langman, 1994; Niaz et al., 2015). WHO international standards for drinking water proposed a health-based guideline value of 0.5 mg/L and an aesthetic value concentration of 0.02 mg/L based on the reported odor threshold (WHO, 2003d).

2.3 CARBON BASED INJECTATES FOR TREATMENT OF PHCs

Carbon Based Injectates (CBI) is an emerging remedial technology for the *in-situ* treatment of groundwater polluted with organic contaminants (e.g., petroleum hydrocarbons (PHCs)) (Fan et al., 2017; Lewis, 2012; USEPA, 2018). CBI technology is fundamentally based on adsorption (activated carbon, AC) and degradation processes working in conjunction. The adsorption/degradation processes working together are expected to be more efficient than conventional treatments that rely solely on just one mechanism; adsorption retards contaminant migration and as a result enhances degradation by extending contact times between contaminants and additives (e.g., bacteria) (Fan et al., 2017).

CBI has been defined as a slurry made of powdered or colloidal activated carbon (as the principal ingredient) mixed with water and chemical or biological additives to promote degradation (e.g., electron acceptors, bacteria, zerovalent iron, etc.), which is injected into the subsurface to remediate soil and groundwater impacted with PHCs (Lewis, 2012). So far, several commercially available AC-based products have been developed (Table 2.2) and applied at contaminated sites including those with leaking underground storage tanks and gasoline release sites (Simon, 2015; USEPA, 2018).

A remediation project from the consultant company LT Environmental Inc. used BOS-200® to remediate impacted benzene and methyl tert-butyl ether (MTBE) groundwater at a retail gasoline station site in Colorado. During the injection program, 2,268 kg of CBI were emplaced. As a result, they obtained a decrease in benzene concentration from 1 mg/L before the emplacement to non-detected levels (<0.0001 mg/L) after CBI injection and an MTBE concentration from over 25 mg/L to 0.004 mg/L in a large portion of the defined plume (LTE, 2006).

Another project of an active retail service station in Sacramento, California was conducted by BB&A Environmental in 2013 to remediate soil and groundwater impacted with gasoline-range total petroleum hydrocarbons (TPH) and volatile organic compounds. During the injection program, a total of 1,846 kg of BOS-200® was injected. The results from the post-injection soil sampling estimated a 45 to 85 % reduction in the mass of TPH (BB&A, 2015).

Table 2.2. Comparison of five AC-based products used for in situ applications. (from Fan et al., 2017).

Product	Physical Property	Additive	Target	Degradation Pathway
BOS-100®	Granular manufactured by Calgon	Impregnation of zerovalent iron	Chlorinated solvents	Abiotic reductive dechlorination
BOS-200®	Powdered manufactured by Calgon	Electron acceptors, phosphorus, nitrogen nutrients, CaSO4, Facultative bacteria mix	Petroleum hydrocarbons	Short-term aerobic and long-term anaerobic bioaugmentation
COGAC®	Granular or powdered	Calcium peroxide, sodium persulfate, Nitrate occasionally	Petroleum hydrocarbons and chlorinated solvents	Chemical oxidation, aerobic and anaerobic biostimulation
PlumeStop®	Colloidal sized AC suspension	Proprietary organic polymer, hydrogen or oxygen release compounds, bacterial strains	Chlorinated solvents or Petroleum hydrocarbons	Anaerobic biodegradation for chlorinated solvents or aerobic biodegradation for petroleum hydrocarbons (augmetation or stimulation)
Carbon-Iron	Colloidal sized AC suspension	Carboxymethyl cellulose as the colloidal stabilizer, impregnation of nano zerovalent iron	Chlorinated solvents	Abiotic reductive dechlorination

2.3.1 ADSORPTION BY ACTIVATED CARBON

One of the fundamental processes of contaminant removal in CBI technology is the adsorption of contaminants by activated carbon (AC). As a broad definition, AC is an amorphous carbonaceous material exhibiting a high degree of porosity and a high interparticle surface area (Bansal & Goyal, 2005), that has been obtained by carbonization of raw material following thermal or chemical activation processes (Marsh & Reinoso, 2006). Common precursors of AC are wood, coconut shells, or coal.

During the carbonization process, noncarbon elements are eliminated and carbon atoms are left forming stacks of aromatic sheets arranged in irregular patterns leaving free interstices or pores. The pores are further cleared by the activation processes which boost the quantity, shape, and size of pores resulting in an extremely high surface area making activated carbon an excellent adsorbent (Bansal & Goyal, 2005).

The porous nature of AC is its principal characterization property, and according to the International Union of Pure and Applied Chemistry (IUPAC), pores can be classified into three groups, based on their pore width (Everett, 1971):

- Macropores with a pore width larger than 0.05 µm.
- Mesopores with a pore width between 0.05 µm to 0.002 µm.
- Micropores with a pore width not exceeding about 0.002 µm.

The high surface area of AC is mainly due to the contribution of micropores (90-95% of the total surface area) and in addition, it is where most of the adsorption of molecules takes place (e.g., benzene) due to similar volume sizes between adsorbate molecules and pores that allow multiple contact points between molecules and pore walls. The mesopores or transitional pores are <5% of the total surface area of the AC, and contribute to the adsorption of molecules; however, they also act as conduits that transport adsorbates to the micropore cavities (Bandosz, 2006; Fan et al., 2017). Macropores generally serve as highways to transport molecules by intraparticle diffusion inside the AC matrix and can adsorb some large size organic molecules; however, they are not usually considered important contributors to adsorption due to their small surface area (Bansal & Goyal, 2005).

During the adsorption processes, molecules or atoms are fixed on the AC surface by physical and/or chemical interactions between adsorbate molecules and the AC surface. Physical interactions such as electrostatic or dispersive forces are the dominant adsorption mechanisms under typical subsurface temperatures (5-10 ºC) (Fan et al., 2017; Williams & Gold, 1976). Additionally, the pH of the point of zero charge (pH_{Pzc}) can be used as an indicator of the surface charge of AC at a specific pH. The point of zero charge expresses the condition when the electrical charge density on a surface is zero (Song et al., 2010). In AC, the pH of the point of zero charge (pH_{Pzc}) depends on the properties of the functional groups on its surface (Song et al., 2010). The surfaces are positive below the pH_{PZC} and negative above pH_{PZC}.

The adsorption of aromatic compounds (e.g., BTEX) from water on AC is related to van der Waals interactions, this occurs by a π - π electron-donor-acceptor mechanism. This dispersion interaction occurs between the delocalized π-electrons in the AC surface and the aromatic rings of the PHCs. This process is determined by the chemical properties of the molecules, its molecular size, hydrophobic nature, and the particular characteristics of the AC (Canzano et al., 2014).

To determine the applicability of the sorption process for operation, and to describe the fixation capacity of the sorbents (Quintelas et al., 2010) requires characterization of sorption equilibrium. To determine the equilibrium adsorption capacity, adsorption isotherms are used by performing bottle point experiments to obtain isotherms points. In this experiment, a set of bottles are filled with an adsorbate solution of different known concentrations C_0 (mg/L), at a specific volume V_L (L), and are amended with a defined adsorbent mass m_A (g). The bottles are shaken until equilibrium is reached and the residual adsorbate concentration in the liquid phase C_e is measured. Then, the sorbed amount of adsorbate q_e (mg/g) or equilibrium adsorption capacity can be calculated by (Worch, 2012):

$$q_e = (C_0 - C_e)\frac{V_L}{m_A} \tag{2.1}$$

Each equilibrium or isotherm point are plotted versus the equilibrium adsorbate residual concentration C_e for the solution studied. Isotherm data reflects the interactions between adsorbate and adsorbents. The equilibrium experimental data for AC is usually fit to the empirical Freundlich isotherm model and is often applied in water treatment studies. The Freundlich model assumes a heterogeneous surface of the adsorbent, and that the adsorption capacity depends on the concentration of the adsorbate in the solution under equilibrium conditions (Dada et al., 2012). The mathematical expression of the Freundlich isotherms model is (Worch, 2012):

$$q_e = K_f \times {C_e}^{n_f} \tag{2.2}$$

where q_e is the amount of sorbate (mg) adsorbed per unit weight of AC (g) at equilibrium conditions, C_e represents the residual adsorbate concentration at equilibrium, expressed in mg/L, K_f represents the adsorption strength where the higher the K_f value the higher adsorbent loading achieved, and n_f is the energetic heterogeneity of the adsorbent surface. If n_f = 1 the isotherms become linear. When n_f < 1 high adsorbent loading at low concentrations are achieved (favorable adsorption), on the other hand, when n_f > 1 isotherms are characterized as unfavorable (Worch, 2012). In addition, the removal efficiency can be determined by the percentage of adsorption using (Dada et al., 2012):

$$\% \, Sorption = \frac{C_0 - C_e}{C_0} \times 100 \quad (2.3)$$

Yakout & Daifullah, (2014) found that the adsorption capacity of BTEX on rice husk AC increased in the order X>E>T>B reflecting the decrease in solubility and increase in molecular weight. Compounds with low solubility have a lower affinity for water and a high affinity for AC. The molecular weight of *p*-xylene and ethylbenzene is the same, however, molecular configuration differs. Therefore, the adsorption of organic compounds is influenced by the physicochemical properties of each individual compound, these results are consistent with previous studies using different AC sources (Daifullah & Girgis, 2003).

Canzano et al. (2014) studied the performance of a commercial AC for the adsorption of toluene, *o*-xylene, ethylbenzene, and naphthalene from artificial groundwater in single and binary systems. The goal was to determine the adsorption capacity of each compound and the possible adsorption interactions between compounds (toluene + naphthalene and o-xylene + ethylbenzene). For the single compound experiments, all compounds showed a significant adsorption capacity on the selected AC, confirming the suitability of the use of AC for adsorption of PHCs in groundwater. Toluene and naphthalene showed higher adsorption capacities with similar values. In binary systems, a competitive effect occurred between toluene and naphthalene observed by the lower adsorption capacity for both compounds compared to that of a single-compound system because adsorption occurs on

the same active sites. AC adsorption sites decrease with increasing sorbed mass which results in the loss of adsorptive capacity of the AC (Yakout & Daifullah, 2014).

Within the physical sorption mechanisms, adsorption and desorption processes are in dynamic equilibrium since adsorption is a reversible process. When equilibrium conditions shift, the adsorbed compounds desorb from the AC into the water by back diffusion (Fan et al., 2017; Yakout & Daifullah, 2014). In addition, adsorbed compounds can be displaced due to competitive sorption by more strongly adsorbing compounds (Yakout & Daifullah, 2014).

Chemical interactions between the surface groups in the AC and the adsorbates are another type of important adsorption mechanism which is referred to as chemisorption. At the edge of the basal planes in the AC structure, carbon atoms are unsaturated, possessing unpaired electrons. At these sites, different heteroatoms can be bonded to the carbon atoms giving rise to surface groups. Among this later, oxygen-containing groups are the most common surface groups in AC. Furthermore, this influences the surface characteristics of the AC (polarity, acidity, electrical and chemical reactivity, etc.) and affects how the AC interacts with different molecules. In addition to oxygen, other surface groups can be formed with hydrogen, sulfur, nitrogen, and halogens (Bansal & Goyal, 2005).

Several studies have shown the suitability of using AC for the treatment of PHCs in water due to the good performance shown by AC in adsorbing aromatic compounds (Faisal et al., 2018; Kalmykova et al., 2014). Ayotamuno et al. (2006) examined the adsorption capacity of different AC materials (granular activated carbon, GAC or powdered activated carbon, PAC) to treat groundwater polluted with petroleum hydrocarbons. The experiments were conducted under laboratory conditions using groundwater samples collected from a polluted aquifer in Nigeria. The reported a significant decrease of dissolved total petroleum hydrocarbons (96% by GAC and 99.9% by PAC).

2.3.2 DEGRADATION PROCESSES INVOLVED IN CBI

A critical process in CBI technology is the degradation of contaminants following adsorption by AC. This synergism leads to a higher contaminant removal than what could be expected from adsorption and degradation alone. Also, this allows for continued contaminant removal far beyond the normal AC adsorption capacity (Voice et al., 1992).

Degradation coupled with adsorption using AC has been extensively studied and established for *ex-situ* water treatment (Çeçen & Aktaş, 2011; Luo et al., 2014; Riley et al., 2018). In addition*, in situ* degradation processes such as chemical oxidation and/or reduction and biodegradation (enhanced by biological stimulation and/or augmentation), has proven to be successful (Fan et al., 2017). Consistent with the scope of this research, this review will focus only on biological processes.

Biodegradation is defined as the transformation of compounds by living organisms through a series of reactions that take place as part of their metabolism (Vidali, 2001). The use of living organisms, primarily microorganisms has been widely applied *in situ* for the treatment of contaminated soil and groundwater (Adams et al., 2015; Bewley & Webb, 2001; Chapelle, 1999; Chiu et al., 2017; Cunningham et al., 2001; Farhadian et al., 2008; Phelps & Young, 1999).

Bioremediation can involve two processes, bioaugmentation which requires the inoculation of exogenous degrading microorganisms into the subsurface to promote degradation, and/or biostimulation which is the addition of nutrients to enhance the metabolic activity of microbes (Wu et al., 2016). In CBI technology, the addition of bacterial strains capable of degrading target pollutants, electron acceptors and nutrients to the AC-based amendment products (Fan et al., 2017) integrates both biostimulation and bioaugmentation processes to enhance microbial biodegradation.

The use of AC as a support material for microbial growth has numerous advantages. The rough porous nature of AC with its high surface area facilitates microbial attachment and colonization leading the growth of significant biomass or biofilm (Simpson, 2008). In other words, bacteria can be immobilized and concentrated on the AC surface. At the same time, bacteria are protected from shear forces which result in better attachment. AC promotes extended contact times between adsorbed contaminants (or a carbon source for microbes) and growing biofilms as they feed on the rich carbon supply (Fan et al., 2017; Simpson, 2008). AC adsorptive nature prevents shock loads (high contaminant concentration that can result in biotoxicity) to microbes which ensures that bacterial metabolic activity remains unaffected (Mason et al., 2000). Bacteria with an average size of 1 µm attach to the outer surface of the AC and are unable to reach the AC internal structure due to size exclusion (AC pore sizes range from 0.002 to 0.05 µm). As a result, biodegradation of contaminants is hypothesized to occur by different mechanisms.

The first mechanism involves total or partial biodegradation of the organic compound before it reaches the microporous structure of the AC. If partial biodegradation occurs, smaller by-product compounds will diffuse and sorb into the micropores. In this mechanism, an active microbial community should be fully established so that the degradation rate surpasses the contaminant influx (Fan et al., 2017; Simpson, 2008). If the concentration of the organic compound in the bulk water decreases, a shift in equilibrium conditions will occur and cause the desorption of organic compounds from inner micropores of the AC and back diffuse due to a reversal of the concentration gradient towards the biofilm will occur, allowing further contaminant degradation. This second mechanism might be dominant when degradation rates decrease (Fan et al., 2017; Simpson, 2008). In the third mechanism it is hypothesized that exoenzymes secreted by bacteria diffuse into the inner pores of the AC where organic compounds are adsorbed and induce transformation, desorb and become accessible for degradation in the biofilm (Klimenko et al., 2002; Nath & Bhakhar, 2011). However, this would be a slow process due to the low diffusivity of large-sized enzymes (21-44 A), which would only have access to the meso- and macropores (Aktaş & Çeçen, 2007;

Klimenko et al., 2002). These three degradation mechanisms rely on direct contact of the microorganisms and the target compound so that the contaminant is readily accessible.

Another mechanism which has recently been postulated is known as direct interspecies electron transfer (DIET) and suggests that AC as an electrically conductive material can provide electrical connection between degrading bacteria and methane-producing bacteria which can increase the rate of methanogenesis. The microorganisms capable of performing DIET can transfer electrons to the AC. Then, electrons will travel through the AC, until they reach the adsorbed target compound. As a result of this process, bacteria do not need to be in direct contact with the organic compound to be able to degrade it. This mechanism suggests that organic compounds entrapped within the micropores out of the reach of microorganisms, will still be bioavailable for degradation; however, further studies to completely address this mechanism need to be evaluated (Liu et al., 2012; Summers et al., 2010).

When assessing evidence of hydrocarbon biodegradation, different lines of evidence are usually used to understand ongoing treatment behavior (Wittebol & Dinkla, 2015). These techniques can include geochemical monitoring (e.g., electron acceptors (nitrate, iron or sulphate), gases (CH_4, CO_2), redox conditions), compound-specific monitoring of organic compounds and their intermediates, stable isotope probing, and in situ microcosms. These techniques can provide indirect evidence for the actual in situ biodegradation; however, the use of molecular analysis of functional genes involved in the biodegradation pathways can provide further direct evidence of the degradation potential (Wittebol & Dinkla, 2015).

The change in redox conditions can provide evidence of biodegradation through reduction processes (Weelink et al., 2010). During anaerobic BTEX biodegradation, microorganisms depend on electron acceptors (e.g., sulphate, CO_2) which are reduced, thereby decreasing its availability and increasing reductant concentrations (e.g., sulphide, CH_4) (Wittebol & Dinkla, 2015). Isotopic analysis assess biodegradation, independent of concentration, and

is based on the principle that ^{12}C substrates are preferentially biodegraded, thus an enrichment of heavy isotopes ^{13}C supports biodegradation (Wittebol & Dinkla, 2015).

Another method to monitor in situ biodegradation is to use in situ microcosms (e.g., BACTRAPs). In situ microcosms are useful for isotopic analyses and identification of microorganisms involved. These are assemblages consisting of activated carbon (well known to absorb BTEX) loaded with ^{13}C labeled substrate that provides an appropriate surface for biofilm formation.

Finally, the analysis of deoxyribonucleic acid (DNA) from aquifer samples can provide information on the presence of the species and functional genes involved in BTEX biodegradation, acquired by quantitative polymerase chain reaction (qPCR) (with previous knowledge of what is expected to be present). Next-generation sequencing can analyze all the genetic material in a sample with the possibility of showing all the genes that have been transcribed. Thus, known and unknown genes involved in BTEX biodegradation can be identified (Wittebol & Dinkla, 2015).

2.3.3 ACTIVATED CARBON MATURING

Although AC possesses a large surface area for contaminant sorption, in the course of any treatment, the sites available for adsorption become exhausted resulting in the loss of adsorption capacity (Aktaş & Çeçen, 2007). Due to this fact, one of the most important factors to sustain the long-term effectiveness of CBI is the regeneration of AC sorption sites. Bioregeneration can be understood as the process where sorbed contaminants desorb/degrade due to microbial activity and releasing sorption sites (Klimenko et al., 2002). For this reason, bacteria on AC plays an essential role in the AC-adsorption/degradation system. In bench-scale studies and wastewater treatment, it has

been shown that biodegradation can extend the lifetime of AC through regeneration of sorption sites.

Desorption from activated carbon occurs due to a shift in equilibrium conditions between the liquid (bulk water) and solid phase (AC), and it is a prerequisite step for regeneration (Aktaş & Çeçen, 2007). However, some strongly sorbed compounds can experience irreversible adsorption or sorption hysteresis. The reversibility of adsorption is attributed to weak van der Waals forces. Nevertheless, interactions between adsorbed compounds and specific functional groups on the carbon surface can result in high energy covalent bonding, therefore resisting desorption (Aktaş & Çeçen, 2007; Yonge et al., 1985). Also, it has been observed that at lower bulk contaminant concentrations, the loading on AC is consequently lower, promoting interactions with high-energy adsorption sites (Putz et al., 2005).

The reversibility of adsorption or degree of hysteresis can be expressed by using (Aktaş & Çeçen, 2007):

$$w\ (\%)\ = \left(\frac{n_{ads}}{n_{des}}\ -\ 1\right) \times 100 \qquad (2.4)$$

where n_{ads} and n_{des} are the inverses of adsorption and desorption intensities obtained from Freundlich isotherms. If $n_{des} < n_{ads}$ a slower rate of desorption is experienced, resulting in a higher degree of hysteresis.

The adsorption energy influencing adsorption reversibility is associated to the change in Gibbs free energy of adsorption ($-\Delta G^{\circ}_{ads}$), where the higher the $-\Delta G^{\circ}_{ads}$ of a compound, the lower its ability to desorb from the sorbent surface (Klimenko et al., 2002). Thus the energy of adsorption could be used to determine which compounds might be efficiently desorbed and removed in the adsorption/biodegradation processes (Aktaş & Çeçen, 2007). As mentioned before, bioregeneration of AC is restrained by adsorption reversibility (Aktaş &

Çeçen, 2007; Klimenko et al., 2003; Nath & Bhakhar, 2011). As microorganisms degrade the absorbable compounds, a shift in equilibrium conditions is experienced resulting in desorption and degradation of compounds. However, loading of AC with non-desorbable compounds or compounds with a high degree of hysteresis prevents bioregeneration (Nath & Bhakhar, 2011).

Klimenko et al. (2003) studied the bioregeneration of three different AC materials saturated with a mixture of oxyethylated alkylphenols (SAS) in static conditions. The bioregeneration efficiency was calculated as the ratio between equilibrium adsorption capacity (q_e) of fresh and regenerated AC (quantity of solute adsorbed from solution per unit weight of AC (mg/g)) at a specific equilibrium concentration (C_e), as given by:

$$Bioregeneration\ (\%) = \frac{qe_{regenerated}}{qe_{fresh}} \times\ 100 \qquad (2.5)$$

The quantification of bioregeneration efficiency should be evaluated under equilibrium conditions with no biodegradation occurring. Their results showed that the degree of regeneration due to biodegradation was only 20-23% of the value of adsorption on fresh AC. The low degree of AC regeneration appeared to be a result of the high degree of hysteresis of SAS molecules, where slow diffusion rates have been previously observed. In addition, adsorption occurring in the inner part of the AC was not subjected to microbial activity as exoenzymes and bacteria did not penetrate this portion of the AC and therefore did not regenerate the sorption sites. Nevertheless, as microbial biofilms began to form on the outer surface of AC, diffusion of contaminants from the bulk water to the inside of the AC may become limited as a result of an increased mass transfer resistance (Mason et al., 2000; Rattier et al., 2012).

Mason et al. (2000), evaluated the change in adsorption characteristics of PAC in a mixed bioreactor. In these experiments, an aerobic BTEX degrading biofilm was grown on the PAC. To determine the influence of biofilm attached to the PAC on the adsorption characteristics

of PAC, a series of isotherms were carried out using methyl-tert-butyl ether (MTBE) as a test compound (which was not metabolized by the bacterial mixture) and compared to fresh PAC. The Freundlich constants K_F and n for the fresh PAC were 3.37 and 1.86 respectively, while for the biofilm coated PAC, K_F ranged from 0.42 to 0.82 and n ranged from 1.14 to 1.35. These results indicate that the adsorption capacity of PAC was significantly reduced in the presence of a biofilm. Martin et al. (2004) observed similar results and reported that the estimated adsorption capacity of a commercial PAC combined with activated sludge was smaller than that predicted by the adsorption isotherm. This decrease was considered to be caused by a reduction in mass transfer due to the biomass surrounding the PAC.

Adsorption capacity can be considerably hampered either by the adsorption of lysed cells, microbial metabolites, and non-biodegradable substances or adsorption of organic matter that outcompete for sorption sites (Nath & Bhakhar, 2011). Zhao et al. (1999) evaluated the adsorption capacity of a biofilm coated GAC from an aerobic biological fluidized bed reactor which treated toluene contaminated water. They observed that the adsorption capacity of biofilm coated GAC remained <70% for the first two months, however, after six months it decreased to 40-57%. They also examined the relationship between the loss in adsorption capacity and the biofilm thickness. Physical dislodging of biofilm by shaking and chemical digestion of the biofilm and sorbed proteins was performed by base wash (0.5 M NaOH). No direct relationship was determined for the loss of adsorption capacity and the biofilm thickness; however, the duration of biofilm/GAC exposure or bioactivity was thought to influence the loss of adsorption capacity. They suggested that the loss in the adsorptive capacity of GAC might have been due to the adsorption of soluble microbial metabolites excreted by the biofilm, which accumulated over time. Thus biological fouling (by biomass production and microbial metabolites) might have consequential impacts on bioregeneration (Leong et al., 2018a) and deteriorate CBI performance.

2.4 BIOFILMS IN GROUNDWATER REMEDIATION

The use of microorganisms has been broadly applied in the *in-situ* remediation (bioremediation) of groundwater impacted by petroleum hydrocarbons (Adams et al., 2015; Bewley & Webb, 2001; Chapelle, 1999; Chiu et al., 2017; Cunningham et al., 2001; Farhadian et al., 2008; Phelps & Young, 1999). Biofilm enhancing remediation such as CBI, offers an advantage over bioremediation with planktonic microorganisms, since it provides microbes with a protective micro-environment and thus a better chance of adaptation and survival under resource limiting environments such as in groundwater (Singh et al., 2006). For this reason, understanding the role and development of these microbial assemblages on engineered substrates such as AC is important. The study of biofilm diversity, composition, and structure have been developed in recent decades, and the use of microscopic and molecular tools have facilitated the analysis of the spatial organization and phylogenetic composition of biofilm communities (Singh et al., 2006).

2.4.1 MICROBIAL BIOFILMS

Microbial biofilms are among the first life forms on Earth (Trevors, 2011). Fossil evidence of biofilms in rocks date back to 3.5 billion years ago (Westall et al., 2003). IUPAC has defined biofilms as:

"Aggregates of microorganisms in which cells that are frequently embedded within a self-produced matrix of extracellular polymeric substance adhere to each other and/or to a surface. " (Ahmad & Husain, 2017)

Biofilms are present in different aquatic environments such as lake sediments, river beds, sea beds, in suspended particles in rivers, lakes, sea, and aquifers (Besemer, 2015; Sabbagh, 2013) and any other surface exposed to adequate moisture (Sutherland, 2001).

Furthermore, microbial biofilms are responsible for many of the biogeochemical processes occurring in aquatic environments (Griebler & Lueders, 2009; Weaver et al., 2015; Wilhartitz et al., 2009). These microbial communities are known to be the dominant mode of microbial life. They can comprise of single species or multi-species communities, with the later most commonly found in natural environments (Lueders, 2017).

Biofilms are comprised primarily of microbial cells and extracellular polymeric substances (EPS) (Carrel et al., 2018). Water accounts for up to 97% of biofilm composition and can be found within the capsules of microbial cells or as a solvent within the EPS (Sutherland, 2001). EPS accounts for 50-90% of the total organic carbon of biofilms, thus considered the primary matrix component of the biofilm (Donlan, 2002). Only 2-15% of total organic carbon represents cellular material (Sutherland, 2001).

EPS is a remarkable component of biofilm composition. It is primarily comprised of polysaccharides, proteins, and eDNA (Zhang et al., 2015). EPS provides biofilm structure and its physical properties are highly dependent on the solutes dissolved on it (Sutherland, 2001). It serves as a protective barrier against changes in extracellular environmental conditions (pH-shift, contaminant shock loads, desiccation and shear forces) and allows complex network interactions (Capozzi et al., 2019a; Carrel et al., 2018; Fröls et al., 2012; Zhang et al., 2015). Additionally, it increases the residence time of the microbial communities which promotes the metabolism of dissolved substances (Besemer, 2015).

The sessile lifestyle of biofilms has numerous advantages over their planktonic counterpart especially in carbon and nutrient-poor environments (Lueders, 2017; Wilhartitz et al., 2009). EPS has shown to be essential for microbial communication. This chemical communication mechanism is known as Quorum sensing. Quorum sensing regulates cellular functions such as nutrient acquisition and exchange, cell-cell signaling compounds, horizontal gene transfer, and secondary metabolite production (Renner & Weibel, 2011). As well it

facilitates interactions of microorganisms with their bio-physicochemical environment (Capozzi et al., 2019; Fröls et al., 2012; Zhang et al., 2015).

The arrangement and specific composition of biofilms depend on intrinsic processes such as cell division, environmental factors such as pH, temperature, oxygen, nutrients or shear forces, as well as the microbial type and diversity (Purevdorj et al., 2002; Stoodley et al., 1999; Sutherland, 2001). The diversity of biofilms will determine the metabolic performance of the communities and the ecosystem services they provide (Besemer, 2015). In aquatic systems (lake sediments, river beds, sea beds, in suspended particles in rivers, lakes, sea and groundwater, as well as treatment plants) biofilms are considered to provide important services, since they contribute to the biogeochemical cycling of nutrients and the removal of anthropogenic contaminants from water (Characklis & Wilderer, 1989; Weaver et al., 2015).

2.4.2 BIOFILM DEVELOPMENT

Biofilm development occurs through different stages including substrate colonization, maturation, maintenance, and dissolution (Toole et al., 2000). These stages have been described by Renner & Weibel (2011) and illustrated in Figure 2.1. In the initial stage, cells are transported from the bulk water to a distance of several microns above the surface (McClaine & Ford, 2002). At this point, bacteria are attracted to the surfaces by electrostatic repulsion or attraction interactions (van de Waal forces) and hydrophobic interactions (by extracellular organelles) (Renner & Weibel, 2011). At this stage, the attachment is reversible.

In the second stage, irreversible attachment occurs where microbial cells form microcolonies and secrete EPS that enhance the irreversible adhesion to substrates and act as a “glue”. Then, cells replicate and accumulate embedding into the EPS, which serves as a

physical barrier protecting them from the extracellular environment (Renner & Weibel, 2011). The EPS also serves as a medium where bacteria can communicate with each other by Quorum sensing (Donlan, 2002). In the fourth stage, the community grows in multiple layers, the EPS accumulates, and microbial colonies mature into a biofilm. A mature biofilm is characterized by the complete embedment of microbial cells forming tridimensional structures. In the final stage, cell propagation takes place where some cells detach from the biofilm and disperse into the bulk liquid providing the opportunity to be re-adsorbed and colonize new surfaces to form biofilms. This process also serves as a regulator of community dynamics (Renner & Weibel, 2011).

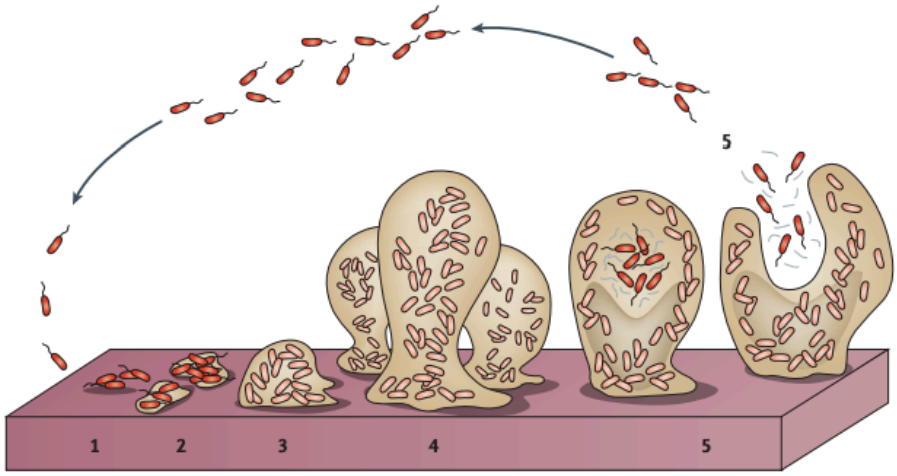

Figure 2.1. Conceptual model of biofilm formation as a developmental process. (1) Initial attachment of planktonic cells adhering to a surface. (2) Cells aggregate to form microcolonies and production of EPS starts, and attachment becomes irreversible. (3) Development of biofilm leading to a mature biofilm forming multi-layered clusters. (4) 3D growth and complete maturation of biofilm. (5) Cell release or dispersion.

2.4.3 PHYSICOCHEMICAL PROPERTIES THAT INFLUENCE ADHESION TO SURFACES

In bioremediation, a portion of the injected bacteria will be transported through the subsurface with the groundwater flow, while another portion will attach to soil or AC particles to develop biofilms (McClaine & Ford, 2002). The initial attachment to surfaces occurs by the transport of cells from the bulk liquid to close proximity of several microns above the surface (McClaine & Ford, 2002). In addition, some microbes are capable of chemotaxis (movement of organisms in response to a chemical gradient or nutrient, promoting bacteria to find optimum conditions for growth and survival), which allows microbial degraders to move toward the contaminants (Singh et al., 2006), such as those sorbed to soil or AC. This mechanism is an advantageous behavior for bacteria, especially in nutrient-limited environments such as groundwater.

Once the bacteria are close to the surface microscopic transport takes place. Bacteria are attracted to the surfaces by electrostatic repulsion or attraction interactions and van der Waal forces (McClaine & Ford, 2002; Renner & Weibel, 2011). Most bacteria possess a net negative charge, thus are attracted principally to positively charged surfaces (Renner & Weibel, 2011). This is an important implication in AC based amendments as a positive surface charge in AC will promote bacterial adhesion. Electrostatic repulsion forces can be overcome by the use of extracellular organelles, such as flagella, pili, curli, and fimbriae (Renner & Weibel, 2011). These organelles present hydrophobic moieties that enhance surface attachment with hydrophobic surfaces containing electrolytes and macromolecules (Donlan, 2002; Renner & Weibel, 2011). The hydrophobic interactions tend to increase with the increasing nonpolar nature of both cells and surfaces (Donlan, 2002).

Additionally, surface topography plays an important role in bacterial attachment. The surface roughness at the nanoscale enhances the adhesion of bacteria during the first stages of colonization, providing further surface area for attachment (Renner & Weibel, 2011). Also, surface roughness protects bacteria from shear forces occurring in

environments where fluids are flowing (Renner & Weibel, 2011; Simpson, 2008). Chemical properties of surfaces are also important for regulating the attachment of bacteria. The "conditioning layer" as described by Renner & Weibel, consists of an adsorbed layer of molecules (e.g,. proteins, ions, and macromolecules) on the surface of materials that vary with particular environmental conditions (e.g,. pH and temperature). Humic acids are one of the main components of the conditioning layer in nutrient-poor environments. Ions such as Mg^{2+} and Ca^{2+} could reduce electrostatic repulsion forces between the negative surface of bacteria and substrates (Renner & Weibel, 2011).

2.4.4 BIOFILMS IN GROUNDWATER ENVIRONMENT

Groundwater systems are characterized by being oligotrophic; limited oxygen replenishment, low availability of organic carbon and nutrients, lack of light, and low temperatures (Griebler & Lueders, 2009). Therefore, microbial diversity in groundwater is generally comprised of heterotrophic organisms well adapted to nutrient-poor and oligotrophic environments, and lithoautotrophs which oxidize inorganic electron donors and fix CO_2 (Griebler & Lueders, 2009).

Microbial biomass in groundwater systems are frequently found attached to surfaces (e.g., sediment particles) forming thin biofilms (Griebler & Lueders, 2009; Weaver et al., 2015). Microbial biofilms are advantageous, especially in oligotrophic environments compared to their planktonic counterparts. The reason is that macromolecules and organic compounds tend to accumulate on surfaces (Griebler et al., 2002), leading to better access to nutrients and carbon sources which can be concentrated and retained into the biofilm, providing long-lasting energy sources to microorganisms (Griebler & Lueders, 2009; Singh et al., 2006). In addition, biofilm-forming microorganisms can form synergistic communities, performing combined processes that planktonic cells cannot (Griebler & Lueders, 2009). The diversity in biofilm communities has been observed to be absent or diverge from the

ones found in the aqueous phase (planktonic counterpart) (Rickard et al., 2004; Wilhartitz et al., 2009).

Bacterial biomass present in groundwater vary between 10^2 to 10^6 cells per cm^3 of groundwater and between 10^4 to 10^8 cells cm^3 of sediment (Griebler & Lueders, 2009). From these estimates, planktonic bacteria contribute only to 0.01 to 10% of the total biomass (Griebler et al., 2002). Similar observations were made in laboratory microcosm studies (Griebler et al., 2002). The ratio between planktonic and attached microbes in groundwater is mostly dependent on nutrient availability, dissolved organic carbon, sediment particle size, and groundwater velocity (Griebler & Lueders, 2009).

Slow groundwater velocities of few meters per day and low shear rates are characteristic of groundwater environments. But changes in flow conditions might occur in zones of high hydraulic conductivity. Microbial biofilm diversity, structure, and surface adhesion has shown to be flow-dependent (Donlan, 2002; Karwautz, 2015). It has been observed that shear forces have the potential of affecting the microbial diversity of biofilms (Rickard et al., 2004). At low velocities associated with lower shear stress, multispecies communities are more diverse compared to those growing in the presence of high shear forces or fluid velocities (Rickard et al., 2004). Also, in higher velocity regimes is expected that more cells would come into contact with surfaces, compared to lower velocity regimes (Donlan, 2002). Under laminar flow conditions, biofilm structure consist of roughly circular-shaped microcolonies (Stoodley et al., 1999). Changes in biofilm morphology will directly impact the biofilm porosity and thickness, which will affect the transfer of solutes from the bulk liquid into and through the biofilm (Karwautz, 2015; Stoodley et al., 1999).

Another factor impacting biofilm development and structure, is the availability of carbon sources, nutrients, and electron donors and acceptors that are essential for microbial growth (Donlan, 2002; Griebler & Lueders, 2009). Groundwater systems which are often oligotrophic, extensive EPS production is not common due to the high energy needed for

its production. However, EPS production could be enhanced when energy sources become available (Karwautz, 2015). In this type of nutrient and carbon-limited systems mixed substrate uptake is common (Karwautz, 2015). Table 2.3 provides a summary of the properties influencing cell attachment to surfaces and biofilm formation.

In biofilms, synergistic microbial communities performing combined processes, facilitate the degradation of recalcitrant compounds (Griebler & Lueders, 2009; Karwautz, 2015). This synergism allows the uptake of diverse carbon sources, which otherwise could not be utilized by planktonic cells, and indeed could exert toxic effects (Capozzi et al., 2019a; Carrel et al., 2018; Fröls et al., 2012; Karwautz, 2015; Singh et al., 2006; Zhang et al., 2015).

Table 2.3. Properties influencing cell attachment and biofilm formation (Modified from Donlan, 2002).

Properties of the substratum	**Properties of the bulk liquid**	**Properties of the cells**
Texture or roughness	Flow velocity	Cell surface hydrophobicity
Hydrophobicity	pH	Extracellular organelles
Conditioning film	Temperature	EPS
	Nutrients	

2.4.5 ROLE OF BIOFILMS IN CONTAMINANT DEGRADATION AND IMPLICATIONS FOR CBI

The biodegradation of PHCs in groundwater systems relies largely on anaerobic processes (Farhadian et al., 2008; Lueders, 2017) since these systems are oxygen limited. The increased organic carbon input by contamination, results in a rapid depletion of any available oxygen (Johnson et al., 2003; Lueders, 2017). Microbial transformation of aromatic compounds under sulfate-reducing, methanogenic and denitrifying conditions had shown to occur naturally in groundwater systems (Alegbeleye et al., 2017; Johnson et al., 2003; Logeshwaran et al., 2018). Furthermore, aromatic compounds (e.g., BTEX) are thermodynamically favorable electron donors (Table 2.4) for microbial growth (Weelink et al., 2010).

Table 2.4. Thermodynamics of toluene oxidation under anaerobic conditions. (Modified from Lueders, 2017)

Electron acceptor (oxidised/reduced)	Stoichiometry	ΔG° [kJ (mol C_7H_8)$^{-1}$]
NO_3^-/N_2	5 C_7H_8 + 36 NO_3^- + H^+ → 35 HCO_3^- + 18 N_2 + 3 H_2O	−3555 kJ
$Fe(OH)_3/FeCO_3$	C_7H_8 + 36 $Fe(OH)_3$ + 29 HCO_3^- + 29 H^+ → 36 $FeCO_3$ + 87 H_2O	−1497 kJ
SO_4^{2-} /HS^- (complete)	2 C_7H_8 + 9 SO_4^{2-} + 6 H_2O → 14 HCO_3^- + 9 HS^- + 5 H^+	−203 kJ
SO_4^{2-} /HS^- (incomplete)	2 C_7H_8 + 3 SO_4^{2-} +6 H_2O → 6 CH_3COO^- + 2 HCO_3^- + 3 HS^- + 5 H^+	−61 kJ
CO2/CH4 (sum)	2 C_7H_8 + 15 H_2O → 9 CH_4 + 5 HCO_3^- + 5 H^+	−130 kJ
Fermenter	2 C_7H_8 + 18 H_2O → 6 CH_3COO^- + 2 HCO_3^- + 8 H^+ + 12 H_2	+166 kJ
Hydrogenotroph	12 H_2 + 3 HCO_3^- + 3 H^+ → 3 CH_4 + 9 H_2O	−203 kJ
Acetotroph	6 $CH3COO^-$ + 6 H_2O → 6 CH_4 + 6 HCO_3^-	−93 kJ

Under methanogenic conditions, degradation of PHCs requires syntrophic associations between fermentative bacteria and methanogens (Archaea). In the first step, fermenters transform hydrocarbons into acetate, formate, and/or H_2. This first step is

thermodynamically unfavorable under standard conditions. However, it becomes favorable when methanogens consume these products and transform them to CH_4 and CO_2, through hydrogenotrophic and acetoclastic methanogenesis. Hydrogenotrophs use H_2 as an electron donor and reduce CO_2 to CH_4. Acetotrophs break acetate to form CH_4 and CO_2. (Toth, 2017).

In the degradation of toluene and xylene isomers, the first step is the addition of the methyl group of toluene to fumarate to form benzylsuccinate by the enzyme benzylsuccinate synthase (*bssABC)* (Lueders, 2017; Washer & Edwards, 2007; Weelink et al., 2010; Wittebol & Dinkla, 2015). This enzyme is present in fermenting bacteria as well as nitrate-, iron-, and sulphate- reducing bacteria (Wittebol & Dinkla, 2015). Benzylsuccinate is then activated to benzylsuccinyl-CoA by a succinyl-CoA-dependent CoA-transferase (*bbsEF)*, which is then converted to succinyl-CoA and benzoyl-CoA (Lueders, 2017; Weelink et al., 2010). Benzoyl-CoA has been recognized as the central intermediate in the anaerobic biodegradation of many aromatic compounds (Lueders, 2017; Weelink et al., 2010). Then, benzoyl-CoA reductase (*bcrCABD)* initiates the degradation of benzoyl-CoA (Weelink et al., 2010). The first step of ring reduction can be conducted by an ATP-dependent class I benzoyl-CoA reductase (*BcrA-D*) (facultative anaerobes) or an ATP-independent class II benzoyl-CoA reductase (strict anaerobes and fermenters) (Lueders, 2017). Then, ring cleavage by 6-oxocyclohex-1-ene-1-carbonyl-CoA hydrolase (*BamA*) is followed by β-oxidation-like reactions to acetyl-CoA for assimilation or complete oxidation to CO_2 (Lueders, 2017).

Implications for CBI

Microbes in biofilms require macronutrients (e.g. nitrogen and phosphorus), micronutrients (e.g., Ca^{2+}, Mg^{2+}, Na^{+}, K^{+}, S^{2-}), electron acceptors, and optimal environmental conditions (e.g., pH, temperature). The uptake of nutrients and other carbon source molecules by microorganisms occurs through the cell walls and membranes. The cell wall is hydrophobic

in nature and consists of a lipid bilayer and membrane proteins which provide a protective barrier to cells. This membrane is selectively permeable to molecules (e.g., ions, nutrients, and also to some contaminants) since it has pores of <4 nm and water and dissolved molecules with molecular weights <100 Da can permeate to the inside of the cells (Whitacre, 2010).

Small, hydrophobic, weakly polar compounds such as alcohols, fatty acids, BTEX compounds (e.g., benzene), can penetrate the lipid phase of the cell membrane. Thus, a concentration gradient between the inside/outside of the cell (through pores and water channels) is one of the main driving forces for contaminant uptake. Consequently, this concentration gradient is highly dependent upon the local availability of the contaminant (Singh et al., 2006). The bioavailability of the contaminants to the microbial degraders depends on the degree on which the contaminants are sorbed into substrates or dissolved in water (Alegbeleye et al., 2017; Canzano et al., 2014). As mentioned previously, BTEX compounds have relatively high solubility and are partitioned into soil pore water, leading to increased mobility with water (Balseiro-Romero et al., 2018; Logeshwaran et al., 2018). In CBI, the use of AC for PHCs impacted groundwater treatment will decrease dissolved contaminant concentrations in the bulk liquid due to uptake by the AC (Ayotamuno et al., 2006). Nevertheless, groundwater flow and chemiotaxis allow microbial degraders to move toward the contaminants sorbed to the AC. Once microbes are brought into close contact with AC, surface interaction processes occur between the cells and the AC, thus biofilm formation mechanisms are initiated. This initial attachment to surfaces occurs due to electrostatic charges, van der Waal forces, and hydrophobic interactions (Renner & Weibel, 2011).

A mentioned before, most bacteria possess a net negative charge, thus are attracted principally to positively charged surfaces (Renner & Weibel, 2011). In a study made by Liu, (2017) characterization of PAC (WPC®, Calgon Carbon) properties was undertaken. The pH_{PZC} value of this PAC was 10.1, indicating that its surface would be positively charged

below a pH of 10. As a result, adsorption of bacteria to WPC® PAC could be enhanced by electrostatic charges. Also, it has been observed that microbial activity is dramatically increased upon adsorption to AC (Simpson, 2008). One hypothesis for this is that upon biofilm attachment to the AC surface, bacteria undergo physiological modifications that promote activation of certain genes. Another hypothesis is that biofilm components (e.g., EPS) increase the local concentration of nutrients, enzymes, and carbon sources and protects them from environmental changes, maintaining a relatively consistent micro-environment (Simpson, 2008).

In biofilm coated AC (granular) reactors, it was observed that the biofilms completely colonized the AC surface. Also, the biofilm thickness was heterogeneous within the same AC particles with the presence of cell-free spaces. These open channels connected the outside environment (bulk liquid) with the deeper inner layers of the biofilm. Thus, it can be speculated that this type of arrangement might facilitate the transport of substrates deeper into the matrix (Massol-Deya et al., 1995).

2.4.6 METHODS TO DETECT BIOFILMS

The knowledge of biofilm function, composition, and architecture have become relevant, due to its role in industrial processes, environment and human diseases (Drago et al., 2016). Various techniques have been developed to examine biofilms produced in different substrates (Drago et al., 2016). When using rough, porous materials such as AC particles, it is of particular interest to acquire more information about biofilm development, biomass accumulation, biofilm morphology, etc. (Caizán-Juanarena et al., 2019).

Biofilm morphology and spatial distribution studies are generally based on microscopic techniques. Visualization of structures in 2D planes can be undertaken by staining techniques and light microscopy. 3D visualization can be performed by scanning electron

microscopy (SEM) and confocal scanning laser microscopy (CLSM) (Wilson et al., 2017). Biomass accumulation measurements can be performed by determination of total dry or wet mass, the total number of cells (e.g., flow cytometry) or heterotrophic plate count (HPC) (Caizán-Juanarena et al., 2019; Waller et al., 2018). Table 2.5 provides a summary of commonly used techniques for the analysis of biofilms.

Table 2.5. Commonly used techniques for biofilm detection (Azeredo et al., 2017; Singh & Gaur, 2019; Singh et al., 2006; Wilson et al., 2017).

Type of analysis	Techniques	Application
Physical methods	Dry or wet weight, Electrochemical impedance spectroscopy	Biomass estimation
	Nuclear magnetic resonance, X-ray tomography	Biofilm thickness
Plate count (colony forming units, CFUs)	Heterotrophic plate count	Quantification of live culturable organisms
Flow-based cell counting	Flow cytometry, Coulter counter	Cell quantification
Microscopy	Light microscopy	Morphological observation, cell quantification
	Confocal laser scanning microscopy	Morphological observation, cell, EPS components, biomass (biovolume), thickness quantification, spatial organization 3D reconstruction
	Scanning electron microscopy	Morphological observation, spatial organization
	Fluorescence in situ hybridization (FISH)	Phylogenetic identification, spatial organization of communities, metabolic activity
Molecular	qPCR	Cell quantification, taxonomy

2.4.6.1 QUALITATIVE CHARACTERIZATION TECHNIQUES

Qualitative characterization of biofilms can include the observation of the physiological biofilm surface, morphology, spatial organization, evaluation of the surface roughness, and interaction of the biofilm with the environment (Wilson et al., 2017).

Scanning Electron Microscopy (SEM) is one of the most frequently used techniques to assess qualitative characteristics of biofilms due to the high resolution it offers (Asahi et al., 2015; Gomes & Mergulhão, 2017). In principle, basic SEM methods require samples of biofilm to be fixed with glutaraldehyde and/or osmium tetroxide, dehydrated in ethanol, alcohol or acetone series, critical-point dried, mounted on an SEM stub, sputter-coated with heavy metals, typically gold or palladium to increase their electrical conductivity, and imaged at an appropriate voltage (Kaláb et al., 2008). SEM can provide resolutions of 1 nm (magnifications up to 1,000,000x) (Henini, 2000), thus enabling to study bacteria in great detail. One of the main limitations of conventional SEM is the need to fix, dehydrate, and metalize the samples before observation. Biofilms are highly hydrated structures (Sutherland, 2001), thus dehydration might alter the morphology. As an example, when EPS is investigated by this technique, it often appears as fibers connecting bacteria (Vuotto & Donelli, 2014).

2.4.6.2 QUANTITATIVE CHARACTERIZATION TECHNIQUES

Quantification of the bacterial population embedded in a biofilm is one of the most acquired measurements. Direct quantification methods rely on the observation and enumeration of the desired parameter such as the number of cells. It can be performed using automated cell counting such as flow cytometry, or imaging using microscopy. In contrast, indirect methods rely on the measurement of some quantifiable biofilm property, such as colony-forming units (CFUs). Most of these methods require detachment, homogenization, and

dispersion of the biofilm in a liquid medium prior to analysis (Wilson et al., 2017), which can add experimental uncertainty.

From the indirect methods, CFU methods such as HPC are one of the most commonly used in microbiology for the determination of the number of viable cells (Allen et al., 2004; Reasoner, 2004; Sartory, 2004). It is based on the resuspension of the biofilm in a solution using serial dilutions. The dilutions are membrane filtered or plated and placed under specific nutrient agar growing mediums. Then, the samples are incubated for a particular length of time and temperature. Finally, the bacterial colonies are enumerated and reported as CFU/mL (Allen et al., 2004; Health Canada, 2012). However, significant errors can be introduced with this method in quantifying cells forming biofilms. This method just allows quantifying viable and culturable organisms, excluding death biomass and organisms that are difficult to culture in laboratory conditions (González-Rivas et al., 2018; Waller et al., 2018).

For direct measurements, flow-based cell counting is an automated way to count biofilm cells with flow cytometry as a commonly used technique (Cerca et al., 2011; Kerstens et al., 2015). These methods involve cells to flow through narrow apertures which are measured as they pass. A laser is used to detect the cells via scattering, absorbance, or fluorescence measurements. It has the advantage of being fast, simple, and accurate. In addition, it can provide information on cell dimension, surface properties, metabolic activity, and state of the cells by coupling it with fluorescent stains (Wilson et al., 2017). However, it requires the homogenization and suspension of the biofilm in liquid cultures.

Cell counting and biofilm characterization can be performed by using microscopy techniques. Light microscopy can be used to visualize biofilms in 2D planes. Immature biofilms attached to translucent surfaces can be stained and visualized. However, mature biofilms that are characterized by their 3D structure, require the suspension and homogenization into a liquid medium. After resuspension, cells can be visualized and

manually counted using chamber counting slides. This microscope slides feature a 2D grid on the bottom, to help to count in each grid and determine the cell density of the suspension. The average count from several grids can be used to calculate the number of cells on a known volume of liquid (Wilson et al., 2017).

Fluorescent microscopy can improve the information acquired by conventional light microscopy by exciting fluorescent molecules of particular components on biofilms. Fluorescent dyes known as fluorophores are molecules which absorb and emit light when incorporated in the biological structure (Wilson et al., 2017). Fluorescent microscopes are equipped with high-intensity lamps (e.g., argon lamps) and fluorescent filters which allow specific bands of excitation and emission light to interact with the sample and the observer.

Confocal laser scanning microscopy (CLSM) is one of the most sensitive assays to study biofilms (Drago et al., 2016). It is a specialized form of microscopy capable of producing high-resolution images of 3D biofilms. The 3D visualization is possible as the area of focus of the sample is scanned in layers to produce 2D slices at successive depths. These slices are then assembled to produce a final 3D image. With CLSM it is possible to observe biofilms attached to opaque surfaces such as sediment grains, metals, and AC particles (Doll et al., 2016; Waller et al., 2018). In addition, CLSM allows the observation of undisturbed, fully hydrated biofilms, and thus eliminates experimental variables associated with cell detachment (required with other techniques)(Drago et al., 2016).

When CLSM is combined with a range of fluorescent stains, images of various cellular and extracellular biofilm components (e.g., live and dead cells, proteins, EPS) can be obtained (Garny et al., 2010; González-Machado et al., 2018). Therefore, it is possible to assess qualitative (organization, distribution, morphology, etc.) and quantitative (cell biomass, biofilm thickness, etc.) biofilm information.

As a first approach for CLSM biofilm imaging, fluorescent stains are used to label specific components of biofilms. Many commercial fluorescent stains are available in a variety of emission colors (green, red, orange, and violet) which allow the analysis of multiple components simultaneously (Wilson et al., 2017). In Table 2.6, a summary of commonly used stains is provided. Highly selective nucleic acid stains such as SYBR-green and SYTO®9 can be used to label microbial cells in a population. In addition, SYTO®9 can be coupled with propidium iodide (PI) to discriminate between live and dead cells (SYTO9 target all cells and PI only targets cells with damaged membranes, reducing SYTO®9 fluorescence when both present) (Drago et al., 2016; Powell et al., 2018). Lectins are used to visualize EPS as they preferentially bind to polysaccharides, a major part of the EPS (Donlan, 2002; Garny et al., 2010). Lectins are capable to bind to carbohydrates without altering their structures (Zhang et al., 2015). The most frequently used lectin is Concanavalin A (Con A), binding to mannose and glucose residues (α-D-glucose and α-D-mannose) (Powell et al., 2018; Zhang et al., 2015).

Table 2.6. Commonly used fluorescent stains (fluorophores) to target specific biofilm components.

Fluorophore	Biofilm binding location	Reference
SYBR-GREEN	Nucleic acids	(Capozzi et al., 2019a; Zhang et al., 2015)
SYTO ® 9	Nucleic acids	(Artyushkova et al., 2016; Doll et al., 2016; Drago et al., 2016; (Banagan et al., 2010; Marchal et al., 2011; Powell et al., 2018; Waller et al., 2018; Zhang et al., 2015)
Propidium Iodide	Nucleic acids of damaged cells	(Artyushkova et al., 2016; Doll et al., 2016; Drago et al., 2016)
Concanavalin A **Alexa Fluor 633**	Polysaccharides (α-D-glucose and α-D-mannose)	(Banagan et al., 2010; Garny et al., 2010; Marchal et al., 2011; Powell et al., 2018)
TOTO-1	Extracellular DNA	(Powell et al., 2018)
SYPRO®	Protein content	(Powell et al., 2018; Zhang et al., 2015)

2.4.7 ANALYSIS OF BIOFILM CONFOCAL IMAGES

Biofilm digital image acquisition using confocal microscopes allows the user to characterize quantitatively and qualitatively desired parameters of biofilm samples. Currently, there are numerous software packages available that allow data analysis and image processing of confocal image stacks to make 2D or 3D representations. Imaris®, ImageJ + COMSTAT, and Daime are popular software packages (Azeredo et al., 2017).

Within the image acquisition of confocal images, slices (called image stacks) of images are recorded at successive focal planes within the *Z* coordinate (different heights). Each fluorophore is captured in a single channel; thus, each image stack is represented by one image per channel used (Azeredo et al., 2017). To obtain a 3D representation of a biofilm, several image stacks should be acquired and reconstructed, resulting in an image with *X*, *Y* and *Z* coordinates. The digitalized images acquired by the microscope are represented as pixels with a certain fluorescent signal. Each pixel in the image represents a certain area at the µm scale. For quantitative analysis, the first step is the to stablish a threshold in which all values below the threshold are considered noise (Azeredo et al., 2017). For thresholding, the images in grey scale format are transformed to binary scale, where $p(i, j) = 0$ or 1. A pixel with a $p(i, j) = 1$ is considered background (void), while a pixel with a $p(i, j) = 0$ is considered a cluster (e.g., bacteria, EPS, PAC)(Lewandowski et al., 1999). Thresholding is a subjective process where the user attempts to represent a distinction between the void space and the biomass (X. Yang et al., 2000). However, automatic thresholding methods have been developed to allow the user to remove the bias caused by manual thresholding. A popular method is Otsu's method. This algorithm determines the thresholds in the images that minimizes the intra-class intensity variance.

Various parameters can be used to quantitatively describe biofilms (e.g., biovolume, biomass, biofilm thickness, roughness coefficient) (Azeredo et al., 2017). Biomass ($\mu m^3/\mu m^2$) is the amount of biologic material on a given sample. This is an expression of

how much of the image stack is covered by a biofilm (pixels). Thickness (μm) is the distance at which biofilm clusters rise from the surface. Usually, biofilms colonizing on surface are not homogeneous. Thus, thickness distribution, local thickness, and average can be obtained to correctly describe a biofilm growing on a rough surface. Average thickness is also used to calculate other biofilm parameters, such as the fractal dimension.

As mentioned previously, biofilms are heterogeneous structures, thus the fractal dimension or roughness coefficient helps to describe the degree of uniformity of the biofilms. The higher the roughness coefficient, the more heterogeneous the biofilm is (Yang et al., 2000). The determination of these parameters allows for information related to the stage of biofilm development, composition, and architecture to be assembled.

CHAPTER 3

MATERIALS AND METHODS

This chapter describes the materials and methods used to characterize an anaerobic biofilm growing on powdered activated carbon (PAC) and determine its influence on the sorption of an organic compound to the PAC. Toluene was used as the model PHC in this work. The experimental design was divided into three phases.

In Phase 1 the baseline sorption characteristics of toluene to a commercial PAC was evaluated by collecting sorption/desorption isotherm data. The primary objective of this phase was to investigate the sorption properties of a model PHC to fresh PAC in an aqueous matrix and to generate baseline performance data to be compared to an aged PAC (with a biofilm attached - Phase 3). Adsorption in the liquid phase is influenced by factors such as pH, temperature, properties of the adsorbate such as its solubility in the solvent, concentration, the chemical composition of the solvent and the properties of the adsorbent (Canzano et al., 2014; Hindarso et al., 2001; Yakout & Daifullah, 2014). The bottle-point method was used to investigate the equilibrium sorption capacity of aqueous phase toluene (initial concentration 1 to 30 mg/L) to fresh PAC at pH 7. Aqueous and solid phase (PAC) analytical data were collected.

In Phase 2 an anaerobic toluene degrading biofilm attached to PAC in bench-scale microcosms was established. The objective of this phase was to assess the colonization and growth of a toluene degrading enrichment culture on PAC under anaerobic conditions to obtain a final product state (bio-coated PAC) that could be used in the Phase 3 sorption experiments. An established microbial culture was used to explore the role that a biofilm could potentially have on the sorption of PHCs to PAC used in CBI systems. Thus, several conditions were required including: (1) an anaerobic culture since oxygen is often depleted

in PHC impacted systems, (2) the culture had to be capable to readily metabolize toluene with degradation rates known to be relatively fast, and (3) the culture could be used in bioaugmentation efforts. The microbial activity in these microcosms systems was monitored by gas production (CO_2 and CH_4) and toluene depletion. The microbial community attached to the PAC was examined by Confocal Laser Scanning Microscopy (CLSM). To quantify specific parameters of biofilm growth and to perform 3D reconstructions of PAC particles, images from the bio-coated PAC were processed using the FIJI software coupled with COMSTAT.

In Phase 3 the sorption characteristics of toluene to the biofilm-coated PAC was evaluated by collecting sorption isotherm data. The objective of this phase was to assess the impact of a biofilm attached to PAC on the sorption characteristics of toluene, and compare these data to those collected in Phase 1 using fresh PAC. Batch sorption experiments were performed using biofilm-coated PAC samples obtained from the microcosm experiment at two time points (Day 80 and Day 180).

3.1 MATERIALS

The sorbent material used in all the experimental work was a coconut-based PAC product (WPC®, < 325 US mesh) obtained from Calgon Carbon Corporation (Pittsburg, PA, USA). Toluene was analytical grade from Sigma-Aldrich (San Luis, MO, USA) with purity >99%. High purity water used for all solutions was obtained from a Millipore Milli-Q® water system.

An artificial groundwater (AGW) solution (Table 3.1) was used in the experiments (see Appendix 1 for a detailed recipe for the AGW modified from Middeldorp et al. (1998)). For all tests, the pH of the AGW was maintained at 7. The AGW prepared for these microcosms experiments used ferrous sulfide (FeS) as a reducing agent. FeS forms a black precipitate

that settles, and therefore only the AGW supernatant was used as the liquid medium for these microcosms.

Table 3.1. Chemicals used for the AGW solution.

Salt solution	[d]NH_4Cl, [e]$MgCl_2$, [e]$MnCl_2$ $4H_2O$, [d]NaCl, [d]$CaCl_2$, [c]Na_2HPO_4 $2H_2O$, [c]KH_2PO_4, [b]Na_2SO_4, [e]$NaHCO_3$.
Trace mineral stock solution	[e]H_3BO_3, [a]$ZnCl_2$, [a]$NiCl_2$ - $6H_2O$, [e]$MnCl_2$ - $4H_2O$, [a]$CuCl_2$ - $2H_2O$, [e]$CoCl_2$ - $6H_2O$, [a]Na_2SeO_3, [e]$Al_2(SO_4)_3$ - $16H_2O$, [e]H_2SO_4.
Amorphous ferrous sulfide solution	[e]$(NH_4)_2Fe(SO_4)_2$ - $6H_2O$, [e]Na_2S - $9H_2O$
Redox indicator stock solution	[e]$C_{12}H_7NO_4$
Phosphate buffer stock solution	[e]KH_2PO_4, [c]K_2HPO_4

[a] Alfa Aesar (Ward Hill, MA, USA)

[b] Anachemia Canada Inc. (Motreal, Canada)

[c] Fisher scientific (Hampton, NH, USA)

[d] Merck KGaA (Darmstadt, Germany)

[e] Sigma-Aldrich (San Luis, MO, USA)

The cell culture used in this work was a methanogenic toluene-degrading enrichment culture (DGG-T), maintained by the University of Toronto and described by Edwards & Grbic-Galic (1994), Ficker et al. (1999), and Washer & Edwards (2007). The DGG-T culture is a well-established methanogenic mixed culture that was enriched from creosote-contaminated aquifer sediments and has been maintained on toluene as the sole carbon source and electron donor for three decades. This consortium is composed of bacterial (hydrolytic fermentative bacteria and syntrophic acetogenic bacteria) and archaeal species (methanogenic archaea) (Ficker et al., 1999). Originally the culture was maintained in an anaerobic mineral salt medium reduced with ferrous sulfide (FeS).

Crimp top Mininert® valves obtained from Sigma-Aldrich (San Luis, MO, USA) were used to cap the microcosms and to allow repeated sampling. Dichloromethane (DCM) was obtained from Sigma-Aldrich (San Luis, MO, USA) and contained internal standards (m-fluorotoluene and 2-fluorobiphenyl (25 mg/L), Sigma-Aldrich; San Luis, MO, USA). For the staining procedure, fluorescent stains SYTO®9 (Invitrogen™; Carlsbad, CA, USA) and Concanavalin A, Alexa Fluor 633™ Conjugate (Invitrogen™; Carlsbad, CA, USA) were obtained from Thermo-Fisher Scientific (Waltham, MA, USA).

3.2 METHODS

This section provides a description of the experimental design of the isotherm and microcosms experiments, and the general sample preparation and handling involved in each experimental phase. Analyses were conducted in triplicate bottles. While each experimental phase is detailed below, detailed protocols are contained in Appendix 1.

3.2.1 SORPTION/DESORPTION EXPERIMENTS

Sorption isotherms and single-step desorption experiments were evaluated by using the bottle point method and 160 mL serum bottles (Wheaton® borosilicate glass, DWK life Sciences; Millville, NJ, USA). For the experimental set-up (Figure 3.1), each bottle was amended with 10 mg (dry weight, dw) of PAC. A toluene stock solution (30 mg/L) was prepared by adding the required amount of pure toluene (250 µL) to the AGW in a 4 L glass vessel (Kimax ™, Fisher Scientific; Hampton, NH, USA) with no headspace. The vessel was sealed with a Teflon® covered septa and stirred for 24 hrs. To generate data for a sorption isotherm of toluene to PAC, seven initial concentrations of toluene (from 1 to 30 mg/L) were prepared in a 2 L glass conical separatory funnel (Pyrex® borosilicate glass, Sigma-Aldrich; San Luis, MO, USA) by diluting the toluene stock solution with fresh AGW. Aliquots from

each initial concentration were then dispensed into a 160 mL serum bottle contained the PAC. Each bottle was filled without headspace and sealed using Teflon® lined silicone septa and crimped with aluminum seals. Control bottles with the same initial concentration but without PAC were also constructed. Triplicates bottles for each initial toluene concentration were assembled.

Figure 3.1. Isotherm experimental set-up, (a) shows the 4 L vessel with toluene stock solution and (b) shows the 160 mL control and PAC bottles used in the bottle point experiments.

The bottles were shaken on a platform shaker for 24 hrs. Previous sorption studies for the PAC and toluene system showed that equilibration time occurred within 1 hr. (Marrocco et al., 2019). Following agitation, the bottles were left undisturbed for 24 hrs so that the PAC could settle. For the sorption experiment bottles, both the aqueous and solid phase were sampled. For aqueous phase sampling, a 19 mL aliquot was removed using a 20 mL glass syringe (Gastight® PTFE luer lock, Hamilton Co.; Reno, CA, USA), placed in a 20 mL glass vial

(KIMBLE® borosilicate glass, DWK life Sciences; Millville, NJ, USA) and extracted by aqueous phase solvent extraction. For solid phase sampling, the remaining aqueous phase was discarded, and solid phase solvent extraction was directly performed on the remaining PAC in the bottle. Following extraction, the DCM was analyzed to estimate the residual toluene concentration in the aqueous phase, and the mass sorbed to the PAC.

For the single-step desorption experiments, after the first 48 hrs. which was assumed to be equilibrium, the aqueous phase was removed and discarded leaving the just the PAC. The bottles were refilled without headspace using fresh AGW solution, sealed using Teflon® lined silicone septa and crimped with aluminum seals. The bottles were shaken on a platform shaker for 24 hrs. Following agitation, the bottles were left undisturbed for 24 hr. so that PAC could settle. Then, the aqueous and solid phases were sampled, extracted and analyzed in the same fashion as in the sorption experiments.

3.2.2 MICROCOSM EXPERIMENT

The microcosm experiment (Phase 2) was designed with the objective to develop a biofilm attached to the PAC (bio-coated PAC) reflective of an aged CBI system. The microcosms were constructed using 22 mL glass serum bottles (Wheaton® borosilicate glass, DWK Life Sciences; Millville, NJ, USA) and sealed with Mininert® valves to allow for repeated sampling. A total of 83 microcosms were constructed (see Table 3.2). For the active treatment (AT) series (for the biofilm-PAC system, 69 microcosms), each bottle was filled with 9 mL of AGW supernatant, 1 mL of culture, 10 mg (dw) PAC, and 1 µL neat toluene. The killed PAC controls (KP) were assembled in a similar fashion as the active treatment but with autoclaved culture (30 min at 121ºC for three consecutive days) to account for abiotic degradation (3 microcosms). Starved control microcosms (SC) were constructed similar to the active treatment microcosms but without the addition of toluene to account for background methane production (3 microcosms). Active controls microcosms (AC) (for a

planktonic cell system, 3 microcosms) were filled with 9 mL of the AGW supernatant, 1 mL of culture and 1 µL neat toluene. Finally, the killed control microcosms (KC) were assembled similar to the active controls but with autoclaved culture (30 min at 121ºC for three consecutive days) to account for abiotic degradation (3 microcosms). Resazurin control microcosms (2 microcosms) were constructed with the redox indicator (resazurin) added to the AGW supernatant and without PAC to visually monitor for oxygen presence in the microcosm systems. The reason for including a redox indicator in these separate microcosms was to ensure that the AGW was anaerobic and to quickly visualize (resazurin changes from clear to pink when oxygen is present) any oxygen input that could occur to the microcosms during the experiment. Note that the anaerobic chamber has oxygen input when bringing materials inside. Also, PAC was not added in these bottles since in previous experiments (data not shown) it was observed that resazurin sorbed to the PAC, so any change in color due to oxygen input would not have been observed. A representative image of a microcosm from each series is shown in Figure 3.1(a).

Prior to microcosm construction, all glassware items were washed with Extran® 300 detergent (Merck KgaA; Darmstadt, Germany), rinsed with deionized (DI) water and autoclaved prior to use. Non-autoclavable items were washed with detergent, rinsed with DI water and disinfected with 70% ethanol solution prior to use. All materials were stored in an anaerobic chamber (COY Laboratory Products Inc.; Grass Lake, MI, USA) for a week to remove residual oxygen (Figure 3.1(b)). The construction, incubation and sampling of the microcosms was performed inside the anaerobic chamber to ensure that anaerobic conditions were maintained. The microcosms were stored at room temperature in a semi-inverted position in the dark (covered with foil), and undisturbed (gently shaken once every two weeks). Three microcosms (3) from each series; active treatment, active control, killed PAC control, killed control and starved control were repeatedly sampled (Day 1, 14, 28, 30, 47, 62, 78, 82, 111, 114, 126, 140, 150 and 175) to monitor toluene degradation and gas production (CH_4 and CO_2).

Figure 3.2. (a) Representative microcosm bottle for each system inside the anaerobic chamber and (b) anaerobic chamber used.

Prior each sampling event, the Mininert valve was wiped with an alcohol wipe. To assess microbial activity, a 1 mL aliquot of the microcosm gas phase (headspace) was removed using a 10 mL glass syringe (Micro-Mate®, Popper & Sons Inc.; New Hyde Park, NY, USA) to which a two-way stop valve was added and analyzed for CO_2 and CH_4. A 200 µL aliquot of the aqueous phase was removed using a 1 mL glass syringe (Gastight®, Hamilton Corporation; Reno, CA, USA) and analyzed for the concentration of toluene. Based on the concentration of toluene observed, additional spikes of neat toluene (0.77 ± 0.29 µL) were added to sustain microbial growth.

Table 3.2. Microcosm experimental design.

Series	PAC	Toluene	No. microcosm
Active treatment (AT)	amended	amended	69[1]
Active control (AC)	-	amended	3
Killed PAC control (KP)	amended	amended	3
Killed control (KC)	-	amended	3
Starved control (SC)	amended	-	3

[1] AT microcosms breakdown:
3 sampled repeatedly for toluene and CH_4/CO_2
12 sampled for PAC solvent extraction
15 used for 80-Day bio-coated PAC isotherm
21 used for 180-Day bio-coated PAC isotherm
12 used to examine biofilm formation at time points 50, 80, 140 and 180
3 used for cell density enumeration
3 left for additional sampling

The pH, oxidation-reduction potential (ORP) and dissolved oxygen (DO) were measured in the AGW prior to microcosm setup, as well as in aliquots of the microcosm supernatant at various time points (Day 50, 80, 140 and 180). A 2 mL aliquot of the aqueous phase from the microcosms was removed using a 3 mL glass syringe (Gastight®, Hamilton Corporation; Reno, CA, USA) and transferred to a 5 mL plastic vial for analysis. pH was measured using an Oakton pH 50S pH meter (Oakton Instruments; Vernon Hills, IL, USA). ORP was measured using an Orion™ Star A325 meter (Thermo Scientific; Waltham, MA, USA). DO was measured using an Orion™ 5Star- 083005MD DO probe (Thermo Scientific; Waltham, MA, USA).

The presence, growth and organization of a biofilm on PAC was examined by CLSM at various time points (Day 50, 80, 140 and 180). The PAC from a AT microcosm was transferred to a 2 mL plastic microcentrifuge tube (Eppendorf®; Hamburg, Germany) and washed with a 150 mM NaCl solution (washing solution). After washing, the sample was stained with a 30 µM of fluorescent dye SYTO®9 for 30 min in the dark. The residual stain was washed with the washing solution before a 200 mg/mL solution of Concanavalin A, Alexa Fluor 633™ Conjugate was added and incubated in the dark for additional 30 min.

Then the residual stain was removed with the washing solution and the samples were mounted on microscope slides and examined under a confocal microscope (LSM 700, Carl Zeiss; Oberkochen, Germany) the same day. A representative image of the confocal microscope is shown in Figure 3.3.

Samples of fresh PAC without microbial culture contact were stained in the same fashion as the active treatment microcosms to detect any signal coming from PAC-stain interactions. Samples of fresh PAC without stain or microbial culture interaction were used to determine if PAC alone had autofluorescence, and to determine and differentiate true biomass from any fluorescent signal coming from PAC.

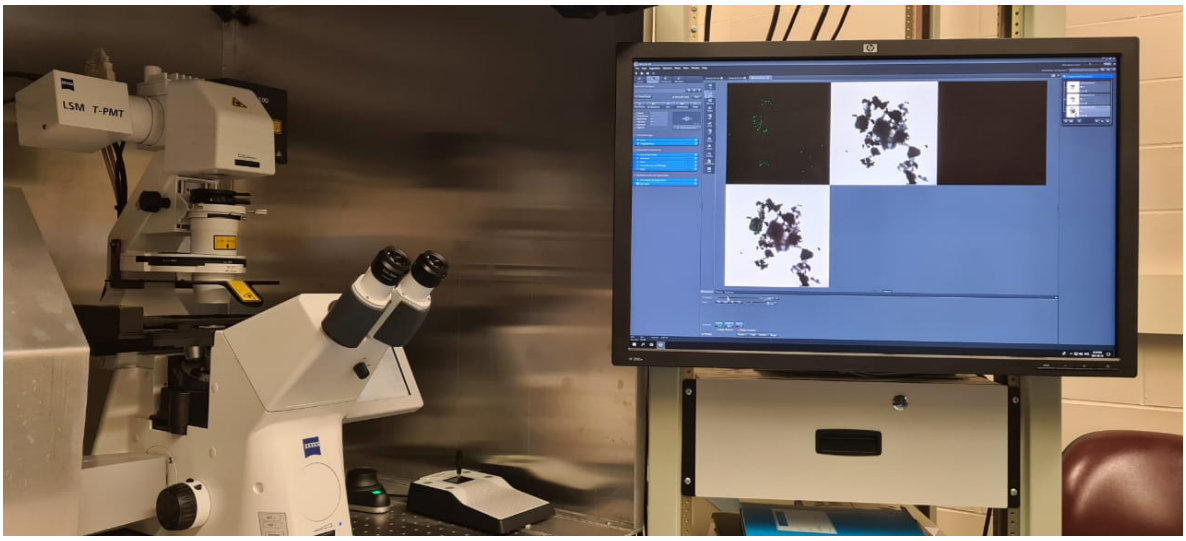

Figure 3.3. LSM 700 confocal microscope using for scanning PAC samples.

SYTO®9 is a highly selective nucleic acid stain and it was used to label microbial cells. Concanavalin A (Con A) is a lectin that binds to polysaccharides (α-D-glucose and α-D-mannose) and it was used to label the EPS (see Appendix 1a for a detailed description on the steps followed to stain the PAC samples). The use of different dyes allowed for the different components of the biofilm (cells and EPS) to be observed.

The biomass density from the bio-coated PAC was determined by a manual cell counting method. First, the biofilm was detached from the PAC with a method modified from Saccani et al. (2014) (refer to Appendix 1 for details), then 1 mL of the homogenized sample (after detachment) was stained with SYTO®9 to a final concentration of 15 µM in a 2 mL plastic microcentrifuge tube (Eppendorf®; Hamburg, Germany) in the dark for 30 minutes. Then, the sample was centrifuged (5417R-Centrifuge, Eppendorf®; Hamburg, Germany) at 6000 x g for 30 min to obtain a cell pellet. The supernatant was discarded, and the cell pellet was resuspended in 100 µL of a 150 mM NaCl solution. Then, 10 µL of the sample was placed on a microscope slide. The samples were observed under the CLMS, and single images were acquired from five different random positions per sample. Cells were counted using the automated cell counter available in the FIJI software, and the average cell count was used to estimate the total cells. Values are reported as the number of cells per gram of PAC.

3.2.3 BIO-COATED PAC SORPTION EXPERIMENTS

The "bio-coated PAC" from the active treatment microcosms was used to perform sorption experiments for Phase 3. Before its use, the microcosms were starved for a couple of weeks to decrease the system toluene concentration. The remaining mass of toluene sorbed on PAC was determined. Sorption experiments using the bio-coated PAC were performed on Day 80 and Day 180. For the Day 80 isotherm, five initial toluene concentrations (from 1 to 30 mg/L) were prepared by diluting the toluene stock solution in fresh AGW solution, while for the Day 180 isotherm seven initial toluene concentrations were (from 1 to 30 mg/L) used.

Adsorption isotherms were evaluated (by bottle point experiments in 160 mL serum bottles), sampled and analyzed in a similar fashion as in Phase 1 (Figure 3.4). However, the bio-coated PAC from each of the selected active treatment microcosms (10 mg PAC, dw) was transferred into different serum bottles before filling the bottles with different initial

toluene concentration solutions. As in Phase 1, control bottles with the same initial toluene concentration but without bio-coated PAC were constructed. Triplicates bottles for each initial toluene concentration were assembled. The aqueous and solid phase was sampled after 48 hrs. which was assumed to be equilibrium. The residual toluene concentration in the aqueous phase and the mass sorbed to the bio-coated PAC were determined.

Figure 3.4. Isotherm experimental set-up, 160 mL serum bottles on a platform shaker.

3.3 ANALYSES

3.3.1 TOLUENE

3.3.1.1 AQUEOUS PHASE

The aliquot collected from the batch sorption bottle was transferred to a 20 mL glass vial while the aliquot collected from the microcosm bottle was transferred into a 2 mL glass autosampler vial (Agilent; Santa Clara, CA, USA) (Figure 3.5). The vials were preloaded with 1 mL of dichloromethane containing internal standards (m-fluorotoluene and 2-fluorobiphenyl (25 mg/L)) and capped with Teflon® lined silicone septa and plastic screw caps.

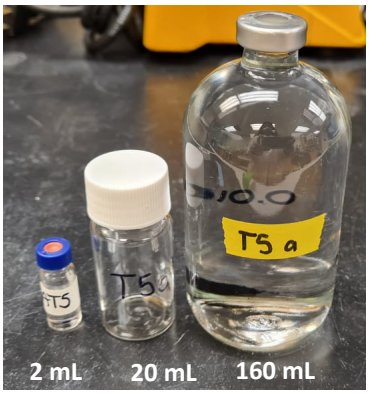

Figure 3.5. Vials (2 mL and 20 mL) used for the aqueous phase extractions, and the 160 mL serum bottle used in bottle point experiments.

The vials were placed in a horizontal position on a platform shaker, and then agitated at 250 rpm for 15 mins. Then the vials were inverted in a vertical position, and the water-solvent phases were allowed to separate for 20 mins. For the sorption experiment samples, the bottom phase (the extract) corresponding to dichloromethane phase was removed with a 1 mL glass syringe (Gastight® LTN, Hamilton Corporation; Reno, CA, USA) and transferred into 2 mL glass autosampler vials. For the microcosms experiment samples, the top phase

(water) was removed and discarded leaving just the dichloromethane phase in the vial. Analysis of the dichloromethane was performed by gas chromatography (GC-FID).

3.3.1.2 SOLID PHASE

To extract the mass of toluene sorbed to the PAC, 1 mL of dichloromethane containing internal standards (m-fluorotoluene and 2-fluorobiphenyl (25 mg/L)) was added to the bottles in which the PAC sample was left (after removing the aqueous phase from the bottle), then the bottles were sealed using Teflon® lined silicone septa and aluminum seals. The bottles were placed vertically on a platform shaker and agitated at 25 rpm for 2 hrs. Following shaking, the bottles were allowed to equilibrate for 24 hrs. before the dichloromethane phase (~0.7 mL) (Figure 3.6) was recovered using a 1 mL glass syringe (Gastight® LTN, Hamilton Corporation; Reno, CA, USA) and placed in a 2 mL autosampler vial. Analysis of the dichloromethane was performed by GC-FID.

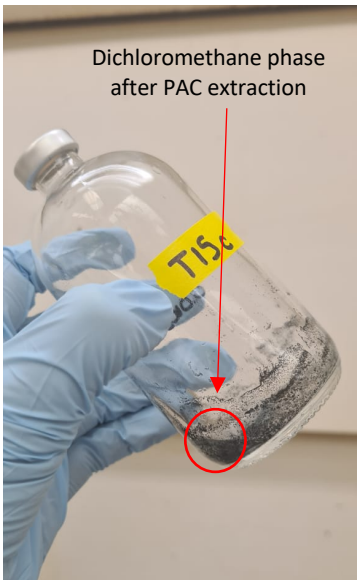

Figure 3.6. Dichloromethane phase after solid phase extraction in a 160 mL serum bottle.

3.3.2 GC-FID ANALYSES

A 3 µL aliquot of dichloromethane sample from extractions was injected into a GC equipped with a FID (GC-7890A, Agilent; Santa Clara, CA, USA). A glass DB5 capillary column (0.25 mm diameter x 30 m length, with a stationary phase film 0.25 µm thick) was used. The GC was run in spitless mode (purge on 0.5 min, purge off 10 min), with a column flow rate of 1 mL/min using helium as the carrier gas. The chromatographic conditions were: 275 ºC in the injection port, the temperature programming was an initial of 35ºC for 0.5 min, then a heating rate of 15ºC/min until a final temperature of 300ºC maintained for 2 min. The method detection limit (MDL) based on an extraction ratio (sample: dichloromethane) 0.2:1 mL is 285 µg/L and 5 µg/L based on a 19:1 mL extraction ratio.

3.3.2 GAS ANALYSES

Gas samples collected from the microcosm headspace were manually injected into a Greenhouse and Atmospheric Gas Analyzer (GC-2014, Shimadzu; Kyoto, Japan). The injection port was set at 100ºC, the column temperature was set at 80ºC and the FID detector at 250ºC, with an equilibration time of 0.5 min. The approximate retention time was 4.9 min for CH_4 and 7.6 min for CO_2. The method detection limit (MDL) for CH_4 was 0.38 mg/L and for CO_2 was 17.15 mg/L.

3.2.5 IMAGE ACQUISITION – CLSM

Images of fluorescently labeled samples were acquired using a LSM 700 (Carl Zeiss, Oberkochen, Germany) with a 63x 1.4 Numerical Aperture (NA) objective lens. The laser lines used for the excitation of the fluorophores were 488 and 633 nm, with a laser intensity of 2.0%. Images were recorded at an excitation/emission wavelength of 488/498 nm for

SYTO®9 and was assigned the colour green, and 633/647 nm for Con A and was assigned the colour red. The PAC was visualized using transmitted light. Images were acquired using the three channels simultaneously in separate tracks to avoid signal overlap. Image resolution was 1028 X 1028 pixels. Images were acquired at five different random locations per sample and never twice from the same area to prevent negative effects of the laser on the biofilm sample. Z-stacking imaging method (in which multiple images are taken at different focal distances to provide a composite image) was used to capture images over the visible top half of the particles by vertical sectioning through the biofilm with z-step increments of 0.5 µm. The microscope settings were constant for all images acquired to reduce bias. Table 3.3 summarizes the parameters used to acquire all images.

Table 3.3. Microscope settings for image acquisition.

Fluorophore	[4]Ex/Em wavelength	Filter	Laser line (nm)	Beam splitter	Target
SYTO®9	488/498 nm	[1]BP	488	[3]MBS	Cells
Con A, Alexa Fluor 633 ™ Conjugate	633/647 nm	[2]LP	633	[3]MBS	EPS

[1]BP: Band Pass
[2]LP: Long Pass
[3]MBS: Mean beam splitter
[4]Ex/Em: Excitation/Emission

3.2.6 IMAGE ANALYSIS – FIJI (ImageJ)

The images obtained were analyzed using FIJI software (ImageJ, Wayne Rasband National Institutes of Health) with the COMSTAT plug-in. First, all the images acquired were processed using a median filter to remove salt and pepper noise by applying a despeckle function. Next, each image was converted to grey scale in tagged image file format (TIFF) using the Bio-Format exporter function in ImageJ. Then, the images were uploaded to the COMSTAT plugin. COMSTAT processed each image by implementing a binary system based

on setting a threshold value on the pixel intensity of the images using the Otsu's method (automated image thresholding). The parameters selected for analysis were biovolume, biomass, thickness, and roughness coefficient.

The biovolume is the volume of the biofilm components given in μm^3. To estimate the biovolume, the number of biofilm pixels (given by COMSTAT) in the image was multiplied by the voxel size (given by COMSTAT) as given by

$$biovolume = \sum biofilm\ pixels * voxel\ size \tag{3.1}$$

A voxel is the 3-D analog of a pixel and is related to the pixel size (length and width) and slice thickness (vertical sectioning of the biofilm, thickness). Biovolume can be used to estimate the cell density of the biofilm based on average cell measurements.

Biomass is a standardized measurement used to compare the amount of any living material covering different substrates or locations. For image analysis it is given in units of volume per unit surface area ($\mu m^3/\mu m^2$). Biomass is an estimation of the amount of biofilm formation attached to the PAC as defined by

$$biomass = \frac{biovolume}{\frac{C^2}{\frac{\pi}{2}}} \tag{3.2}$$

where PAC surface area was estimated using the measured the circumference of the particle (*C*).

The thickness (average thickness) is an indicative of the general architecture of the biofilm and was calculated by COMSTAT using

$$Thickness = \frac{\sum value\ (pixels)}{\sum pixels \neq 0} \tag{3.3}$$

Where value (pixels) is the pixel height multiplied by the number of slices in the column counted as biomass. In the binary image the algorithm looks from the top to the bottom of the image stack and locates the highest point above each pixel in the bottom layer containing biomass. The number pixels counted as biomass in the same column are multiplied by the height of the slice. All the values obtained from above calculations are stored. Then the average of the heights of all pixel columns is calculated. It ignores pores and voids inside the biofilm.

The roughness coefficient provides a measure of how much the thickness of the biofilm varies with respect of its average and is a measure of heterogeneity, the smaller the value, the greater uniformity of the biofilm. The roughness coefficient was estimated by COMSTAT using

$$Roughness = \frac{1}{n_{spots} \times thickness} \sum_{i=1}^{slices} spots\,[i]\; x\; (thickness\,[i] - thickness) \qquad (3.4)$$

Where n_{spots} is the total number of spots found with biomass, thickness refers to the average thickness from Equation 3.3, spots [i] contains the spots found on slice i, thickness [i] contain the thickness defined by slice i.

To obtain 3D impressions of the structures of interest, the maximum intensity *Z*-projection function in ImageJ was used. This function applies a mathematical algorithm to remove the out of focus information, so that sharper images can be produced. To obtain 3D reconstructions from the image stacks, the 3D volume viewer plugin was used. First, the image stacks (8-bit) were transformed to RGB stacks and then uploaded to the 3D volume viewer plugin as a volume with a 3D-(xyz)-space. The viewing angle of the images was adjusted to rotate and visualize the particles from different angles. By capturing several images from different angle views, it was possible to create rotating animations of the particles.

3.2.7 DATA AND STATISTICAL ANALYSIS

For the statistical analysis of the experimental data the OriginPro® software version 2021 (Origin-Lab Corporation; Northampton, MA, USA) was used.

Sorption experimental data were fit to the Freundlich model using IsoFit (Mattot, 2007). The K_f and n_f model parameter values, standard errors and 95% confidence intervals were determined.

Microcosm experimental data (e.g., toluene and methane) from the AC, KC and KP microcosms was corrected for sampling loses at each sampling time point (see Appendix 2 for list of steps used), then toluene degradation and methane production was evaluated. In the AT microcosms the methane produced was used as a proxy for methanogenic toluene biodegradation by

$$C_7H_8 + 7.102\ H_2O + 0.072\ NH_4^+ \rightarrow 2.318\ HCO_3^- + 4.32\ CH_4 + 2.39\ H^+ + 0.072\ C_5H_7O_2N \quad (3.5)$$

to determine the mass of toluene degraded.

The mass of toluene in the AT microcosm system was estimated by

$$M_s = M'_{sp} - M_d \quad (3.6)$$

where M_s is the mass of toluene in the system (at that current time point) in mg, M'_{sp} is the mass of toluene (mg) in the system in the previous sampling point (after correcting from sampling losses) and M_d is the mass of toluene degraded over that time interval (from previous sampling point to the current time point). The mass of toluene sorbed to the PAC (M_{PAC}) was then estimated based by mass balance as given by

$$M_s = M_w + M_g + M_{PAC} \quad (3.7)$$

where M_s in the mass of toluene in the system in mg, M_w is the mass of toluene in the aqueous phase, M_g is the mass of toluene in the gas phase and M_{PAC} is the mass of toluene sorbed to PAC in mg.

The mass sorbed to PAC was also estimated from

$$M_{PAC} = m_{PAC} K_f C_w^{n_f} \quad (3.8)$$

where M_{PAC} is the mass of toluene sorbed to PAC (mg), m_{PAC} is the mass of PAC (dw) in g, K_f and n_f are the Freundlich parameters and C_w is the concentration of toluene in the aqueous phase (mg/L). The Freundlich parameters obtained from the model best fit for in Fresh PAC and bio-coated PAC at Day 80 and 180 were used.
At four time points (Day 62, 78, 149 and 175), PAC solid phase solvent extraction was performed to determine the mass sorbed to PAC (observed).

The concentration of toluene sorbed to PAC is given by

$$C_{PAC} = \frac{M_{PAC}}{m_{PAC}} \quad (3.9)$$

Where C_{PAC} is the concentration of toluene sorbed to PAC in mg/g, m_{PAC} is the mass of PAC (dw) in g, and M_{PAC} is the mass of toluene sorbed to PAC (mg).

The quantitative biofilm experimental data were analyzed statistically using the non-parametric two-tailed Mann-Whitney-U-test to compare two independent groups of data. The significance level was set at p = 0.05 (95% confidence level) to determine whether there were significant differences in the parameters (biovolume, biomass, thickness, and roughness) analyzed at different time points of biofilm growth.

CHAPTER 4

RESULTS AND DISCUSSION

As described in Chapter 3, this research was conducted in three sequential phases. Figure 4.1 shows the 180-day experimental timeline including the sampling and characterization events performed during the course of this research.

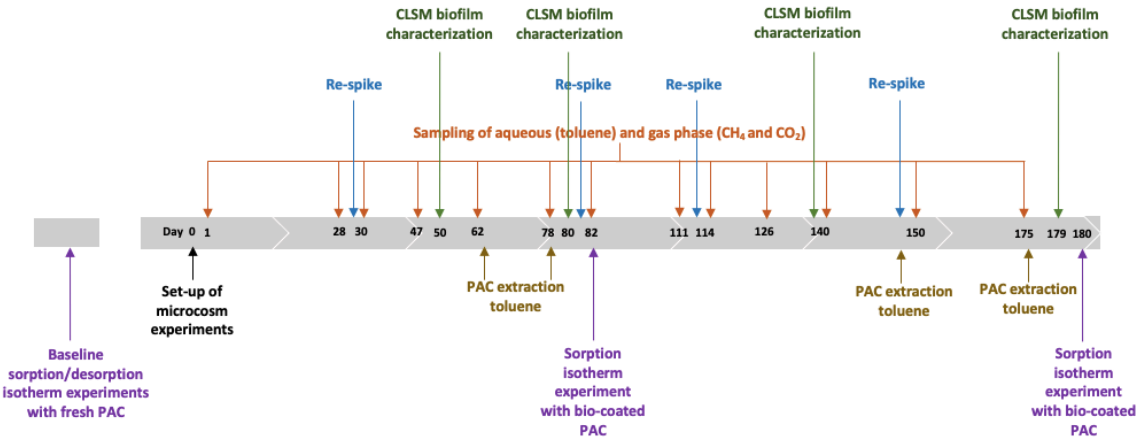

Figure 4.1. Experimental research timeline. The microcosm set-up was selected as Day 0.

4.1 BATCH SORPTION EXPERIMENTS WITH FRESH PAC

It has been demonstrated that the Freundlich isotherm represents the adsorption of aqueous PHCs to PAC, and is given by:

$$q_e = K_f {C_e}^{n_f} \quad (4.1)$$

where q_e is the equilibrium mass of sorbate per gram of sorbent (mg/g), K_f ((mg/g)(L/mg)^n) and n_f (dimensionless) are the Freundlich parameters indicating sorption capacity and intensity respectively, and C_e is the equilibrium aqueous phase sorbate concentration in mg/L. The Freundlich model assumes a heterogeneous surface of the sorbent material, where the adsorption capacity is strongly influenced by the concentration of the adsorbate in the solution under equilibrium conditions (Canzano et al., 2014; Dada et al., 2012). The Freundlich parameter (K_f) is indicative of sorption capacity, and compounds with K_f values > 10 (mg/g)(L/mg)^n can be considered to be well removed by AC (Summers et al., 2010).

Figure 4.2 represents the sorption isotherm data for toluene on fresh PAC. The data show that the adsorption capacity steepens rapidly at low concentrations indicating readily abundant and accessible sorption sites on the PAC surfaces. However, as the toluene concentration increases, the isotherm becomes asymptotic indicating that available sorption sites are saturated by the increased number of adsorbate molecules.

The adsorption equilibrium data generated in the bottle-point experiments were fit to the Freundlich model using IsoFit (Mattot, 2007). The estimated model parameters along with their 95% confidence intervals (CI) are listed in Table 4.1. The K_f value obtained (79.8 (mg/g)(L/mg)$^{0.35}$) indicates a good affinity of PAC for toluene. This is not surprising given the hydrophobicity of toluene (log K_{ow} 2.69) and its molecular configuration, as well as the high surface area of the WPC ® PAC (89% of the pore volume are micropores (Liu, 2017)). The Freundlich exponent n_f represents the adsorption intensity, and indicates how favorable the adsorption process is with values of n_f < 1 denoting favorable adsorption (Bandosz, 2006). In addition, a lower n_f value indicates greater sorption capacity at low aqueous concentrations as noted above. The n_f value obtained (0.35) indicates that sorption of toluene to fresh PAC was favorable. The detailed data from the experiments (aqueous and solid phase concentrations) can be found on Appendix 2. A mass balance analysis using the aqueous and solid phase concentrations indicated that < 3% of the toluene mass was

unaccounted. This suggest that the generated model parameters are reliable for use in Phase 3.

Table 4.1. Freundlich sorption model parameters and 95% confidence interval (CI) for toluene/PAC system.

Parameter	Value	CI
K_f [(mg/g)(L/mg)^n]	79.8	67.3 – 92.2
n_f	0.35	0.29 – 0.42
R^2	0.98	

A similar observation was reported by Zhao et al. (1999) who evaluated the adsorption characteristics of toluene to fresh GAC and obtained a K_f of 79.3 ± 3.3 and n_f of 0.37 ± 0.03. Voice et al. (1992) obtained a K_f value of 83 and n_f value of 0.44 for toluene sorption to fresh GAC. Chatzopoulos et al. (1993) determined a K_f of 88.5 and n_f of 0.27 for equilibrium toluene concentrations between 0.7 and 50 mg/L on PAC.

To investigate the reversibility of the adsorption process, single step desorption experiments were conducted as discussed in Chapter 3. These desorption data (Figure 4.2) lie slightly above the adsorption data indicating that a fraction of the toluene (68.75 ± 8%) was not desorbed. The toluene mass balance error was < 11%. For reversible adsorption, the sorption and desorption data sets should be statistically similar, indicating similar retention irrespective of the pathway (González-Machado et al., 2018). Hysteresis can occur for a number reasons including: (1) when molecules experience high energy bonding to the carbon surface functional groups (Aktaş & Çeçen, 2007; Klimenko et al., 2002; Yonge et al., 1985); (2) due to presence of molecular oxygen on the AC surface which interacts with functional groups of the adsorbate (e.g. methyl groups) and can result in oxidation reactions promoting irreversible adsorption (Aktaş & Çeçen, 2007; De Jonge et al., 1996; Vinitnantharat et al., 2001); and (3) due to the high surface area of WPC®PAC that allows

multiple contact points between molecules and pore walls, resulting in entrapment of the molecules within the carbon matrix and consequently the blocking of the diffusion network (Aktaş & Çeçen, 2007; Bandosz, 2006; Bansal & Goyal, 2005; Fan et al., 2017; Yakout & Daifullah, 2014; Yonge et al., 1985).

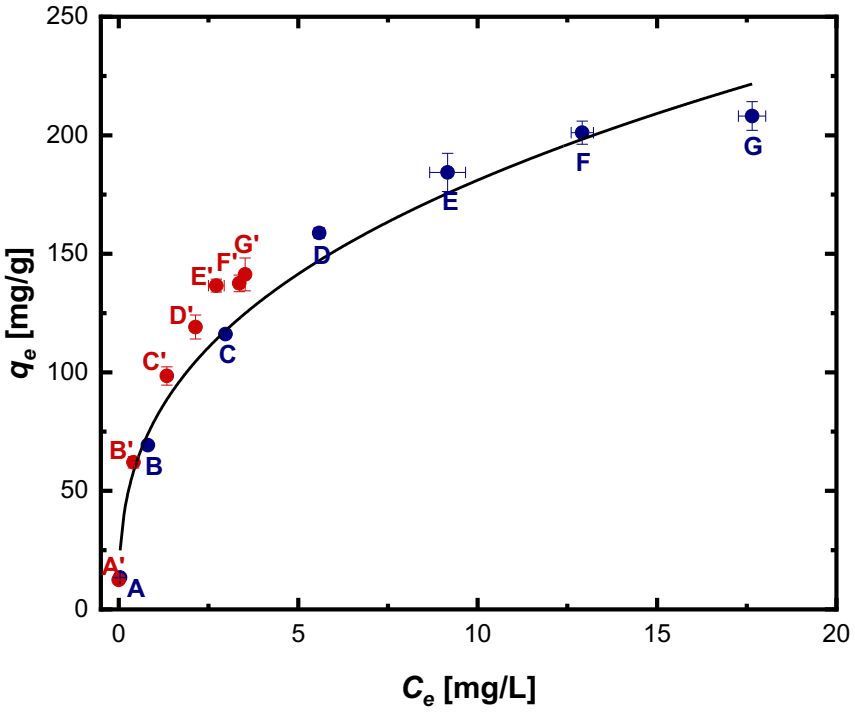

Figure 4.2. Sorption (●) and desorption (●) equilibrium data for toluene on fresh PAC. The symbols are the actual data points, while the solid line represents the least-squares fit for Eq (4.1). The connected sorption-desorption data are indicated by A-A', B-B', C-C', D-D', E-E', F-F', and G-G'. Error bars represent the standard deviation of triplicate bottles.

Yakout & Daifullah (2014) reported that about 67% of toluene remained sorbed to AC prepared from rice husk following desorption. This suggests strong adsorption of aromatic compounds to AC. In contrast, a study using PAC F300® observed that the extent of hysteresis of toluene was small (5%) suggesting that the adsorption of toluene was highly reversible (Chatzopoulos et al., 1993).

4.2 MICROCOSMS EXPERIMENTS

4.2.1 TOLUENE AND METHANE BEHAVIOR

Toluene and methane mass determined over the 180-day long experimental period are displayed in Figure 4.3. Figure 4.3(a) represents the "active" microcosms that were amended with the live culture, and Figure 4.3(b) represents the "killed" or control microcosms that were amended with autoclaved culture.

All microcosms (except for the SC) were spiked with 7.66 ± 0.3 µmoles/bottle of toluene on Day 0. Variations in mass in the sterile controls are presumed to be related to sampling inconsistencies. In general, the KP microcosms showed minor decreases in toluene, while toluene mass in the KC microcosms was observed to decrease consistently (Figure 4.3b). The KC system is characterized by an aqueous and gas phase, and due to the high volatile nature of toluene (dimensionless Henry's constant of ~0.27) mass partitioned from the aqueous phase to the gas phase and was potentially lost during sampling events or by gas leakage through the Mininert valve. In contrast, the KP system is characterized by three phases, an aqueous, gas and solid (PAC) phase and in this case, toluene was partitioned to a greater extent in the PAC due to the sorption characteristics of PAC for toluene. As a result, the aqueous and gas phase concentrations were less, and thus mass losses due to sampling or gas leakage were lower compared to the KC microcosms.

In both sterile controls (KC and KP), little to no methane was produced (0.003 ± 0.001 µmoles) over the course of the experiment (Figure 4.4). The amended culture in these microcosms was autoclaved for three consecutive days, thus no biological activity was expected. In the starved control (SC), some methane was produced (3.87 ± 1.7 µmoles) and was observed to evolve from Day 0 (Figure 4.3) presumably due to culture decay as no toluene was present.

Toluene degradation was monitored, and microcosms were re-spiked with toluene as required (indicted by the gap in toluene profiles) (Figure 4.3). Between Day 0 and Day 30 a slight toluene loss was observed in the active microcosms (AT: 1.11 ± 0.34 µmoles, AC: 2.01 ± 0.64 µmoles) with similar degradation rates, AT (0.04 ± 0.01 µmoles/ day) and AC (0.07 ± 0.02 µmoles/ day). Over the first 30 days, the AT microcosms produced 4.80 ± 1.50 µmoles of methane and the AC microcosms produced 5.88 ± 2.77 µmoles of methane. Methanogenesis was the degradation pathway occurring in the active microcosms, as methane was detected immediately following experimental setup.

On Day 30, all microcosms (except for the SC) were re-spiked, increasing toluene mass to 10.89 ± 0.79 µmoles/bottle. Biodegradation was evident from this re-spike onwards, as observed by the decrease of toluene and increase of methane. On Day 78, toluene was completely degraded in the AC microcosms (below MDL), whereas in the AT microcosms toluene was not completely degraded (4.37 ± 1.23 µmoles of toluene/bottle remaining) in the system. Between Day 30 and Day 78 degradation rates were 0.12 ± 0.03 µmoles/ day and 0.12 ± 0.04 µmoles/ day in AC and AT microcosms, respectively.

On Day 82, toluene was re-spiked in the AC and AT microcosms increasing toluene mass to 8.56 ± 0.70 µmoles/bottle and 13.09 ± 1.24 µmoles/bottle, respectively. By Day 111 toluene was completely degraded (below MDL) in the AC microcosms, whereas in the AT microcosms 6.73 ± 1.44 µmoles/bottle remained in the system. By Day 111, 20.28 ± 1.3 µmoles of toluene were degraded in the AC microcosms and 14.19 ± 1.44 µmoles were degraded in the AT microcosms (Figure 4.4). Between Day 82 and Day 111, degradation rates of 0.29 ± 0.02 µmoles/ day and 0.22 ± 0.09 µmoles/ day were estimated for the AC and AT microcosms, respectively.

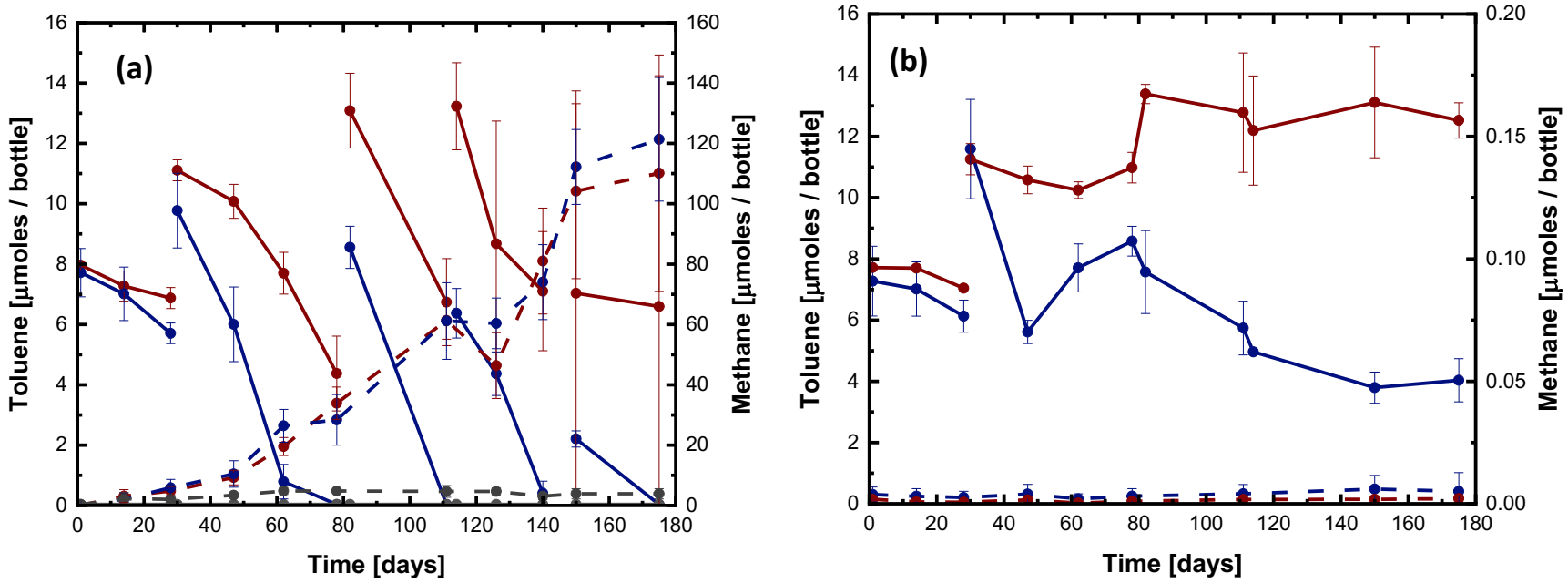

Figure 4.3. Toluene mass (solid lines) and methane production (dashed lines) over the 180-day microcosm period. (a) active microcosms: active treatment (AT, active culture + toluene + PAC, red (●), toluene mass estimated by Equation 3.6 using stoichiometric ratio of methane produced); active control (AC, active culture + toluene, blue (●)); starved control (SC, active culture + PAC, grey (●)). (b) sterile or killed controls: killed control (KC, killed culture + toluene, blue (●)); killed PAC control (KP, killed culture + PAC + toluene, red (●)). Error bars represent the standard deviation of measurements from triplicate bottles. A gap in toluene profiles indicates a re-spike episode.

On Day 114, toluene was re-spiked in the AT and AC microcosm increasing the mass to 13.23 ± 1.44 µmoles/bottle and 6.37 ± 0.82 µmoles/bottle, respectively. By Day 140, most of the toluene was degraded in the AC microcosms (0.41 ± 0.4 µmoles/bottle remaining). In the AT microcosms, toluene mass was ~ 8.68 ± 4.06 µmoles/bottle. Between Day 114 and Day 140 estimated degradation rates were 0.23 ± 0.05 µmoles/day for the AC microcosms and 0.13 ± 0.10 µmoles/day for the AT microcosms.

On Day 150 the active microcosms (AT and AC) were re-spiked increasing toluene mass to 7.03 ± 6.71 µmoles/bottle in the AT microcosms, and 2.21 ± 0.27 µmoles/bottle in the AC microcosms. By Day 175 all toluene was degraded in the AC microcosms (below MDL), and in the AT microcosms between 8 to 10 µmoles toluene remained in the system. Between Day 150 and Day 175 estimated degradation rates were 0.09 ± 0.01 µmoles/day in the AC microcosms and 0.02 ± 0.13 µmoles/ day in the AT microcosms. By Day 175, 121.38 ± 20.48 µmoles of methane were produced in the AC microcosms, and 110.15± 39.17 µmoles of methane were produced in the AT microcosms. Over the duration of this microcosm experiment, 28.42 ± 0.26 µmoles/bottle of toluene were degraded in the AC microcosms and 24.55 ± 10.03 µmoles/bottle of toluene were degraded in the AT microcosms based on methane production (Figure 4.4).

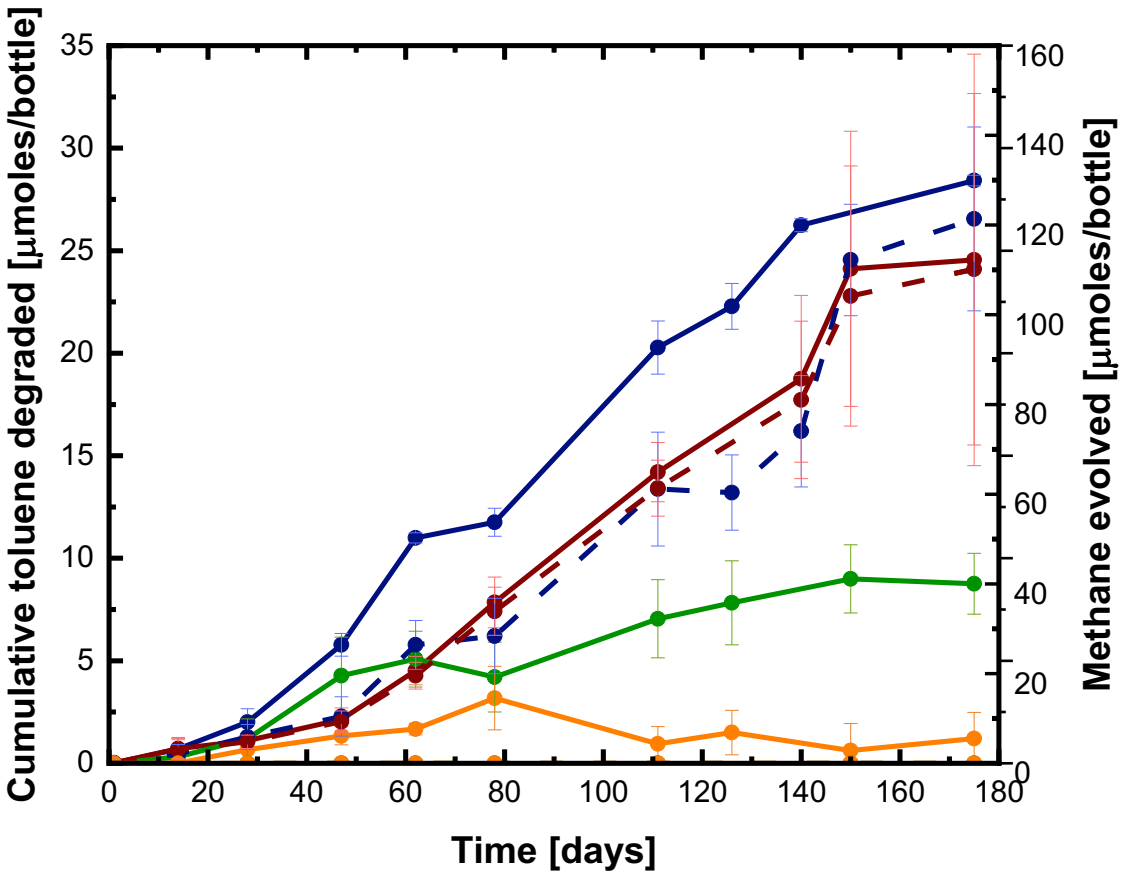

Figure 4.4. Cumulative toluene mass lost and cumulative methane evolved over the 180-day period of the microcosm experiments amended with toluene. Active microcosms: active treatment (AT, active culture + toluene + PAC, red (●), toluene mass estimated by Equation 3.6 using stoichiometric ratio of methane produced); active control (AC, active culture + toluene, blue (●)); sterile or killed controls: killed control (KC, killed culture + toluene, green (●)); killed PAC control (KP, killed culture + PAC + toluene, orange (●)). Error bars represent the standard deviation of measurements from triplicate bottles.

In general, average toluene degradation rates were higher in the AC microcosms compared with the AT microcosms for all degradation cycles (Table 4.2). However, overall rates are statistically similar for both systems. In the AC microcosms, a greater fraction of toluene mass was in the aqueous phase and thus readily bioavailable for microbial oxidation. In contrast, in the AT microcosms a greater fraction of toluene mass was partitioned to the

solid phase (PAC). Since the microorganism size > PAC micropore size, biodegradation should occur external to the PAC matrix and after desorption/diffusion from the micropores (Fan et al., 2017). Thus, the rate of biodegradation of toluene in the AT systems should have been governed by the rate of desorption from PAC.

Table 4.2. Summary of estimated toluene degradation rates for each time interval in the AC and AT microcosms.

	AC		**AT**	
Time interval	**Rate**	**S.D.**	**Rate**	**S.D.**
days	µmoles/ day		µmoles/ day	
1 - 28	0.07	0.02	0.04	0.01
30 -78	0.12	0.03	0.12	0.04
82 - 111	0.29	0.02	0.22	0.09
114 - 140	0.23	0.05	0.13	0.10
150 - 175	0.09	0.01	0.02	0.13
Overall	0.15	0.02	0.14	0.05

Bioregeneration of AC is constrained by adsorption reversibility (Aktaş & Çeçen, 2007; Klimenko et al., 2003; Nath & Bhakhar, 2011). In the AT microcosms, toluene was successfully desorbed from PAC as these microcosms had an active toluene degrading microbiota. The sorption, desorption and degradation of sorbates on PAC amended systems in the presence of active microbial degraders is a result of physical, chemical and biological reactions (Mason et al., 2000). As microorganisms degrade the dissolved toluene, a shift in equilibrium conditions is experienced causing the sorbates (e.g., toluene) to desorb and diffuse from within the PAC particles to areas where biodegradation takes place (Fan et al., 2017; Nath & Bhakhar, 2011; Simpson, 2008).

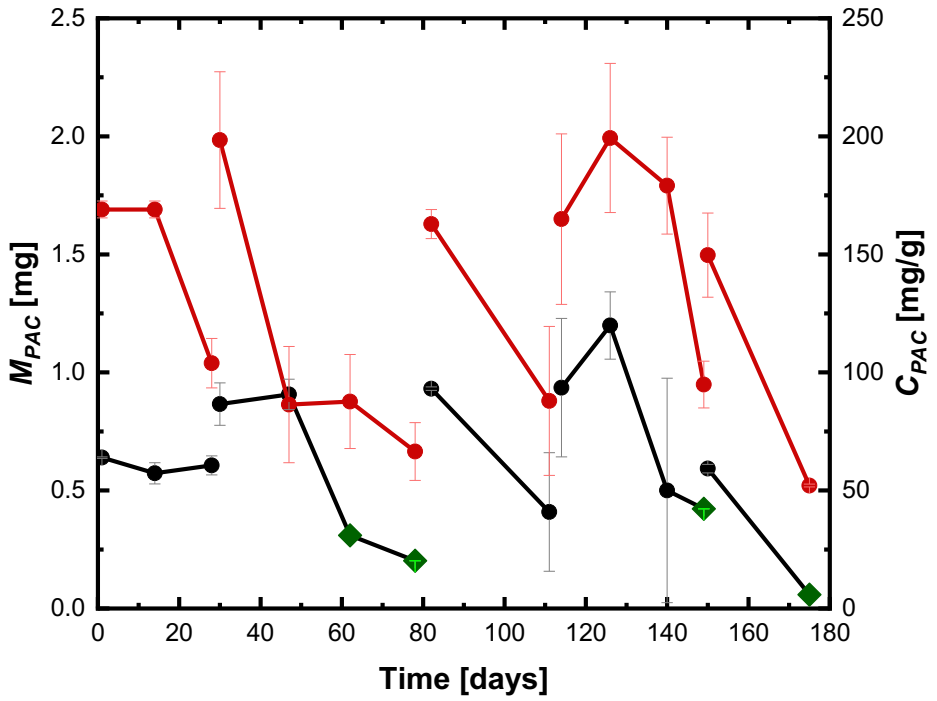

Figure 4.5. Mass (left Y-axis) and concentration (right Y-axis) of toluene sorbed to PAC over the 180-day period in the AT microcosms: M_{PAC} and C_{PAC} were estimated by Equation 3.7 and 3.9, respectively (black (●)); M_{PAC} and C_{PAC} observed from PAC extraction (green (◆)); M_{PAC} and C_{PAC} estimated by Equation 3.8 and 3.9, respectively, using the Freundlich model parameters obtained from the fresh PAC isotherm best fit and aqueous phase toluene concentration (red (●)). Error bars represent the standard deviation of measurements/estimates from triplicate bottles. A gap in toluene profiles indicates a re-spike episode.

Figure 4.5 shows the mass of toluene sorbed to the PAC as estimated from the mass balance Equation 3.7, along with PAC extraction data from Day 62, 78, 149 and 180 as indicated by the different symbols. In addition, Figure 4.5 shows the estimated mass of toluene sorbed to PAC obtained from Equation 3.8 using the Freundlich parameters for fresh PAC (K_f = 79.8; n_f = 0.35). At the beginning of the experiment, the estimated mass of toluene sorbed to the PAC was 0.69 ± 0.003 mg (= 63.91 ± 0.3 mg /g PAC) from mass balance and 1.69 ± 0.03 mg (= 165.17 ± 1.96 mg/g PAC) using the Freundlich equation. After the second re-spike (Day 30), the estimated sorbed mass increased to 0.87 ± 0.09 mg (= 84.62 ± 9.07 mg/g) from

mass balance, while the estimate using the Freundlich equation increased to 1.98 ± 0.29 mg (= 193.79 ± 26.94 mg/g). Near the middle of the experiment (Day 78), data from PAC extraction showed that the toluene mass sorbed to the PAC decreased to 0.20 ± 0.05 mg (= 20.22 ± 5.2 mg toluene/g PAC), whereas when estimated from the Freundlich equation the mass was 0.67 ± 0.12 mg (=65.44 ± 12.16 mg/g). After three re-spiking events, the estimated mass of toluene sorbed to the PAC increased to 1.20 ± 0.14 mg (= 117.23 ± 14.74 mg/g) from mass balance considerations and 1.99 ± 0.32 mg (194.56 ± 28.96 mg/g) from the Freundlich equation. At the end of the experiment (Day 180) the PAC extraction showed that the toluene mass decreased to 0.05 ± 0.007 mg (= 5.5 ± 0.7 mg/g). At the same time point (Day 180) the estimated mass sorbed to PAC using the Freundlich equation was 0.52 ± 0.01 mg of toluene (= 51.40 mg/g). These results show that the mass of toluene sorbed to PAC predicted by the Freundlich model (using fresh PAC parameters) greatly overestimated the observed results from PAC extractions. Nevertheless, it is clear that toluene desorbed from PAC as a result of the decrease in aqueous phase concentration due to microbial biodegradation.

The assembled data set demonstrates: (1) that toluene readily desorbs from PAC when an active microbiota is present and (2) is subsequently degraded. As previously mentioned, the decrease in toluene concentration in the aqueous phase generated a shift in equilibrium conditions causing desorption from the PAC making toluene bioavailable for the microbial degraders. Also, sorption sites can be recovered due to the reversible sorption process allowing further sorption of the adsorbate (Zhao et al., 1999). This reflects the positive impact of microorganisms in regenerating PAC.

4.2.1.1 pH, DO AND ORP

pH, DO and ORP were measured at Day 0, 50, 80, 140 and 180 (refer to Appendix 1). The pH at Day 0 was 7.05 ± 0.02 (optimal growth pH for cells) and decreased to 6.59 ± 0.15 by Day 180. This minor decrease is likely a result of the anaerobic degradation of toluene which produces hydrogen ions, and the increases in CO_2 in the system.

The ORP at Day 0 was -237.8 ± 27.2 mV, reflecting the suitability of using FeS as a reducing agent. By Day 180, the ORP decreased to -286.95 ± 7.5 mV, the decrease in ORP is attributed to the increase in methanogenic microbial activity which is characterized by a highly reduced environment.

The DO concentration Day 0 was 0.03 ± 0.02 mg/L as confirmed by the clear colour in the resazurin microcosm bottles. DO was maintained at similar low concentrations during the experiment, except at Day 180 where concentrations increased to 0.12 ± 0.02 mg/L likely due to a poor probe calibration rather than an actual increase in DO. The microcosms bottles were stored in the anaerobic chamber supplied with $N_2/H_2/CO_2$ and with a palladium catalyst which scavenges oxygen molecules. Although there was potential for some oxygen contamination, especially when material was introduced to the anaerobic chamber, the oxygen levels were always allowed to decrease to non-detect before sampling was conducting.

4.2.2 BIOFILM CHARACTERIZATION

The presence, growth and organization of the PAC biofilm was examined by CLSM. Two negative controls were imaged to determine the autofluorescence of the PAC and/or the PAC-stain interactions so that actual biomass was observed on the bio-coated PAC samples and to understand background noise. The autofluorescence of fresh PAC without microbial culture contact and stain were imaged and no signal was detected indicating that fresh PAC had no autofluorescence. To determine PAC-stain interactions that could produce fluorescence, fresh PAC samples were stained with SYTO9 dye and imaged. No signal was detected consistent with previous findings that SYTO9 dye displays a low intrinsic fluorescence in cell-free systems and fluorescence can only be observed upon binding with DNA (Wlodkowic et al., 2008).

4.2.2.1 QUALITATIVE CHARACTERIZATION

Microbial interaction with AC is primarily influenced by the surface charge since the microbial cell walls have a negative charge. Based on the pH_{PZC}, the WPC® PAC would be positively charged in a system with a pH < 10 (Liu, 2017), and thus electrostatic adsorption should be promoted. A few different cell morphologies were observed attached to the PAC. This included rod-like cells which were predominant with a length of 1.5 ± 0.8 µm; thin rod cells with a length of 0.7 ± 0.1 µm; and sometimes chains of rod-like cells with a length of 3-10 µm (see Figures 4.6 to 4.15). The 3-D reconstructions of the particles allow for visualization of biofilm attachment to the PAC.

By Day 50 the microbial attachment observed on the PAC surfaces were a few individual cells randomly dispersed (Figures 4.7 and 4.8). This type of spotty aggregation represents a transitional state that precedes the formation of a structured biofilm (Bogino et al., 2013). During the early stage of PAC colonization (Day 80) some cells formed clusters on the surface of the PAC (Figures 4.9 and 4.10). These microcolonies were observed particularly

on particles > 10 µm, presumably due to a larger contact surface area between the cells and the PAC which enabled a higher degree of attachment and stability.

By Day 140 (Figures 4.11 and 4.12), an increase of the number of cells and cell clusters attached to the PAC surfaces, compared to Day 80, was observed indicating that the microbes were to attaching to each other. On Day 180 (Figures 4.13 to 4.15), two types of growth were observed: (1) a monolayer of cells completely covering the particles, and (2) a discontinuous multilayer of cells. In addition, thicker cell colonies were observed to have developed on the PAC. This increased coverage and thickness (Figures 4.13 to 4.16) is a result of more surface area contact between the cells and the PAC. Eventually, continual microbial growth would likely have resulted in entire coverage of the PAC particles (Massol-Deya et al., 1995)

Although EPS was not observed to be the prevalent biofilm component, the images clearly show that a biofilm was formed on PAC. The biofilms formed by the DGG-T culture were observed to be characterized by a slow growth in both cells and EPS. Biofilm formation varies by microbial species, some are characterized by rapid growth and extensive EPS production such as *P. aeruginosa*, while others are deficient in certain proteins that play an important role in biofilm formation (D. López et al., 2010).

As described above, cell attachment and biofilm formation on PAC was observed to be heterogeneous with high variability between PAC particles likely related to surface irregularity. Song et al. (2010) and Zhao et al. (1999) reported a similar type of biofilm on AC where a non-uniform biofilm was characterized by localized concentrations of bacteria. Van Der Mei et al. (2008) studied the adhesion of bacteria to AC particles, specifically a positively charged coconut-based carbon from Calgon Carbon (similar to the one used in this study) sieved to a particle size of 25-50 µm. They found highly variable cell adhesion between single particles (n = 10).

Figure 4.5 shows microscopic images from the mixed methanogenic culture biofilm detached from the PAC at Day 180. Based on these images the cell concentration was estimated to be 7.02 ± 0.87 x10^{10} cells/g PAC. Reaume et al. (2014) observed cell concentrations of 4.0 x 10^{10} cells/g GAC in a packed bed biofilter used for treating municipal water. Capozzi et al. (2019) grew an anaerobic biofilm on different carbonaceous materials and after 159 days of biofilm growth reported a cell concentration of 1.2 x 10^{9} and 1.5 x 10^{10} cells/g of AC and bone char respectively. Massol-Deya et al. (1995) reported bacterial concentrations ranging from 10^{9} to 10^{11} cells/g AC, and Combarros et al. (2014) indicated values between 2.8 x 10^{10} to 7.5x10^{10} cells/g of AC. Thus, the cell concentration estimated in this work is consistent with values reported by others for AC systems.

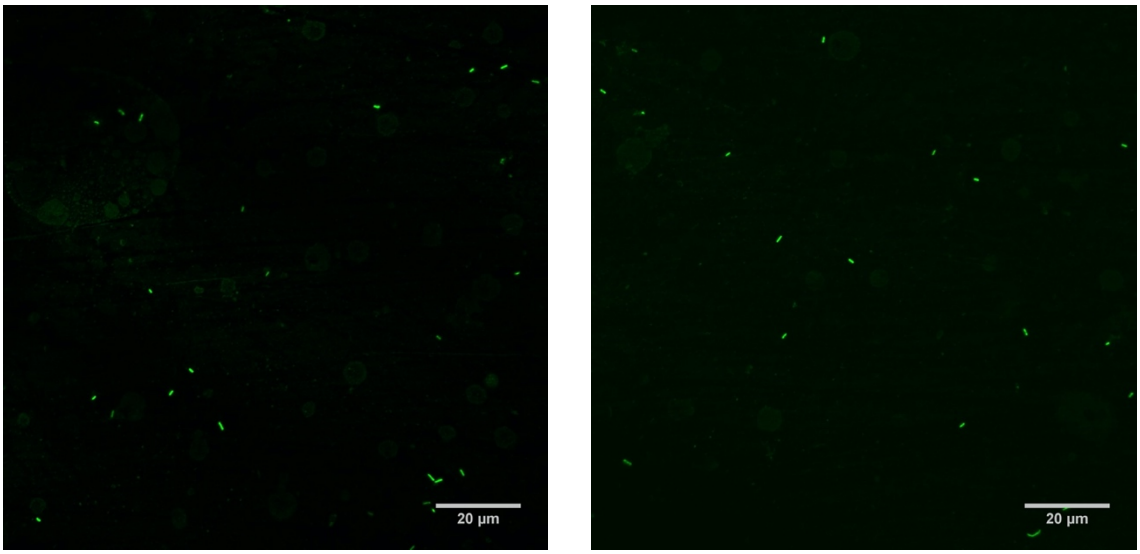

Figure 4.6. Mixed methanogenic toluene degrading culture cells from detached biofilms stained with SYTO 9 for cell density enumeration. Scale bar denotes 20 µm.

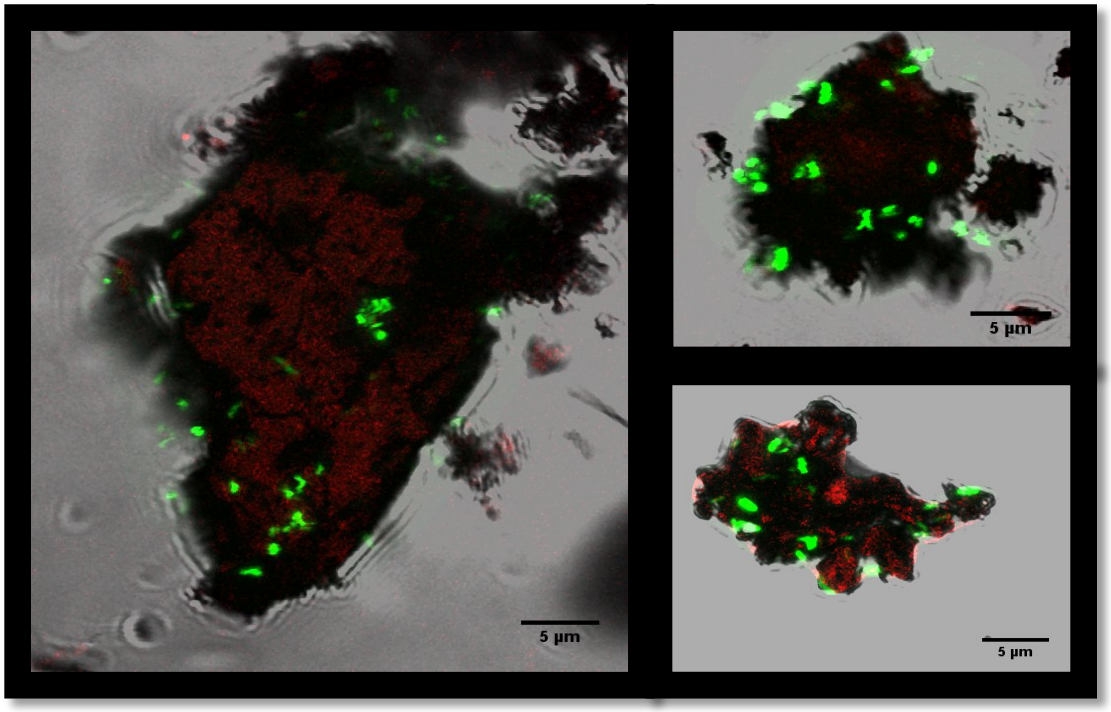

Figure 4.7. Maximum intensity projection CLSM images of biofilms on the surface of PAC particles at Day 50. Cells labeled with SYTO9 stain (green) and EPS labeled with Con A (red), PAC surface (black). The scale bar denotes 5 µm.

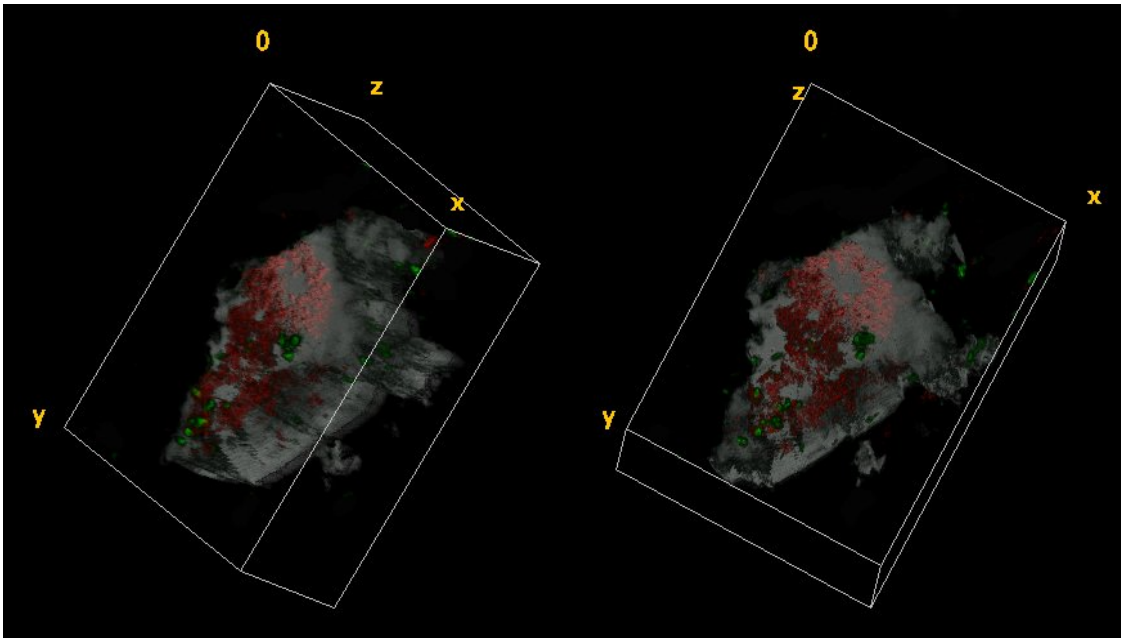

Figure 4.8. Constructed CLSM three-dimensional image of biofilm on surface of a PAC particle at Day 50.

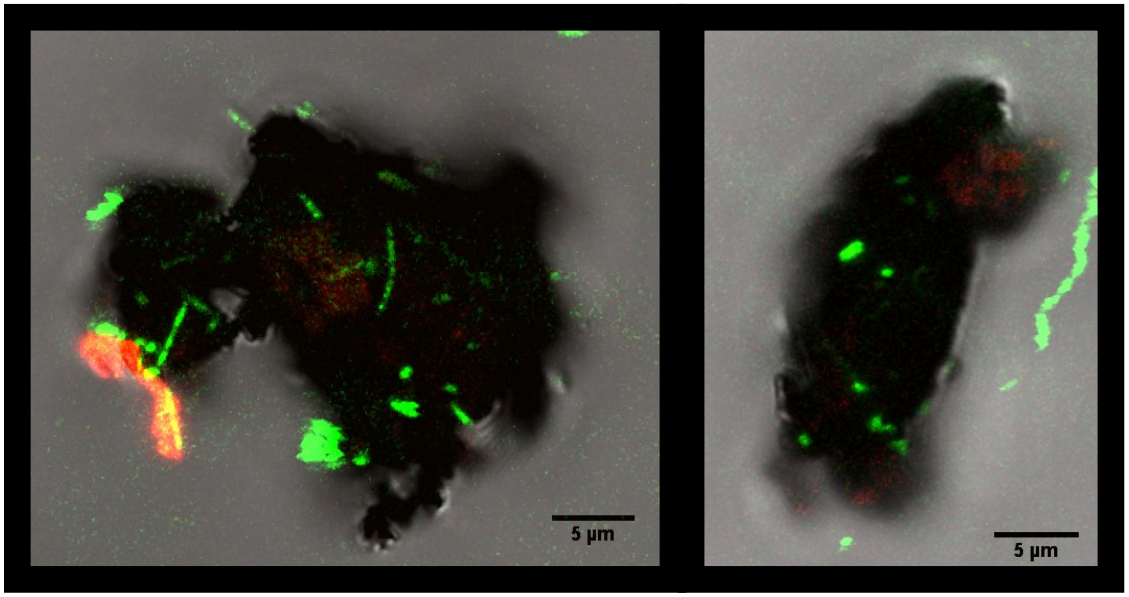

Figure 4.9. Maximum intensity projection CLSM images of biofilms on surfaces of PAC particles at Day 80. Cells labeled with SYTO9 stain (green) and EPS labeled with Con A (red), PAC surface (black). The scale bar denotes 5 µm.

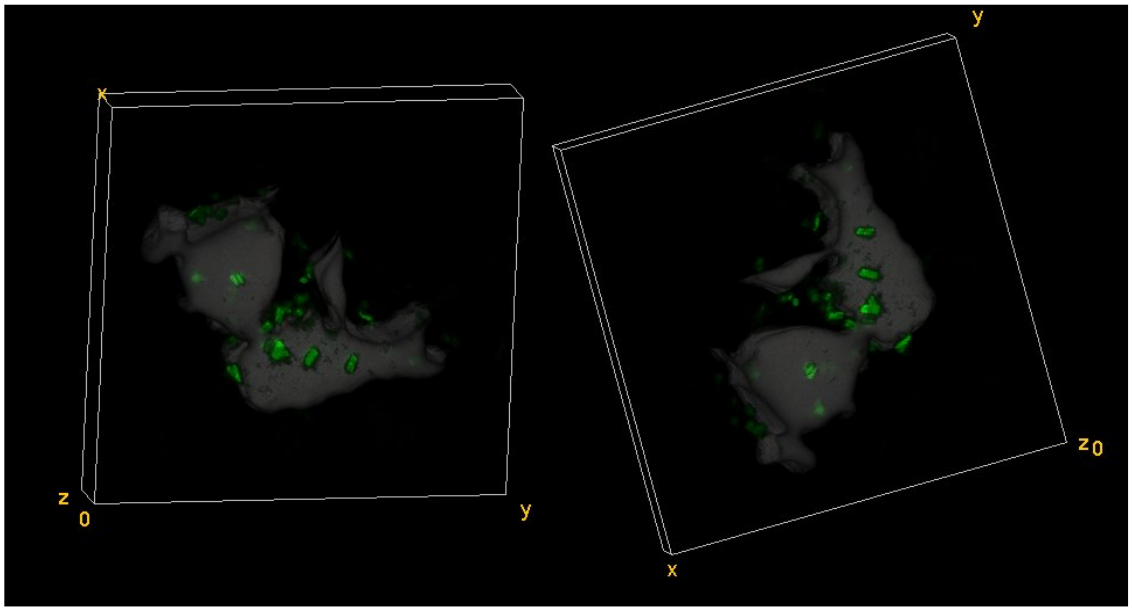

Figure 4.10. Constructed CLSM three-dimensional image of biofilm on surface of a PAC particle at Day 80.

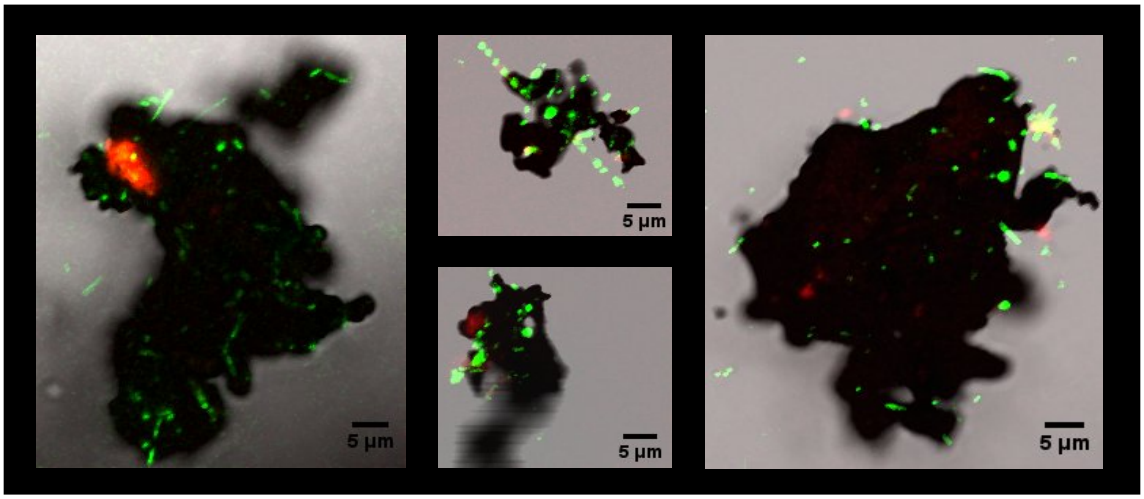

Figure 4.11. Maximum intensity projection CLSM images of biofilms on surfaces of PAC particles at Day 140. Cells labeled with SYTO9 stain (green) and EPS labeled with Con A (red), PAC surface (black). The scale bar denotes 5 µm.

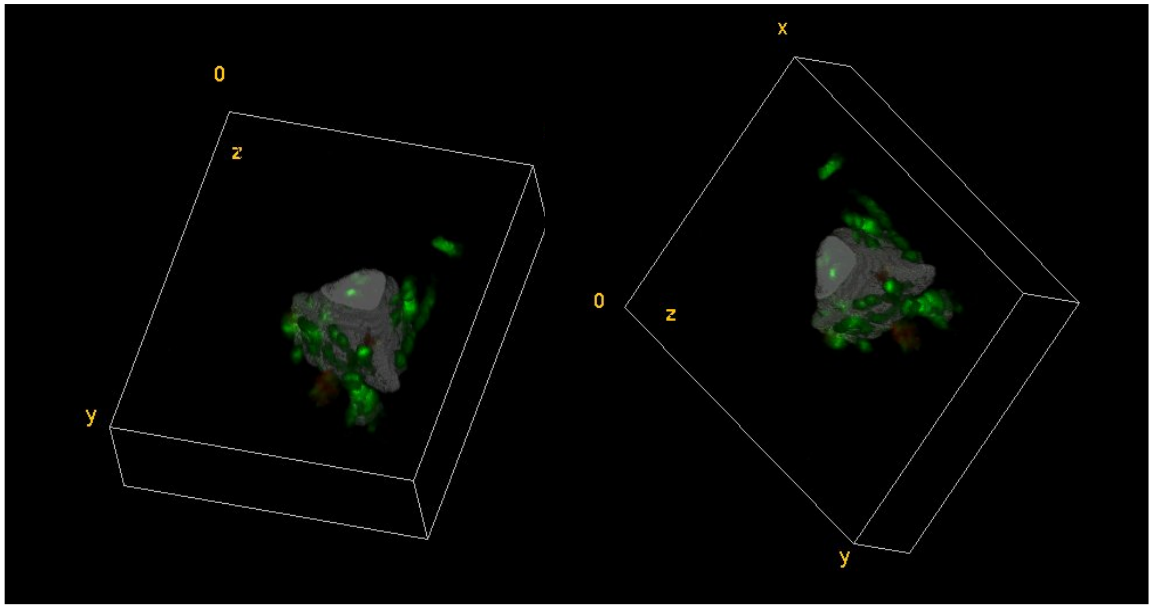

Figure 4.12. Constructed CLSM three-dimensional image of biofilm on the surface of a PAC particle at Day 140.

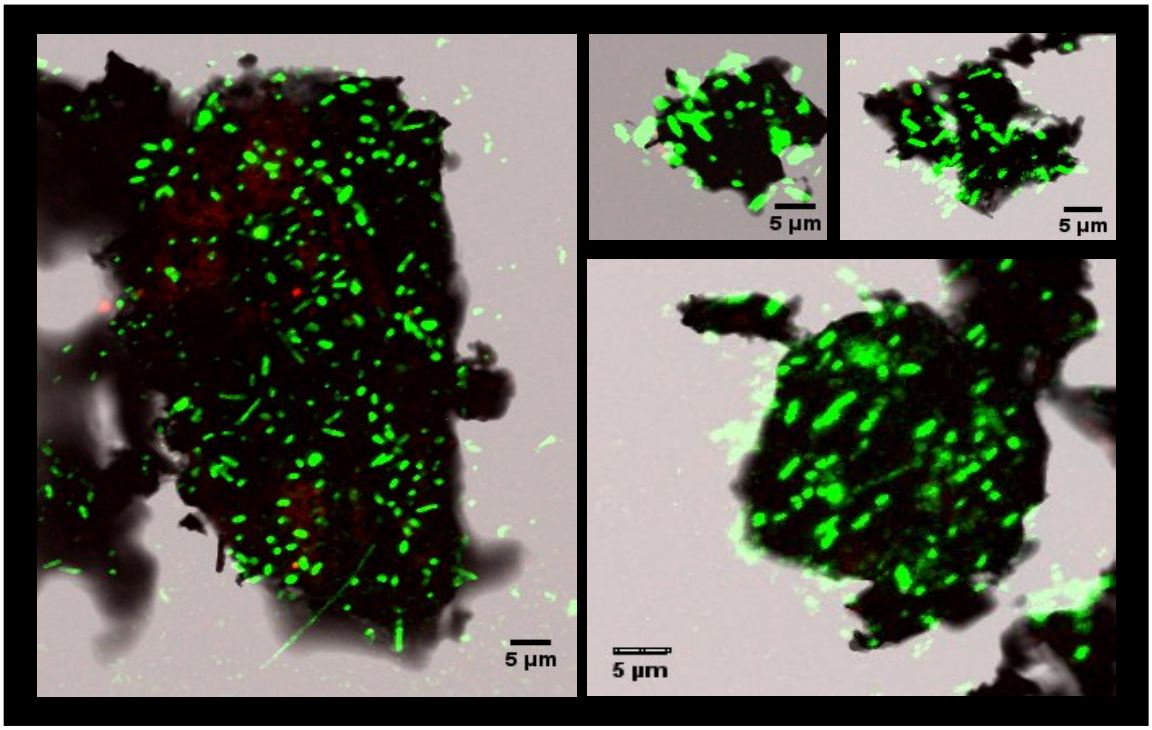

Figure 4.13. Maximum intensity projection CLSM images of biofilms on the surface of PAC particles at Day 180. Cells labeled with SYTO9 stain (green) and EPS labeled with Con A (red), PAC surface (black). The scale bar denotes 5 µm.

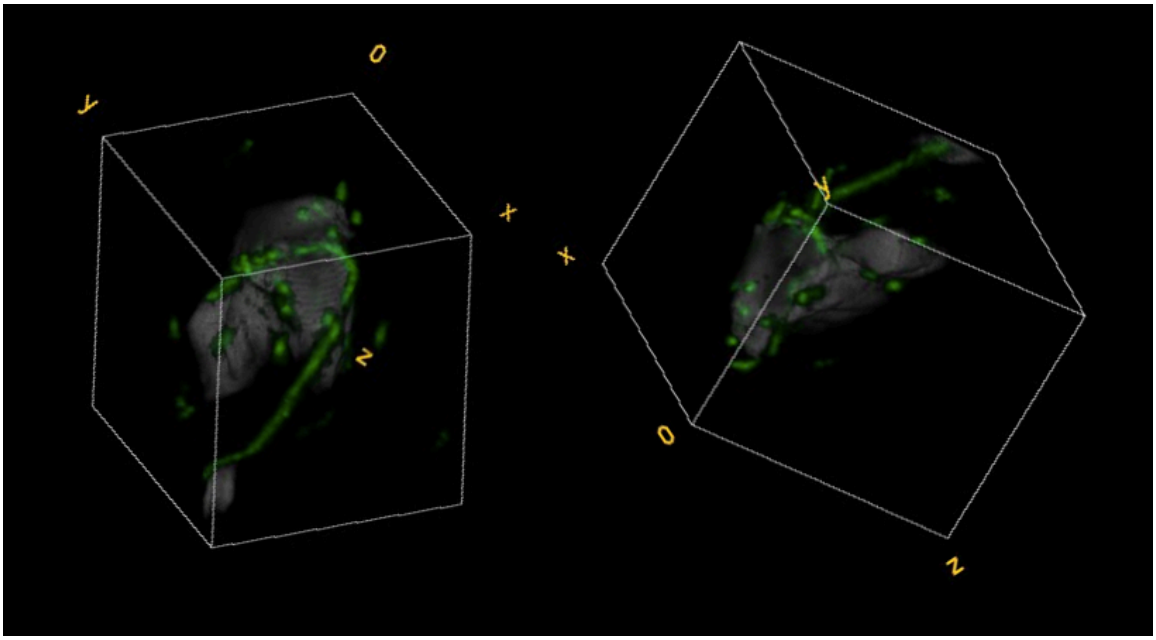

Figure 4.14. Constructed CLSM three-dimensional images of biofilm on the surface of a PAC particle at Day 180.

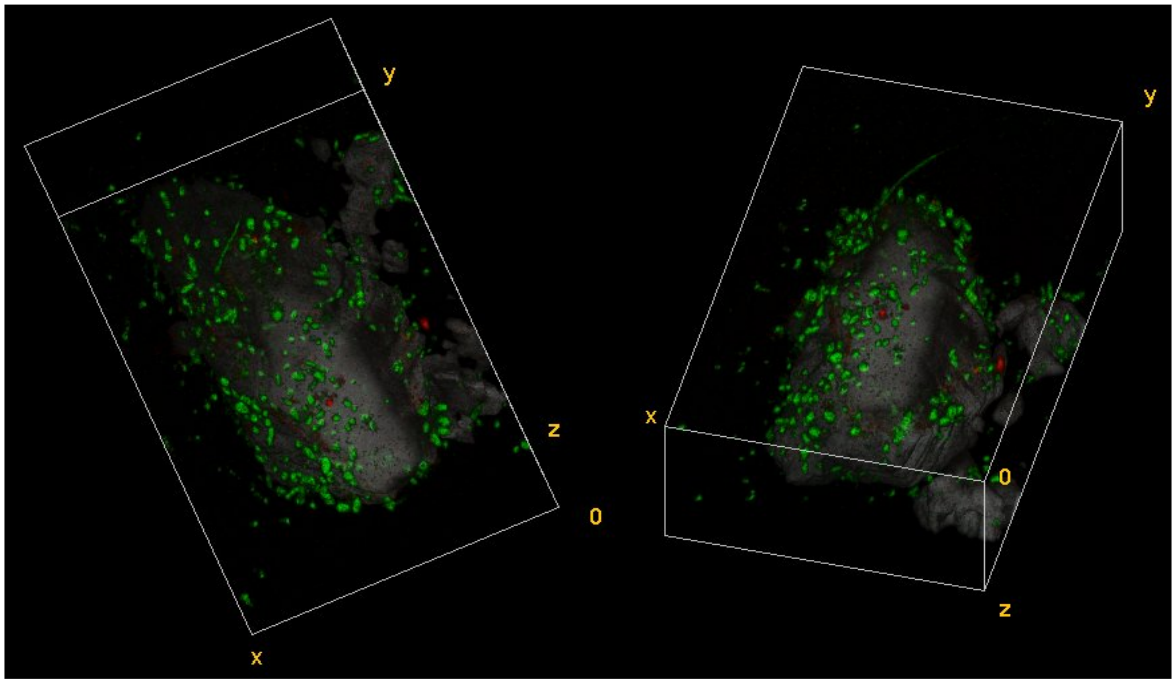

Figure 4.15. Constructed CLSM three-dimensional image of biofilm on the surface of a PAC particle at Day 180.

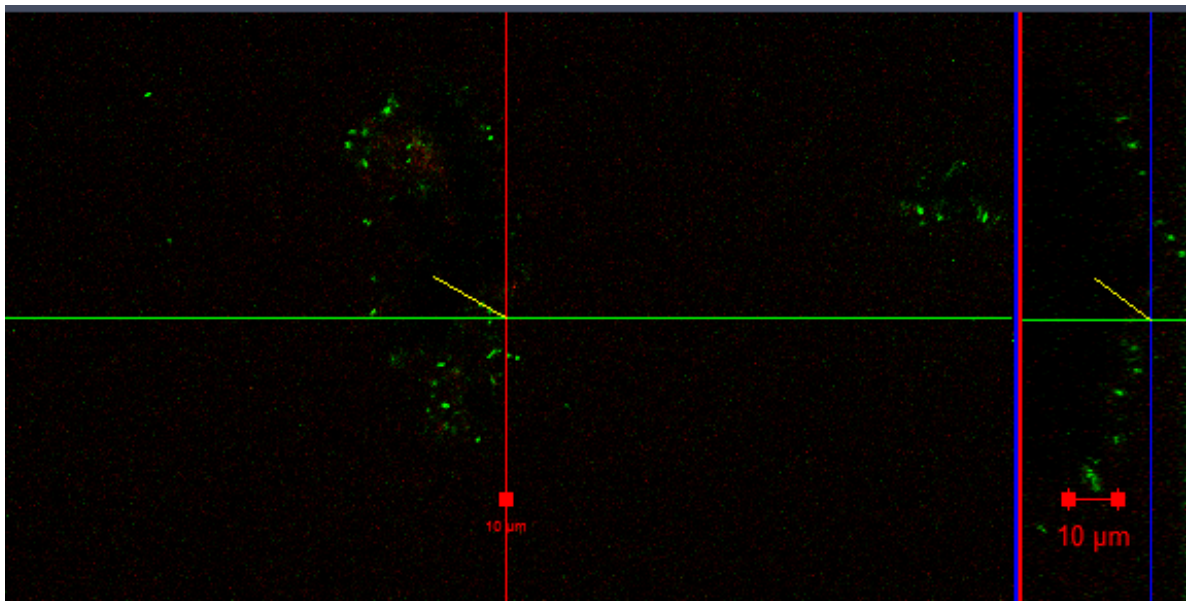

Figure 4.16. Orthogonal view of biofilm formation at Day 180 showing biofilm thickness. Scale bar denotes 10 µm.

4.2.2.2 QUANTITATIVE CHARACTERIZATION

A detailed descriptive statistic of the biofilm parameters (Table A2.4), and the p-values obtained between time points tested (Table A2.5) can be found in Appendix 2.

Biovolume

Biovolume is the volume of the biofilm components (either cells or EPS) attached to the PAC surfaces and can be used to estimate the number of cells based on average cell dimensions. Cell and EPS biovolume was highly variable between PAC particles (n = 50) at all characterization time points and in general increased over the 180-day experimental period for both components (Figure 4.17(a,b)). There was a statistically significant difference ($p < 0.05$) in cell biovolume between all sampling points indicating substantial cell growth over time. This is supported by the visual observation of PAC particles at Day 50 and Day 180 (see Figures 4.7 and 4.13) where an increase in the number of cells attached to the PAC is evident. The EPS biovolume showed a statistically significant increase ($p < 0.05$) between Day 50 and Day 80, and between Day 80 and Day 140, but not between Day 140 and Day 180 ($p > 0.05$). However, when comparing EPS production between Day 80 and Day 180, a statistically significant difference in biovolume was determined.

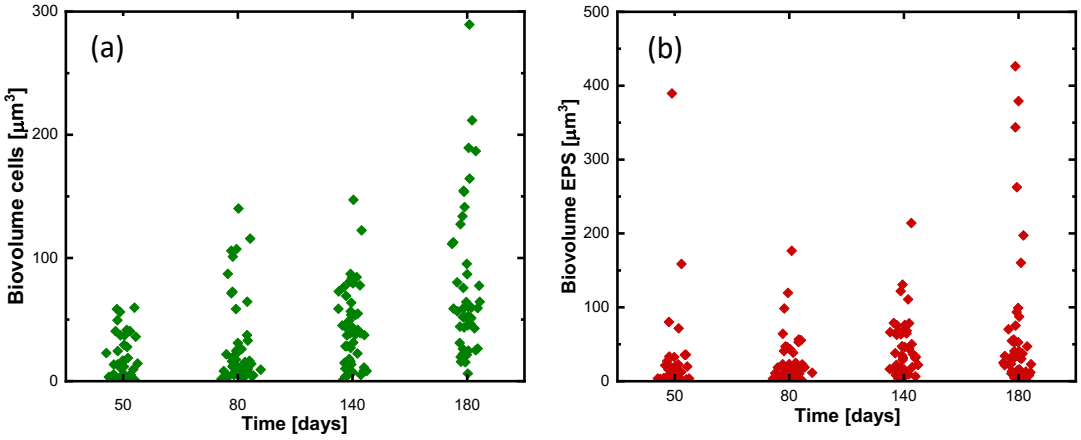

Figure 4.17. Biovolume of (a) cells (■) and (b) EPS (■) of the anaerobic toluene degrading culture biofilm at different time points (n = 50).

Biomass

Biomass is the amount of biological material per unit area of PAC ($\mu m^3/\mu m^2$). It is an estimation of the amount of biofilm formation attached to the PAC surface and is useful when comparing the amount of living material covering different substrates. As observed on Day 50 (Figure 4.18) the average cell biomass was 0.11 $\mu m^3/\mu m^2$ (0.02 (lower quartile, Q1) to 0.17 $\mu m^3/\mu m^2$ (upper quartile, Q3), with a range of 0.15 $\mu m^3/\mu m^2$ covered by the interquartile range (IQR)), and average EPS biomass was 0.09 $\mu m^3/\mu m^2$ and ranged from 0.008 (Q1) to 0.15 $\mu m^3/\mu m^2$ (Q3), with an IQR of 0.146 $\mu m^3/\mu m^2$. From the CLSM images, at this time point, only a few cells were observed randomly attached to the PAC. There was no statistically significant difference between the biofilm components.

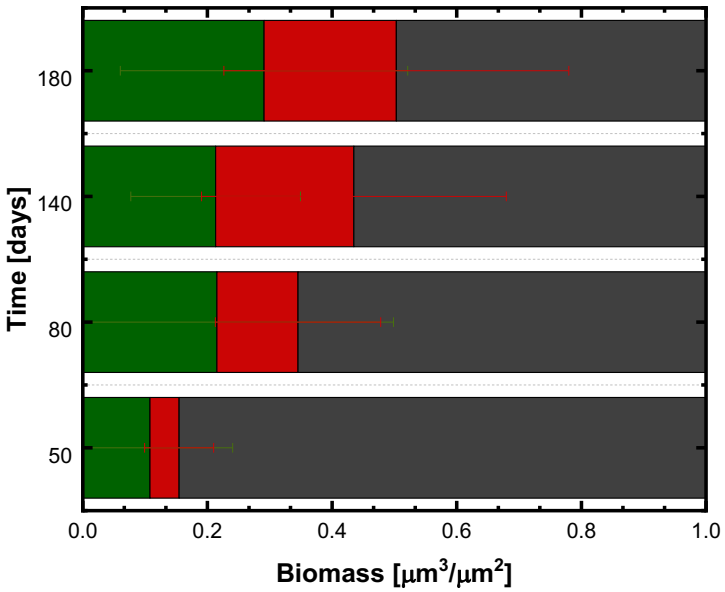

Figure 4.18. Biomass of the anaerobic toluene degrading culture biofilm components (cells (■), green; EPS, (■) red) on PAC ((■) grey) at different time points. Error bars represent ± one standard deviation, (n = 50).

Between Day 50 and Day 80, a statistically significant increase in biomass was determined for both the cells and EPS. The average cell biomass at Day 80 was 0.22 $\mu m^3/\mu m^2$ (0.04 (Q1) to 0.26 $\mu m^3/\mu m^2$ (Q3), IQR of 0.22 $\mu m^3/\mu m^2$ and the average EPS was 0.13 (0.051 (Q1) to

0.15 $\mu m^3/\mu m^2$ (Q3), IQR of 0.10 $\mu m^3/\mu m^2$). A visual inspection of the particles showed some microcolonies forming by Day 80 which resulted in the increase of biofilm biomass. Between Day 80 and Day 180, a statistically significant increase in cell biomass was also determined. The cell biomass at Day 180 increased to an average of 0.29 $\mu m^3/\mu m^2$ (0.64 (Q1) to 0.36 $\mu m^3/\mu m^2$ (Q3)). For the EPS component, the biomass increased to an average of 0.21 $\mu m^3/\mu m^2$ (0.06 (Q1) to 0.25 $\mu m^3/\mu m^2$ (Q3)). A statistically significant increase in biomass was determined between Day 50 and Day 180. The high variability of biomass attachment could be attributed to the irregular surface of AC particles, as well as the variation in sizes between PAC particles. Larger contact surface area between the cells and the PAC will enable a higher degree of attachment and stability which will promote the biomass growth on those surfaces.

Thickness

Biofilm thickness is especially important for biofilms growing on materials where sorption is used for contaminant removal. Thicker biofilms may decrease the sorption kinetics due to increased diffusional resistance. Figure 4.19 shows that the average cell thickness remained relatively constant on Day 50, Day 80 and Day 140 (4.49 ± 1.4 µm, 4.26 ±1.3 µm, and 4.2 ± 2.6 µm respectively) and no statistically significant difference was determined between any of those time points. However, a statistically significant increase in cell thickness was determined at Day 180 with an average thickness of 7.39 ± 3.9 µm. These observations are consistent with Capozzi et al. (2019) who observed that a constant cell thickness (4.4 ± 0.56 µm) remained over 159 days for an anaerobic dehalorespiring biofilm growing on AC.

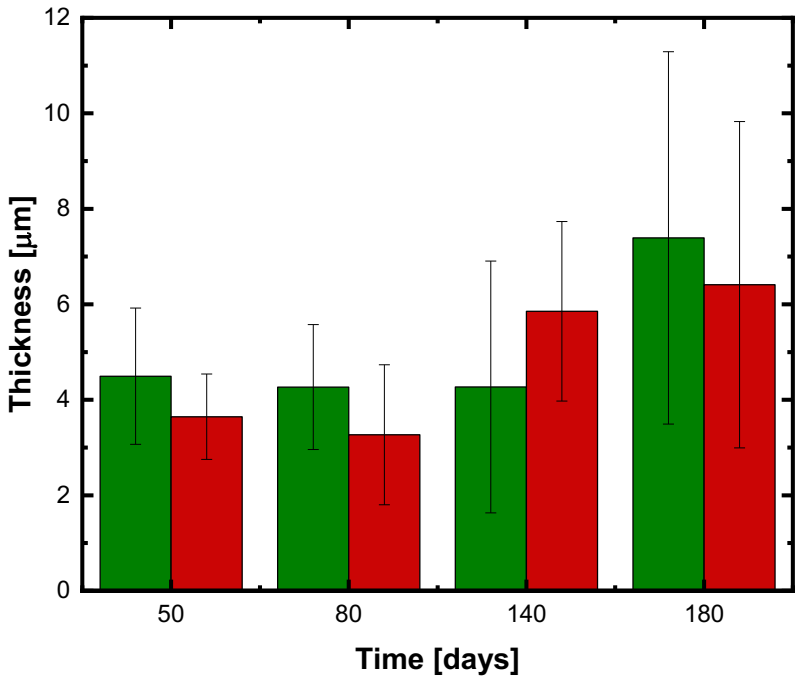

Figure 4.19. Biofilm thickness of the anaerobic toluene degrading culture components (cells (■), green; EPS, (■) red) on PAC at different time points. Error bars represent ± one standard deviation, (n = 50).

The EPS thickness was not statistically significantly different between Day 50 (3.64 ± 0.9 µm) and Day 80 (3.26 ± 1.5 µm), while the increase between Day 80 and 140 (5.85 ± 1.9 µm) was statistically different. The EPS thickness was not statistically different between Day 140 and Day 180 (6.41 ± 3.4 µm) meaning that between those time points the thickness did not increase significantly. However, the EPS thickness was statistically different between Day 50 and Day 180, which means that over the length of the experiment, the EPS accumulated gradually resulting in a significant increase in thickness.

Biofilm thickness is a result of environmental conditions, such as, flow, nutrient availability and temperature, as well as developmental age of the biofilm. As a biofilm ages, it is expected that an accumulation of biofilm components that will result in an increase in thickness. These results are consistent with the observations on the CLSM images where multi-layers of cells were observed on some PAC particles at Day 180.

Roughness

Biofilm roughness describes the degree of uniformity of the developed biofilm. It provides information on biomass structure and architecture to complement the characterization of the biofilm. A roughness coefficient of zero indicates a uniform biofilm, and the greater the roughness coefficient the more heterogeneous the biofilm (González-Machado et al., 2018). The biofilm roughness was similar throughout the experiment (Figure 4.20) with a high roughness coefficient observed (~1.6). Although comparing the cell roughness between Day 50 and Day 180, a statistically significant difference was determined ($p < 0.05$).

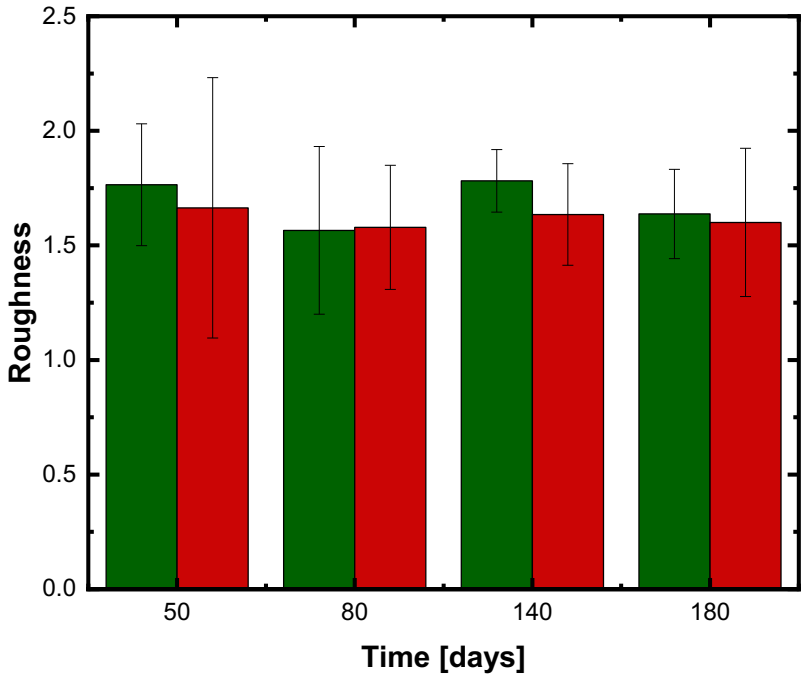

Figure 4.20. Roughness of the anaerobic toluene degrading culture biofilm components (cells (■), green; EPS, (■) red) on PAC at different time points. Error bars represent ± one standard deviation, (n = 50).

The decrease in the roughness on Day 180 can be attributed to the increase of cells attached to the PAC which led to more uniform and thicker biofilms as compared to Day 50 where random cell attachment was observed. On the other hand, the EPS did not show a statistical

difference between the various time points. Although the EPS biovolume and thickness increased over time, due to the interwoven nature of the EPS, its formation is expected to be uneven. These results are consistent with the visual observation of CLSM images where a high degree of variability in attachment was observed on the PAC surfaces. Over time, if a greater accumulation of cells and EPS was achieved, perhaps a smoother layer would have been obtained on PAC surface.

4.3 EFFECT OF BIOMASS ON ADSORPTION

To investigate the influence of a biofilm attached to PAC on the sorption of toluene, biofilm coated PAC samples were obtained from the microcosm experiments at two time points. A series of batch sorption experiments were performed on Day 80 and Day 180. The sorption characteristics of fresh PAC and the one of bio-coated PAC were compared to gain insight into the possible loss of adsorption capacity due to PAC ageing.

The mass of sorbed toluene associated with the bio-coated PAC was determined prior to conducting the sorption experiments. As observed in Figure 4.5, the mass of toluene sorbed to the PAC was 20.22 ± 5.2 mg/g on Day 80, and 5.69 ± 0.7 mg/g on Day 180. As a result of this initial mass sorbed, the data generated from the point-bottle experiments required modification as given by

$$q'_e = \frac{C_0 V + q_{0\,PAC} - C_e V}{m} \quad (4.2)$$

where q'_e is the adjusted equilibrium mass of sorbate per gram of sorbent (mg/g), C_0 is the initial aqueous phase sorbate concentration in mg/L, C_e is the equilibrium aqueous phase sorbate concentration in mg/L, q_{0PAC} is the initial mass of sorbate on the PAC, V is the volume of the aqueous phase in liters (L) and m is the mass of PAC in grams (g). The adsorption equilibrium data generated in the bottle-point experiments were fit to the Freundlich model using IsoFit (Mattot, 2007). The estimated model parameters and 95% confidence intervals (CI) are listed in Table 4.3. A paired t-test was applied to the experimental data showing that bio-coated PAC was significantly successful in removing toluene from the contaminated solution ($p < 0.05$).

The adsorption isotherms of fresh PAC and of bio-coated PAC at Day 80 and Day 180 were compared. An F-test was used to compare the dataset obtained from the model best fit (fresh PAC vs Day 80 bio-coated PAC, fresh PAC vs Day 180 bio-coated PAC). At both time points, the bio-coated PACs showed a statistically significant difference in adsorption ($p <$

0.05) relative to the fresh PAC (Figure 4.21). The K_f value decreased from 79.8 (fresh PAC) to 50.7 at Day 80 and to 47.7 at Day 180. Values of n_f increased to 0.42 at both time points. The results indicate a decrease in sorptive capacity of both bio-coated PACs when compared to the fresh PAC.

With a similar n_f value, the adsorption capacity for toluene was reduced from Day 80 to Day 180; however, an F-test (Day 80 bio-coated PAC vs Day 180 bio-coated PAC) showed no there was no statistical difference ($p > 0.05$). In addition, an examination of the 95% confidence intervals for K_f and n_f at both time points indicates that they are not statistically different.

Biological fouling arises from the proliferation of biomass and microbial by-products on AC surfaces. This causes blocking of AC pores that may limit the mass transfer of the sorbate to the AC matrix, as well as competition with the sorbate for available sorption sites, leading to a deterioration of adsorption performance (Hutchinson & Robinson, 1990; Leong et al., 2018b; Yakout & Daifullah, 2014). Reports on other biofilm coated AC systems observed sorptive properties to deteriorate during biofilm formation/bioregeneration, and was attributed to the adsorption of lysed cells or the adsorption of microbial metabolites, and therefore complete recovery of the adsorption capacity was not achieved (Aktaş & Çeçen, 2007).

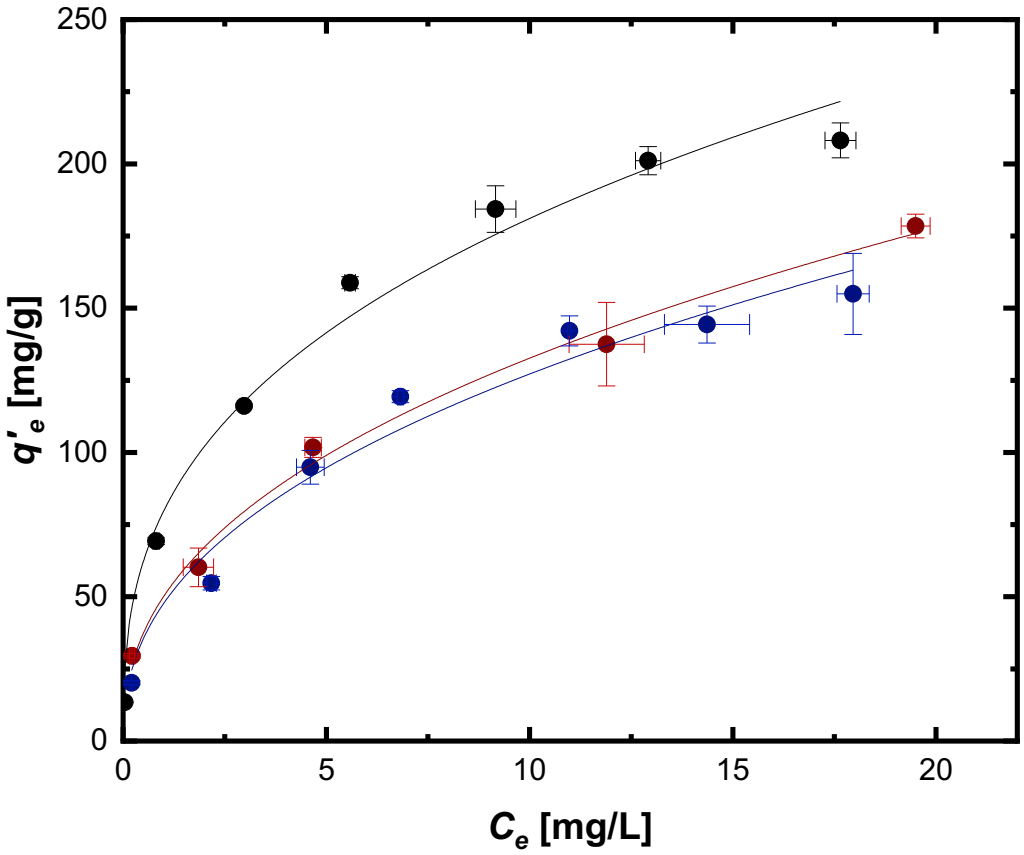

Figure 4.21. Sorption isotherms for toluene on fresh PAC (black (●)), and bio-coated PAC at Day 80 (red (●)), and Day 180 (blue (●)). The symbols are the data points, while the solid line represents the least-squares fit. Error bars represent the standard deviation of triplicate bottles.

Table 4.3. Adsorption isotherm parameters for PAC at different time points of biofilm formation. Confidence intervals (CI) set at 95%.

Time	K_f [(mg/g)(L/mg)^n]	CI	n_f -	CI	R^2
0 (fresh PAC)	79.8	67.3 – 92.2	0.35	0.29 – 0.42	0.98
80 (bio-PAC)	50.2	43.1 – 57.2	0.42	0.37 – 0.48	0.99
180 (bio-PAC)	47.7	36.3 – 59.2	0.42	0.33 – 0.52	0.96

Similar results were found by Zhao et al. (1999) who evaluated the change in adsorption parameters on a bio-coated GAC grown on a fluidized bed reactor system for toluene contaminated water. The K_f value obtained for fresh GAC was 79.3 and the n_f value was 0.37. The K_f values decreased and n_f values slightly increased during the experimental period. At Day 77 and Day 187 the K_f decreased to 46.3 and 37.7 and n_f increased to 0.42 and 0.51 respectively.

Mason et al. (2000) evaluated the change in adsorption characteristics of PAC in a mixed bioreactor. In these experiments, an aerobic BTEX degrading biofilm was grown on the PAC. To determine the influence of a biofilm attached to the PAC on the change of sorption characteristics, a series of isotherms were carried out using methyl-tert-butyl ether (MTBE). The Freundlich parameters K_f and n_f for the fresh PAC were 3.37 and 1.86 respectively, while for the bio-coated PAC, K_f ranged from 0.42 to 0.82 and n_f ranged from 1.14 to 1.35. These results indicate that the adsorption capacity of PAC was significantly reduced due to biofilm presence.

Zhao et al. (1999) observed that the capacity of GAC for toluene during the first 60 days of biofilm-GAC exposure decreased by 70% of the initial value at 3 and 10 mg/L, and then decreased to around 52 and 57% for 3 and 10 mg/L respectively after 200 days. Furthermore, they did not find a direct relationship between the amount of biomass attached to GAC or the thickness of the biofilm with the decreased adsorptive capacity. However, the duration of biofilm/GAC exposure (bioactivity) was considered to have influenced the loss of adsorption capacity. They suggested that the loss of GAC sorption capacity might have been due to the adsorption of soluble microbial metabolites (microbial by-products) excreted by the biofilm, which accumulated over time. Song et al. (2010) investigated the impact of biofilm formation on 2-NSA adsorption to GAC. Adsorption capacity decreased to 91% after 35 days of biofilm growth, however, variations in biofilm thickness and surface coverage (80%) had no effect on the change of adsorption capacity which remained at 90%.

In this study, on Day 80 the biomass present on the PAC was 0.22 ± 0.3 $\mu m^3/\mu m^2$ cells and 0.13 ± 0.1 $\mu m^3/\mu m^2$ EPS, and the average cellular thickness was 4.26 ±1.3 µm and the average EPS thickness was 3.26 ± 1.5 µm. At Day 180, the average biomass was 0.3 ± 0.2 $\mu m^3/\mu m^2$ cells and 0.21 ± 0.2 $\mu m^3/\mu m^2$ EPS, and the average thickness was 7.39 ± 3.9 µm for cells and 6.41 ± 3.3 µm for EPS. The biofilm development was significantly greater ($p < 0.05$) at Day 180 than at Day 80. The K_f value indicates a slight loss in adsorption capacity from Day 80 to Day 180, however, the differences are not statistically significant ($p > 0.05$). Still, this slight decrease in K_f at Day 180 might be influenced by the increase in biofilm attached to PAC resulting from the increased time for bioactivity. From the data obtained, the change in sorption characteristic of the PAC for toluene over an extended period of biofilm formation appears to be a result of biological fouling (by biomass production and/or sorption of microbial metabolites).

Combarros et al. (2014) observed that after a biofilm was developed on GAC surfaces, the GAC was not able to adsorb the test compound (salicylic acid) because the biomass likely plugged the active sites or the GAC was saturated with components of the synthetic water during biofilm formation. Similar results were observed by Klimenko et al. (2003) where the adsorption capacity of bio-coated AC decreased to 20% of the value of sorption on fresh AC and the extent of regeneration did not depend on the type of AC used.

Treatment using PAC amendments generates an immediate reduction of contaminants in groundwater due to rapid adsorption of dissolved-phase sorbates (Fan et al., 2017). After adsorption, microbes degrade the dissolved-phase contaminants in the neighborhood of the PAC, and a shift in equilibrium conditions in which desorption of contaminants and regeneration of PAC sorption sites occur. These steps create a dynamic equilibrium where continuous sorption and degradation of contaminants will provide long-term groundwater treatment (Fan et al., 2017; Klimenko et al., 2003; Simpson, 2008). As such, the potential longevity of CBI is one of the major benefits of this technology (Fan et al., 2017). However, as observed in this research, one of the factors that may affect the long-term effectiveness

of PAC barriers is the fouling of PAC sorption sites due to bioactivity (biofilm formation and/or competitive sorption of microbial by-products generated during the process of biofilm formation), which might disrupt the synergistic interplay between the sorption-desorption-degradation processes. Even when the contaminant (i.e., toluene) was desorbed from PAC and degraded by the microbes, PAC sorption capacity was reduced as a result of biofilm growth.

To explore the impact that biofilm formation may have on the performance of a PAC barrier, a simple and conservative approach was adopted. Following placement of a PAC barrier to cut-off a plume, sorption of contaminants will take place and, after a sufficient time has passed, equilibrium will be reached, and breakthrough will occur if biodegradation is ignored. Figure 4.22 shows a schematic of an ideal PAC barrier with a plume entering from the left and a "treated" plume exiting on the right. The time to barrier saturation or breakthrough can be estimated from (refer to Appendix 2 details)

$$t_{sat} = \frac{\left[\phi\, C_w^{in} + K_f\, C_w^{n_f}\, \rho_b\, f_{PAC}\right] V}{q\, C_w^{in}\, A} \qquad (4.3)$$

where t_{sat} is the time to barrier saturation in days, ϕ is the soil porosity, ρ_b is the soil bulk density in g/m^3, C_w^{in} is the aqueous contaminant concentration entering the barrier in g/m^3, K_f and n_f are the Freundlich parameters, f_{PAC} is the fraction of PAC in the barrier, q is the groundwater specific flux in m/day, V is the volume of the PAC barrier in m^3 and A is the cross-sectional area perpendicular to the direction of flow in m^2. If biodegradation occurs following placement of the PAC barrier, a biofilm will develop over time on the surface of PAC as demonstrated in this research, and PAC sorption sites will be blocked and the rate of mass transfer into the PAC will decrease (Hutchinson & Robinson, 1990). Once a biofilm has sufficiently developed, and assuming that biodegradation rates are less than equilibrium sorption kinetics and the mass loading to the barrier, the contaminant residence time in the PAC barrier would be insufficient for significant biodegradation to occur. As a result, sorption equilibrium will be obtained subject to the biofilm impacted

sorption conditions and breakthrough will occur. Of interest is the percent reduction in t_{sat} of a bio-coated PAC once the above conditions have been established.

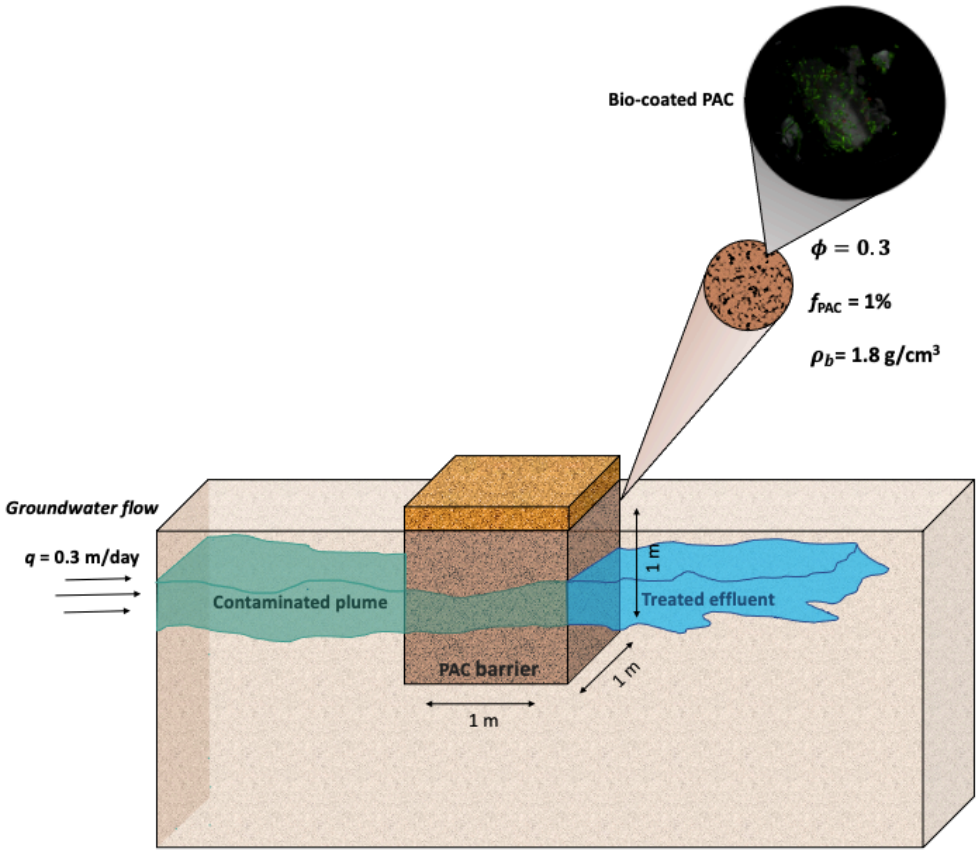

Figure 4.22. Schematic of the simulated PAC barrier.

Figure 4.23 illustrates the percent reduction in t_{sat} for a bio-coated PAC as a function of the aqueous concentration entering the barrier relative to a fresh PAC using the system parameters shown on Figure 4.22. The t_{sat} for the fresh PAC was calculated using the Freundlich parameters obtained from the best fit isotherm (Table 4.3). Similarly, the t_{sat} for the bio-coated PAC was calculated using the Freundlich parameters obtained from the isotherm best fit for the Day-180 PAC (Table 4.3) with "time zero" assumed to be the time when biofilm had been sufficiently developed. The percent reduction in t_{sat} of the bio-coated PAC was then estimated by comparing it to t_{sat} of the fresh PAC. This simple analyses

ignores: (1) the time interval between PAC placement and sufficient biofilm development to occur, (2) mass loss due to biodegradation, and (3) the enhanced biodegradation rate of the mature biofilm.

As expected, the time to breakthrough of the PAC barrier deteriorated with biofilm formation with a greater impact at lower concentrations. However, the reduction in t_{sat} estimated here does not necessarily imply a long-term degradation in treatment since biodegradation mechanisms are expected to be fully established. The long-term dominant contaminant removal mechanism is expected to be biodegradation, and a minor loss of sorption capacity should not be detrimental. Thus, complete PAC regeneration would not be required to sustain barrier treatment. Unfortunately, field data to support this conceptual model are not yet available.

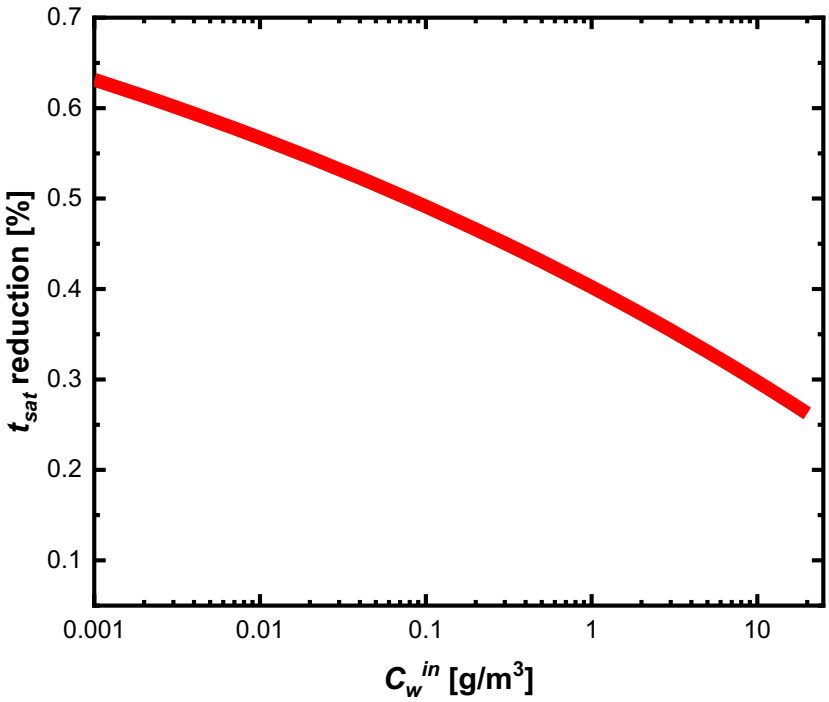

Figure 4.23. Percent reduction in the breakthrough time (t_{sat}) of a bio-coated PAC compared to breakthrough time (t_{sat}) for a fresh PAC as a function of entering concentration (C_w^{in}).

CHAPTER 5

CONCLUSIONS AND RECOMMENDATIONS

5.1 CONCLUSIONS

The change in PAC sorption characteristics for toluene was evaluated using batch sorption experiments following 180-days of biofilm formation. Baseline sorption performance on fresh PAC indicated its effectiveness to remove dissolved toluene present in artificial groundwater. The reversibility of the adsorption process was evaluated using a series of one-step desorption experiments. Results showed hysteretic behavior between adsorption and desorption as a fraction of toluene remained sorbed under equilibrium conditions.

Batch microcosms experiments were used to grow an anaerobic toluene degrading biofilm on PAC to obtain “bio-coated” PAC. CLSM was employed to evaluate the presence, growth and organization of the biofilm formation on the PAC. Cells were randomly dispersed on PAC surfaces by Day 50, and as the biofilm developed a marked increase in cell attachment was observed. The biofilm formation was heterogeneous across all PAC particles scanned. Two types of cell and EPS growth were observed: in some cases, a monolayer of cells completely covered the particles, while in other cases, a discontinuous multilayer of cells was formed. To estimate biofilm growth over time, quantitative characterization biofilm parameters (biovolume, biomass, thickness, and roughness) was determined. The findings demonstrated a consistent growth of biofilm on the PAC that was characteristically heterogeneous with high variability between PAC particles.

Data collected from the microcosm experiments also served to evaluate the simultaneous sorption, desorption and biodegradation of toluene in the presence of active microbial degraders. Initially, the majority of toluene mass added was quickly partitioned to the PAC

which decreased the toluene concentration in the aqueous phase. The active toluene degrading microbiota decreased the aqueous toluene concentration and promoted desorption of toluene from PAC. Desorption from the PAC followed by biodegradation maintained low aqueous concentrations of toluene. This behavior reflects the synergistic effect of microorganisms and the adsorptive capacity of PAC to maintain dissolved concentrations at lower levels.

Desorption of toluene should have contributed to the recovery of the sorption capacity of PAC; however, a biofilm was formed, and a loss of sorption capacity was observed. The change in PAC sorption characteristics was investigated with samples of the “bio-coated” PAC at two time points of biofilm formation (Day 80 and Day 180). The noted decrease of adsorption capacity over time appears to be a result of a combination of blocking of the PAC pores with biomass, and the sorption of microbial decay products and metabolites.

This research clearly illustrated that PAC is an efficient growth surface for microbes to form biofilms. Since PAC sorption capacity is reduced in the presence of biofilms and a reduction in the system breakthrough performance is expected, especially at lower concentrations, the long-term effectiveness of CBI systems for the treatment of PHC plumes will be impacted. The changing sorption characteristics of the PAC will alter the synergistic interplay between sorption, desorption and biodegradation. At the moment, the role that biofilm formation plays in CBI system performance in situ is limited, and the results from this research offer a glimpse into the impact of biofilm formation on sorption, albeit a bench-scale study. Until our understanding matures, the underlying mechanisms occurring in a CBI barrier for PHC treatment will remain unclear.

5.2 RECOMMENDATIONS

This research focused on evaluating the impact of biofilm formation on PAC sorption characteristics for PHCs (e.g., toluene) under controlled bench scale conditions using a well-studied enrichment culture. Under these ideal conditions it was observed that PAC sorption capacity was reduced after biofilm growth. However, the change in sorption capacity of PAC amendments in situ after prolonged exposure to native microbiota and natural organic matter (NOM) is unknown.

Although groundwater tends to have low NOM concentrations, its presence will further impact the PAC sorption capacity to PHCs by blocking external pores and competing for sorption sites. Native microbiota is more likely to outcompete the laboratory enrichment cultures (characterized by its slow growth) for attachment to PAC surfaces and grow extensive biofilms. It is speculated that these two factors would cause the sorption capacity of PAC to quickly diminish, thus further impacting the long-term effectiveness of CBI systems.

To assess biofilm growth on PAC by native microbiota, core samples should be extracted from operational CBI barriers and subjected to CLSM biofilm characterization methods to assess growth under natural conditions. Furthermore, sorption experiments using field-aged PAC sediments, and fresh PAC amended sediments should be conducted. These results would aid in our understanding of the impact of biofilms and other competing sorbates on changes in the of performance of PAC systems in situ.

In addition, microbial characterization (molecular biology markers) would be useful to compare the community structure between PAC zones (treatment zones) and untreated zones, to determine if PAC contributes to the enrichment of PHCs degraders in the treatment zone. The presence of a larger biomass of microbial degraders in the treatment zone is essential for the long-term functioning of a CBI system. As demonstrated in this

research, the sorption capacity is reduced in the presence of a biofilm, thus active microbial PHCs degraders in PAC biofilms should be present in larger proportion to compensate for the decrease in PAC sorption performance for a successful treatment of PHCs using a CBI system.

REFERENCES

Adams, G. O., Fufeyin, P. T., Okoro, S. E., & Ehinomen, I. (2015). Bioremediation, Biostimulation and Bioaugmention: A Review. *International Journal of Environmental Bioremediation & Biodegradation*, *3*(1), 28–39. https://doi.org/10.12691/ijebb-3-1-5

Agency for Toxic Substances and Disease Registry (ATSDR). (2004). Interaction profile for Benzene , Toluene , Ethylbenzene , and Xylenes (BTEX). In *U.S. Department of Health and Human Services, Public Health Service* (Issue May).

Ahmad, I., & Husain, F. M. (2017). Biofilms in Plant and Soil Health. In *Biofilms in Plant and Soil Health*. https://doi.org/10.1002/9781119246329

Aksoy, M. (1989). Hematotoxicity and carcinogenicity of inhaled benzene. *Environmental Health Perspectives*, *82*(1), 97–108. https://doi.org/10.1289/ehp.898297

Aktaş, Ö., & Çeçen, F. (2007). Bioregeneration of activated carbon: A review. *International Biodeterioration and Biodegradation*, *59*(4), 257–272. https://doi.org/10.1016/j.ibiod.2007.01.003

Albert, O. N., Amaratunga, D., & Haigh, R. P. (2018). Environmental Policies within the Context of Compensation for Oil Spill Disaster Impacts: A Literature Synthesis. *Procedia Engineering*, *212*(2017), 1179–1186. https://doi.org/10.1016/j.proeng.2018.01.152

Alegbeleye, O. O., Opeolu, B. O., & Jackson, V. A. (2017). Polycyclic Aromatic Hydrocarbons: A Critical Review of Environmental Occurrence and Bioremediation. *Environmental Management*, *60*(4), 758–783. https://doi.org/10.1007/s00267-017-0896-2

Allen, M. J., Edberg, S. C., & Reasoner, D. J. (2004). Heterotrophic plate count bacteria - What is their significance in drinking water? *International Journal of Food Microbiology*. https://doi.org/10.1016/j.ijfoodmicro.2003.08.017

Alquwaizany, A. S., Alfadul, S. M., Khan, M. A., & Alabdulaaly, A. I. (2019). Occurrence of organic compounds in groundwater of Saudi Arabia. *Environmental Monitoring and Assessment*, *191*(10). https://doi.org/10.1007/s10661-019-7723-6

Artyushkova, K., Roizman, D., Santoro, C., Doyle, L. E., Fatima Mohidin, A., Atanassov, P., & Marsili, E. (2016). Anodic biofilms as the interphase for electroactive bacterial growth on carbon veil. *Biointerphases*, *11*(3), 031013. https://doi.org/10.1116/1.4962264

Asahi, Y., Miura, J., Tsuda, T., Kuwabata, S., Tsunashima, K., Noiri, Y., Sakata, T., Ebisu, S., & Hayashi, M. (2015). Simple observation of Streptococcus mutans biofilm by scanning electron microscopy using ionic liquids. *AMB Express*. https://doi.org/10.1186/s13568-015-0097-4

ATSDR. (2015). Draft Toxicological Profile for Toluene. *U.S. Department of Health and Human Services*, *4*(September), 359–365. https://doi.org/http://www.atsdr.cdc.gov/toxprofiles/tp18.pdf

Ayotamuno, M. J., Kogbara, R. B., Ogaji, S. O. T., & Probert, S. D. (2006). Petroleum contaminated ground-water: Remediation using activated carbon. *Applied Energy*, *83*(11), 1258–1264. https://doi.org/10.1016/j.apenergy.2006.01.004

Azeredo, J., Azevedo, N. F., Briandet, R., Cerca, N., Coenye, T., Costa, A. R., Desvaux, M., Di

Bonaventura, G., Hébraud, M., Jaglic, Z., Kačániová, M., Knøchel, S., Lourenço, A., Mergulhão, F., Meyer, R. L., Nychas, G., Simões, M., Tresse, O., & Sternberg, C. (2017). Critical review on biofilm methods. In *Critical Reviews in Microbiology*. https://doi.org/10.1080/1040841X.2016.1208146

Balseiro-Romero, M., Monterroso, C., & Casares, J. J. (2018). Environmental Fate of Petroleum Hydrocarbons in Soil: Review of Multiphase Transport, Mass Transfer, and Natural Attenuation Processes. *Pedosphere*, *28*(6), 833–847. https://doi.org/10.1016/S1002-0160(18)60046-3

Banagan, B. L., Wertheim, B. M., Roth, M. J. S., & Caslake, L. F. (2010). Microbial strengthening of loose sand. *Letters in Applied Microbiology*. https://doi.org/10.1111/j.1472-765X.2010.02872.x

Bandosz, T. J. (2006). Activated Carbon Surfaces in Environmental Remediation. In *Interface Science and Technology* (Vol. 7, Issue C). https://doi.org/10.1016/S1573-4285(06)80013-X

Bansal, R., & Goyal, M. (2005). *Activated Carbon Adsorption - Roop Chand Bansal, Meenakshi Goyal - Google Books*. https://books.google.ca/books?hl=en&lr=&id=VUluBwAAQBAJ&oi=fnd&pg=PP1&dq=activated+carbon&ots=gsPco6oTaC&sig=A-SvkgATHKkx73YSKJvIEd4gWTY#v=onepage&q=activated carbon&f=false

BB&A. (2015). *BOS 200® CASE STUDIES* (Vol. 97408, Issue 541).

Belvederesi, C., Thompson, M. S., & Komers, P. E. (2018). Statistical analysis of environmental consequences of hazardous liquid pipeline accidents. *Heliyon*, *4*(11), e00901. https://doi.org/10.1016/j.heliyon.2018.e00901

Besemer, K. (2015). Biodiversity, community structure and function of biofilms in stream ecosystems. *Research in Microbiology*, *166*(10), 774–781. https://doi.org/10.1016/j.resmic.2015.05.006

Bewley, R. J. F., & Webb, G. (2001). In situ bioremediation of groundwater contaminated with phenols, BTEX and PAHs using nitrate as electron acceptor. *Land Contamination and Reclamation*, *9*(4), 335–347. https://doi.org/10.2462/09670513.600

Bogino, P., Oliva, M., Sorroche, F., & Giordano, W. (2013). The Role of Bacterial Biofilms and Surface Components in Plant-Bacterial Associations. *International Journal of Molecular Sciences*, *14*(8), 15838–15859. https://doi.org/10.3390/ijms140815838

Caizán-Juanarena, L., Krug, J. R., Vergeldt, F. J., Kleijn, J. M., Velders, A. H., Van As, H., & Ter Heijne, A. (2019). 3D biofilm visualization and quantification on granular bioanodes with magnetic resonance imaging. *Water Research*, *167*. https://doi.org/10.1016/j.watres.2019.115059

Canzano, S., Capasso, S., Di Natale, M., Erto, A., Iovino, P., & Musmarra, D. (2014). Remediation of groundwater polluted by aromatic compounds by means of adsorption. *Sustainability (Switzerland)*, *6*(8), 4807–4822. https://doi.org/10.3390/su6084807

Capozzi, S. L., Bodenreider, C., Prieto, A., Payne, R. B., Sowers, K. R., & Kjellerup, B. V. (2019a). Colonization and growth of dehalorespiring biofilms on carbonaceous sorptive amendments. *Biofouling*, *35*(1), 50–58. https://doi.org/10.1080/08927014.2018.1563892

Capozzi, S. L., Bodenreider, C., Prieto, A., Payne, R. B., Sowers, K. R., & Kjellerup, B. V. (2019b). Colonization and growth of dehalorespiring biofilms on carbonaceous sorptive amendments. *Biofouling*, *35*(1), 50–58. https://doi.org/10.1080/08927014.2018.1563892

Carrel, M., Morales, V. L., Beltran, M. A., Derlon, N., Kaufmann, R., Morgenroth, E., & Holzner, M. (2018). Biofilms in 3D porous media: Delineating the influence of the pore network geometry, flow and mass transfer on biofilm development. *Water Research*, *134*, 280–291. https://doi.org/10.1016/j.watres.2018.01.059

Çeçen, F., & Aktaş, Ö. (2011). Activated Carbon for Water and Wastewater Treatment: Integration of Adsorption and Biological Treatment. In *Activated Carbon for Water and Wastewater Treatment: Integration of Adsorption and Biological Treatment*. John Wiley & Sons. https://doi.org/10.1002/9783527639441

CEPA. (1992). Toluene - Priority substances list assessment report no. 4. In *Canadian Environmental Protection Act* (Vol. 4, Issue 1). https://doi.org/10.1007/BF02937017

CEPA. (1993). *Xylenes (Priority substances list assessment report)*.

Cerca, F., Trigo, G., Correia, A., Cerca, N., Azeredo, J., & Vilanova, M. (2011). SYBR green as a fluorescent probe to evaluate the biofilm physiological state of staphylococcus epidermidis, using flow cytometry. *Canadian Journal of Microbiology*. https://doi.org/10.1139/w11-078

Chapelle, F. H. (1999). Bioremediation of petroleum hydrocarbon-contaminated ground water: The perspectives of history and hydrology. *Ground Water*, *37*(1), 122–132. https://doi.org/10.1111/j.1745-6584.1999.tb00965.x

Characklis, W. G., & Wilderer, P. A. (1989). The structure and function of biofilms. *The Structure and Function of Biofilms*.

Chatzopoulos, D., Varma, A., & Irvine, R. L. (1993). Activated carbon adsorption and desorption of toluene in the aqueous phase. *AIChE Journal*, *39*(12), 2027–2041. https://doi.org/10.1002/aic.690391213

Chiu, H. Y., Verpoort, F., Liu, J. K., Chang, Y. M., & Kao, C. M. (2017). Using intrinsic bioremediation for petroleum–hydrocarbon contaminated groundwater cleanup and migration containment: Effectiveness and mechanism evaluation. *Journal of the Taiwan Institute of Chemical Engineers*, *72*, 53–61. https://doi.org/10.1016/j.jtice.2017.01.002

Clark, C. (2016). *What is BTEX?* Gulf Coast Environmental Systems.

Combarros, R. G., Rosas, I., Lavín, A. G., Rendueles, M., & Díaz, M. (2014). Influence of biofilm on activated carbon on the adsorption and biodegradation of salicylic acid in wastewater. *Water, Air, and Soil Pollution*, *225*(2). https://doi.org/10.1007/s11270-013-1858-9

Corapcioglu, M. Y., & Baehr, A. L. (2011). *Unsaturated Zone*. *23*, 941–941. https://doi.org/10.1007/978-90-481-3585-1_872

Cunningham, J. A., Rahme, H., Hopkins, G. D., Lebron, C., & Reinhard, M. (2001). Enhanced in situ bioremediation of BTEX-contaminated groundwater by combined injection of nitrate and sulfate. *Environmental Science and Technology*, *35*(8), 1663–1670. https://doi.org/10.1021/es001722t

Dada, A. O., Olalekan, A. P., & Olatunya, A. M. (2012). Langmuir, Freundlich, Temkin and

Dubinin–Radushkevich Isotherms Studies of Equilibrium Sorption of Zn 2+ Unto Phosphoric Acid Modified Rice Husk. *IOSR Journal of Applied Chemistry*, *3*(1), 38–45. https://doi.org/10.9790/5736-0313845

Daifullah, A. A. M., & Girgis, B. S. (2003). Impact of surface characteristics of activated carbon on adsorption of BTEX. *Colloids and Surfaces A: Physicochemical and Engineering Aspects*, *214*(1–3), 181–193. https://doi.org/10.1016/S0927-7757(02)00392-8

De Jonge, R. J., Breure, A. M., & Van Andel, J. G. (1996). Reversibility of adsorption of aromatic compounds onto powdered activated carbon (PAC). *Water Research*, *30*(4), 883–892. https://doi.org/10.1016/0043-1354(95)00248-0

Do Rego, E. C. P., & Pereira Netto, A. D. (2007). PAHs and BTEX in groundwater of gasoline stations from Rio de Janeiro City, Brazil. *Bulletin of Environmental Contamination and Toxicology*, *79*(6), 660–664. https://doi.org/10.1007/s00128-007-9300-x

Doll, K., Jongsthaphongpun, K. L., Stumpp, N. S., Winkel, A., & Stiesch, M. (2016). Quantifying implant-associated biofilms: Comparison of microscopic, microbiologic and biochemical methods. *Journal of Microbiological Methods*. https://doi.org/10.1016/j.mimet.2016.07.016

Donlan, R. M. (2002). Biofilms: Microbial life on surfaces. In *Emerging Infectious Diseases* (Vol. 8, Issue 9, pp. 881–890). Centers for Disease Control and Prevention (CDC). https://doi.org/10.3201/eid0809.020063

Drago, L., Agrappi, S., Bortolin, M., Toscano, M., Romanò, C. L., & De Vecchi, E. (2016). How to study biofilms after microbial colonization of materials used in orthopaedic implants. *International Journal of Molecular Sciences*, *17*(3). https://doi.org/10.3390/ijms17030293

Duffy, J. J., Peake, E., & Mohtadi, M. F. (1980). Oil spills on land as potential sources of groundwater contamination. *Environment International*, *3*(2), 107–120. https://doi.org/10.1016/0160-4120(80)90045-8

Edwards, E. A., & Grbic-Galic, D. (1994). Anaerobic degradation of toluene and o-xylene by a methanogenic consortium. *Applied and Environmental Microbiology*, *60*(1), 313–322. https://doi.org/10.1128/aem.60.1.313-322.1994

EIA. (2019). *Use of oil - U.S. Energy Information Administration (EIA)*. https://www.eia.gov/energyexplained/oil-and-petroleum-products/use-of-oil.php

EIA. (2020). Short-Term Energy Outlook April 2020. In *US EIA - Short-Term Energy Outlook* (Issue April 2020). https://doi.org/10.1136/bmjopen-2015-008636

EPA. (1999). Understanding Oil Spills And Oil Spill Response - Understanding Oil Spills In Freshwater Environments. *Chapter 8 - Response to Oil Spills*, *December*, 37-44p.

Everett, D. H. (1971). Manual of Symbols and Terminology for Physicochemical Quantities and Units, Appendix II: Definitions, Terminology and Symbols in Colloid and Surface Chemistry. *Pure and Applied Chemistry*, 577–638. https://doi.org/10.1351/pac197231040577

Faisal, A. A. H., Sulaymon, A. H., & Khaliefa, Q. M. (2018). A review of permeable reactive barrier as passive sustainable technology for groundwater remediation. *International Journal of Environmental Science and Technology*, *15*(5), 1123–1138. https://doi.org/10.1007/s13762-017-1466-0

Fan, D., Gilbert, E. J., & Fox, T. (2017). Current state of in situ subsurface remediation by activated carbon-based amendments. *Journal of Environmental Management*, *204*, 793–803. https://doi.org/10.1016/j.jenvman.2017.02.014

Farhadian, M., Vachelard, C., Duchez, D., & Larroche, C. (2008). In situ bioremediation of monoaromatic pollutants in groundwater: A review. *Bioresource Technology*, *99*(13), 5296–5308. https://doi.org/10.1016/j.biortech.2007.10.025

Fayemiwo, O. M., Daramola, M. O., & Moothi, K. (2017). Btex compounds in water – future trends and directions for water treatment. *Water SA*, *43*(4), 602–613. https://doi.org/10.4314/wsa.v43i4.08

Ficker, M., Krastel, K., Orlicky, S., & Edwards, E. (1999). Molecular characterization of a toluene-degrading methanogenic consortium. *Applied and Environmental Microbiology*, *65*(12), 5576–5585. https://doi.org/10.1128/aem.65.12.5576-5585.1999

Filley, C. M., Halliday, W., & Kleinschmidt-DeMasters, B. K. (2004). The Effects of Toluene on the Central Nervous System. In *Journal of Neuropathology and Experimental Neurology* (Vol. 63, Issue 1, pp. 1–12). https://doi.org/10.1093/jnen/63.1.1

Fröls, S., Dyall-Smith, M., & Pfeifer, F. (2012). Biofilm formation by haloarchaea. *Environmental Microbiology*, *14*(12), 3159–3174. https://doi.org/10.1111/j.1462-2920.2012.02895.x

Garny, K., Neu, T. R., Horn, H., Volke, F., & Manz, B. (2010). Combined application of 13C NMR spectroscopy and confocal laser scanning microscopy-Investigation on biofilm structure and physico-chemical properties. *Chemical Engineering Science*, *65*(16), 4691–4700. https://doi.org/10.1016/j.ces.2010.05.013

Gomes, L. C., & Mergulhão, F. J. (2017). SEM analysis of surface impact on biofilm antibiotic treatment. *Scanning*. https://doi.org/10.1155/2017/2960194

Gong, Y., Zhao, X., Cai, Z., O'Reilly, S. E., Hao, X., & Zhao, D. (2014). A review of oil, dispersed oil and sediment interactions in the aquatic environment: Influence on the fate, transport and remediation of oil spills. *Marine Pollution Bulletin*, *79*(1–2), 16–33. https://doi.org/10.1016/j.marpolbul.2013.12.024

González-Machado, C., Capita, R., Riesco-Peláez, F., & Alonso-Calleja, C. (2018). Visualization and quantification of the cellular and extracellular components of salmonella agona biofilms at different stages of development. *PLoS ONE*, *13*(7). https://doi.org/10.1371/journal.pone.0200011

González-Rivas, F., Ripolles-Avila, C., Fontecha-Umaña, F., Ríos-Castillo, A. G., & Rodríguez-Jerez, J. J. (2018). Biofilms in the Spotlight: Detection, Quantification, and Removal Methods. *Comprehensive Reviews in Food Science and Food Safety*. https://doi.org/10.1111/1541-4337.12378

Goss, M. J., Barry, D. A. J., & Rudolph, D. L. (1998). Contamination in Ontario farmstead domestic wells and its association with agriculture: 1. Results from drinking water wells. *Journal of Contaminant Hydrology*, *32*(3–4), 267–293. https://doi.org/10.1016/S0169-7722(98)00054-0

Griebler, C., & Lueders, T. (2009). Microbial biodiversity in groundwater ecosystems. *Freshwater Biology*, *54*(4), 649–677. https://doi.org/10.1111/j.1365-2427.2008.02013.x

Griebler, C., Mindl, B., Slezak, D., & Geiger-Kaiser, M. (2002). Distribution patterns of attached and suspended bacteria in pristine and contaminated shallow aquifers studied with an in situ sediment exposure microcosm. *Aquatic Microbial Ecology*, *28*(2), 117–129. https://doi.org/10.3354/ame028117

Harp, T. A. (2009). Case studies: Closing solvent sites using activated carbon impregnated with iron. *Contaminated Soils, Sediments and Water*, *14*(January), 217–228.

Health Canada. (2012). Guidance on the Use of Heterotrophic Plate Counts in Canadian Drinking Water Supplies. *Water. Air and Climate Change Bureau, Healthy Environments and Consumer Safety Branch, Health Canada, Ottawa, Ontario*.

Health Canada (HC). (2006). Guidelines for Canadian drinking water quality: guideline technical document - arsenic. In *Water Quality and Health Bureau, Healthy Environments and Consumer Safety Branch*. https://doi.org/10.1016/j.scitotenv.2009.04.006

Henini, M. (2000). Scanning electron microscopy: An introduction. *III-Vs Review*. https://doi.org/10.1016/S0961-1290(00)80006-X

Hindarso, H., Ismadji, S., Wicaksana, F., Mudjijati, & Indraswati, N. (2001). Adsorption of benzene and toluene from aqueous solution onto granular activated carbon. *Journal of Chemical and Engineering Data*, *46*(4), 788–791. https://doi.org/10.1021/je000176g

Huff, J., Chan, P., & Melnick, R. (2010). Clarifying carcinogenicity of ethylbenzene. In *Regulatory Toxicology and Pharmacology* (Vol. 58, Issue 2, pp. 167–169). Academic Press. https://doi.org/10.1016/j.yrtph.2010.08.011

Hutchinson, D. H., & Robinson, C. W. (1990). A microbial regeneration process for granular activated carbon-II. regeneration studies. *Water Research*, *24*(10), 1217–1223. https://doi.org/10.1016/0043-1354(90)90044-7

IARC. (2012). Chemical agents and related occupations. *IARC Monographs on the Evaluation of Carcinogenic Risks to Humans / World Health Organization, International Agency for Research on Cancer*, *100*(Pt F), 9–562.

(IRIS), U. E. (2017). *Benzene (CASRN 71-43-2) | IRIS | US EPA*. http://www.epa.gov/iris/subst/0276.htm

Ivshina, I. B., Kuyukina, M. S., Krivoruchko, A. V., Elkin, A. A., Makarov, S. O., Cunningham, C. J., Peshkur, T. A., Atlas, R. M., & Philp, J. C. (2015). Oil spill problems and sustainable response strategies through new technologies. *Environmental Sciences: Processes and Impacts*, *17*(7), 1201–1219. https://doi.org/10.1039/c5em00070j

Joel, O., & Amajuoyi, C. (2010). Physicochemical Characteristics and Microbial Quality of an Oil Polluted Site in Gokana, Rivers State. *Journal of Applied Sciences and Environmental Management*, *13*(3). https://doi.org/10.4314/jasem.v13i3.55373

Johnson, S. J., Woolhouse, K. J., Prommer, H., Barry, D. A., & Christofi, N. (2003). Contribution of anaerobic microbial activity to natural attenuation of benzene in groundwater. *Engineering Geology*, *70*(3–4), 343–349. https://doi.org/10.1016/S0013-7952(03)00102-9

Kaláb, M., Yang, A.-F., & Chabot, D. (2008). Conventional Scanning Electron Microscopy of Bacteria. *Infocus Magazine*. https://doi.org/10.22443/rms.inf.1.33

Kalmykova, Y., Moona, N., Strömvall, A. M., & Björklund, K. (2014). Sorption and

degradation of petroleum hydrocarbons, polycyclic aromatic hydrocarbons, alkylphenols, bisphenol A and phthalates in landfill leachate using sand, activated carbon and peat filters. *Water Research*, *56*(0), 246–257. https://doi.org/10.1016/j.watres.2014.03.011

Karwautz, C. (2015). *Microbial Biofilms in Groundwater Ecosystems*.

Kershaw, D. S. (1996). *BTEX Removal from Ground . Water Using Ground Tire Rubber*.

Kerstens, M., Boulet, G., Van kerckhoven, M., Clais, S., Lanckacker, E., Delputte, P., Maes, L., & Cos, P. (2015). A flow cytometric approach to quantify biofilms. *Folia Microbiologica*. https://doi.org/10.1007/s12223-015-0400-4

Kim, G. W., Hong, J. Y., Yu, S. Y., Ahn, J. J., Kim, Y., Son, S. W., Park, J. T., & Hwang, S. Y. (2015). Integrative analyses of differential gene expression and DNA methylation of ethylbenzene-exposed workers. *Biochip Journal*, *9*(3), 259–267. https://doi.org/10.1007/s13206-015-9310-4

Klimenko, N. A., Marutovsky, R. M., Pidlisnyuk, V. V., Nevinnaya, L. V., Smolin, S. K., Kohlmann, J., & Radeke, K.-H. (2002). Biosorption Processes for Natural and Wastewater Treatment – Part 1: Literature Review. *Engineering in Life Sciences*, *2*(10), 317–324. https://doi.org/10.1002/1618-2863(20021008)2:10<317::aid-elsc317>3.0.co;2-m

Klimenko, N., Smolin, S., Grechanyk, S., Kofanov, V., Nevynna, L., & Samoylenko, L. (2003). Bioregeneration of activated carbons by bacterial degraders after adsorption of surfactants from aqueous solutions. *Colloids and Surfaces A: Physicochemical and Engineering Aspects*, *230*(1–3), 141–158. https://doi.org/10.1016/j.colsurfa.2003.09.021

Langman, J. M. (1994). Xylene: Its toxicity, measurement of exposure levels, absorption, metabolism and clearance. *Pathology*, *26*(3), 301–309. https://doi.org/10.1080/00313029400169711

Leong, K. Y., Loo, S. L., Bashir, M. J. K., Oh, W. Da, Rao, P. V., & Lim, J. W. (2018a). Bioregeneration of spent activated carbon: Review of key factors and recent mathematical models of kinetics. *Chinese Journal of Chemical Engineering*, *26*(5), 893–902. https://doi.org/10.1016/j.cjche.2017.09.018

Leong, K. Y., Loo, S. L., Bashir, M. J. K., Oh, W. Da, Rao, P. V., & Lim, J. W. (2018b). Bioregeneration of spent activated carbon: Review of key factors and recent mathematical models of kinetics. *Chinese Journal of Chemical Engineering*, *26*(5), 893–902. https://doi.org/10.1016/j.cjche.2017.09.018

Leusch, F., & Bartkow, M. (2010). A short primer on benzene, toluene, ethylbenzene and xylenes (BTEX) in the environment and in hydraulic fracturing fluids. PDF file on http://www.derm.qld.gov.au/environmental_management/coal-seam-gas/pdf/btex-report.pdf, accessed on the 18th of July 2011. *Smart Water Research Center*. https://www.ehp.qld.gov.au/management/coal-seam-gas/pdf/btex-report.pdf

Lewandowski, Z., Webb, D., Hamilton, M., & Harkin, G. (1999). Quantifying biofilm structure. *Water Science and Technology*. https://doi.org/10.1016/S0273-1223(99)00152-3

Lewis, T. B. (2012). *Remediating Petroleum Contaminants with Activated Carbon Injectates*. *July*.

Liu, F., Rotaru, A. E., Shrestha, P. M., Malvankar, N. S., Nevin, K. P., & Lovley, D. R. (2012). Promoting direct interspecies electron transfer with activated carbon. *Energy and Environmental Science*, *5*(10), 8982–8989. https://doi.org/10.1039/c2ee22459c

Liu, Y. (2017). *Treatment of the cyanotoxins cylindrospermopsin, microcystin-LR and anatoxin-a by activated carbon in drinking water*. University of Waterloo.

Logeshwaran, P., Megharaj, M., Chadalavada, S., Bowman, M., & Naidu, R. (2018). Petroleum hydrocarbons (PH) in groundwater aquifers: An overview of environmental fate, toxicity, microbial degradation and risk-based remediation approaches. *Environmental Technology and Innovation*, *10*, 175–193. https://doi.org/10.1016/j.eti.2018.02.001

López, D., Vlamakis, H., & Kolter, R. (2010). Biofilms. In *Cold Spring Harbor perspectives in biology* (Vol. 2, Issue 7). Cold Spring Harbor Laboratory Press. https://doi.org/10.1101/cshperspect.a000398

López, E., Schuhmacher, M., & Domingo, J. L. (2008). Human health risks of petroleum-contaminated groundwater. *Environmental Science and Pollution Research*, *15*(3), 278–288. https://doi.org/10.1065/espr2007.02.390

LTE. (2006). *Case Study: Retail Gasoline Station, Colorado- Sinclair Marketing Co.*

Lueders, T. (2017). The ecology of anaerobic degraders of BTEX hydrocarbons in aquifers. *FEMS Microbiology Ecology*, *93*(1), 1–13. https://doi.org/10.1093/femsec/fiw220

Luo, Y., Guo, W., Ngo, H. H., Nghiem, L. D., Hai, F. I., Zhang, J., Liang, S., & Wang, X. C. (2014). A review on the occurrence of micropollutants in the aquatic environment and their fate and removal during wastewater treatment. In *Science of the Total Environment* (Vols. 473–474, pp. 619–641). Elsevier. https://doi.org/10.1016/j.scitotenv.2013.12.065

Marchal, M., Briandet, R., Halter, D., Koechler, S., DuBow, M. S., Lett, M. C., & Bertin, P. N. (2011). Subinhibitory arsenite concentrations lead to population dispersal in thiomonas sp. *PLoS ONE*. https://doi.org/10.1371/journal.pone.0023181

Marsh, H., & Reinoso, F. R. (2006). *Activated Carbon - Harry Marsh, Francisco Rodríguez Reinoso - Google Books*. https://books.google.ca/books?hl=en&lr=&id=UaOXSk2vFVQC&oi=fnd&pg=PP1&dq=activated+carbon&ots=Qw0hg_IvJu&sig=HlWvh4yuP67qwn0iQLKBOBby1Cg#v=onepage&q=activated carbon&f=false

Mattot, L.S. 2007. IsoFit Documentation and User's Guide Version 1.2. https://www.eng.buffalo.edu/~lsmatott/IsoFit/IsoFitMain.html

Martin, M. J., Serra, E., Ros, A., Balaguer, M. D., & Rigola, M. (2004). Carbonaceous adsorbents from sewage sludge and their application in a combined activated sludge-powdered activated carbon (AS-PAC) treatment. *Carbon*, *42*(7), 1389–1394. https://doi.org/10.1016/j.carbon.2004.01.011

Mason, C. A., Ward, G., Abu-Salah, K., Keren, O., & Dosoretz, C. G. (2000). Biodegradation of BTEX by bacteria on powdered activated carbon. *Bioprocess Engineering*, *23*(4), 331–336. https://doi.org/10.1007/s004499900159

Massol-Deya, A. A., Whallon, J., Hickey, R. F., & Tiedje, J. M. (1995). Channel structures in aerobic biofilms of fixed-film reactors treating contaminated groundwater. *Applied and Environmental Microbiology*, *61*(2), 769–777.

https://doi.org/10.1128/aem.61.2.769-777.1995
McClaine, J. W., & Ford, R. M. (2002). Reversal of flagellar rotation is important in initial attachment of Escherichia coli to glass in a dynamic system with high- and low-ionic strength buffers. *Applied and Environmental Microbiology*, *68*(3), 1280–1289. https://doi.org/10.1128/AEM.68.3.1280-1289.2002
Middeldorp, P. J. M., Van Aalst, M. A., Rijnaarts, H. H. M., Stams, F. J. M., De Kreuk, H. F., Schraa, G., & Bosma, T. N. P. (1998). Stimulation of reductive dechlorination for in situ bioremediation of a soil contaminated with chlorinated ethenes. *Water Science and Technology*. https://doi.org/10.1016/S0273-1223(98)00240-6
Mitra, S., & Roy, P. (2011). BTEX : A Serious Ground-water Contaminant. *Research Journal of Environmental Sciences*, *5*(5), 394–398. https://doi.org/10.3923/rjes.2011.394.398
Nath, K., & Bhakhar, M. S. (2011). Microbial regeneration of spent activated carbon dispersed with organic contaminants: Mechanism, efficiency, and kinetic models. *Environmental Science and Pollution Research*, *18*(4), 534–546. https://doi.org/10.1007/s11356-010-0426-8
NHMRC, & NRMMC. (2011). *Australian Drinking Water Guidelines Paper 6 National Water Quality Management Strategy* (Issue December).
Niaz, K., Bahadar, H., Maqbool, F., & Abdollahi, M. (2015). A review of environmental and occupational exposure to xylene and its health concerns. In *EXCLI Journal* (Vol. 14, pp. 1167–1186). Leibniz Research Centre for Working Environment and Human Factors. https://doi.org/10.17179/excli2015-623
NIOSH. (2016). *NIOSH Pocket Guide to Chemical Hazards Tetrachloroethylene*. Centers for Disease Control and Prevention. https://www.cdc.gov/niosh/npg/npgd0049.html
Onwurah, E., Ogugua, N., Onyike, N., Ochonogor, E., & Otitoju, O. F. (2007). Crude Oil Spills in the En. *International Journal of Environmental Research*, *1*(4), 307–320. http://citeseerx.ist.psu.edu/viewdoc/download?doi=10.1.1.899.4556&rep=rep1&type=pdf
Phelps, C. D., & Young, L. Y. (1999). Anaerobic biodegradation of BTEX and gasoline in various aquatic sediments. *Biodegradation*, *10*(1), 15–25. https://doi.org/10.1023/A:1008303729431
Powell, L. C., Pritchard, M. F., Ferguson, E. L., Powell, K. A., Patel, S. U., Rye, P. D., Sakellakou, S. M., Buurma, N. J., Brilliant, C. D., Copping, J. M., Menzies, G. E., Lewis, P. D., Hill, K. E., & Thomas, D. W. (2018). Targeted disruption of the extracellular polymeric network of Pseudomonas aeruginosa biofilms by alginate oligosaccharides. *Npj Biofilms and Microbiomes*, *4*(1). https://doi.org/10.1038/s41522-018-0056-3
Praveen, D. (2013). *The 10 biggest oil consuming countries*. Hydrocarbons-Technology.Com. https://www.hydrocarbons-technology.com/features/featurethe-10-biggest-oil-consuming-countries-4141632/
Purevdorj, B., Costerton, J. W., & Stoodley, P. (2002). Influence of Hydrodynamics and Cell Signaling on the Structure and Behavior of. *Society*, *68*(9), 4457–4464. https://doi.org/10.1128/AEM.68.9.4457
Putz, A. R. H., Losh, D. E., & Speitel, G. E. (2005). Removal of Nonbiodegradable Chemicals from Mixtures during Granular Activated Carbon Bioregeneration. *Journal of Environmental Engineering*, *131*(2), 196–205. https://doi.org/10.1061/(ASCE)0733-

9372(2005)131:2(196)
Quintelas, C., Silva, B., Figueiredo, H., & Tavares, T. (2010). Removal of organic compounds by a biofilm supported on GAC: Modelling of batch and column data. *Biodegradation*, *21*(3), 379–392. https://doi.org/10.1007/s10532-009-9308-5
Rashid, M. H. (2015). *Electric Renewable Energy Systems*. Academic Press. http://web.b.ebscohost.com.proxy.lib.uwaterloo.ca/ehost/ebookviewer/ebook/bmxlYmtfXzExMDQzNjZfX0FO0?sid=f03a3ae5-18da-4289-87af-1c8ebdf3a199@pdc-v-sessmgr04&vid=0&format=EB&rid=1
Rattier, M., Reungoat, J., Gernjak, W., Keller, J., & Joss, A. (2012). Investigating the role of adsorption and biodegradation in the removal of organic micropollutants during biological activated carbon filtration of treated wastewater. *Journal of Water Reuse and Desalination*, *2*(3), 127–139. https://doi.org/10.2166/wrd.2012.012
Reasoner, D. J. (2004). Heterotrophic plate count methodology in the United States. *International Journal of Food Microbiology*. https://doi.org/10.1016/j.ijfoodmicro.2003.08.008
Renner, L. D., & Weibel, D. B. (2011). Physicochemical regulation of biofilm formation. *MRS Bulletin*, *36*(5), 347–355. https://doi.org/10.1557/mrs.2011.65
Rickard, A. H., McBain, A. J., Stead, A. T., & Gilbert, P. (2004). Shear rate moderates community diversity in freshwater biofilms. *Applied and Environmental Microbiology*, *70*(12), 7426–7435. https://doi.org/10.1128/AEM.70.12.7426-7435.2004
Riley, S. M., Ahoor, D. C., & Cath, T. Y. (2018). Enhanced biofiltration of O&G produced water comparing granular activated carbon and nutrients. *Science of the Total Environment*, *640–641*, 419–428. https://doi.org/10.1016/j.scitotenv.2018.05.228
Sabbagh, L.-A. (2013). *Optimization of Microbial Adsorption (Biofilm Creation) on Activated Carbon by Surface Modification of Substrate*.
Saccani, G., Bernasconi, M., & Antonelli, M. (2014). Optimization of low energy sonication treatment for granular activated carbon colonizing biomass assessment. *Environmental Technology (United Kingdom)*. https://doi.org/10.1080/09593330.2013.853698
Sartory, D. P. (2004). Heterotrophic plate count monitoring of treated drinking water in the UK: A useful operational tool. *International Journal of Food Microbiology*. https://doi.org/10.1016/j.ijfoodmicro.2003.08.006
Schmidt, T. C., Haderlein, S. B., Pfister, R., & Forster, R. (2004). Occurrence and fate modeling of MTBE and BTEX compounds in a Swiss Lake used as drinking water supply. *Water Research*, *38*(6), 1520–1529. https://doi.org/10.1016/j.watres.2003.12.027
Serrano, A., Gallego, M., & Silva, M. (2007). Enhancing sensitivity in headspace-mass spectrometric determination of BTEX in drinking water. *Analytical Chemistry*, *79*(7), 2997–3002. https://doi.org/10.1021/ac070044r
Simon, J. A. (2015). Editor's Perspective—An In Situ Revelation: First Retard Migration, Then Treat. *Remediation Journal*, *25*(2), 1–7. https://doi.org/10.1002/rem
Simpson, D. R. (2008). Biofilm processes in biologically active carbon water purification. *Water Research*, *42*(12), 2839–2848. https://doi.org/10.1016/j.watres.2008.02.025
Singh, R., Paul, D., & Jain, R. K. (2006). Biofilms: implications in bioremediation. *Trends in*

Microbiology, *14*(9), 389–397. https://doi.org/10.1016/j.tim.2006.07.001
Snyder, R. (2000). Overview of the toxicology of benzene. *Journal of Toxicology and Environmental Health - Part A*, *61*(5–6), 339–346. https://doi.org/10.1080/00984100050166334
Snyder, R. (2012). Leukemia and benzene. *International Journal of Environmental Research and Public Health*, *9*(8), 2875–2893. https://doi.org/10.7326/0003-4819-99-6-885
Song, X., Liu, H., Cheng, L., & Qu, Y. (2010). Surface modification of coconut-based activated carbon by liquid-phase oxidation and its effects on lead ion adsorption. *Desalination*, *255*(1–3), 78–83. https://doi.org/10.1016/j.desal.2010.01.011
Stoodley, P., Lewandowski, Z., Boyle, J. D., & Lappin-Scott, H. M. (1999). The formation of migratory ripples in a mixed species bacterial biofilm growing in turbulent flow. *Environmental Microbiology*, *1*(5), 447–455. https://doi.org/10.1046/j.1462-2920.1999.00055.x
Summers, Z. M., Fogarty, H. E., Leang, C., Franks, A. E., Malvankar, N. S., & Lovley, D. R. (2010). Direct exchange of electrons within aggregates of an evolved syntrophic coculture of anaerobic bacteria. *Science*, *330*(6009), 1413–1415. https://doi.org/10.1126/science.1196526
Sutherland, I. W. (2001). The biofilm matrix - An immobilized but dynamic microbial environment. *Trends in Microbiology*, *9*(5), 222–227. https://doi.org/10.1016/S0966-842X(01)02012-1
Thongplang, J. (2016). *What is BTEX and why is it important?* Aeroqual.
Toole, G. O., Kaplan, H. B., & Kolter, R. (2000). *B f m d*. 49–79.
Toth, C. R. A. (2017). *Characterizing and accelerating methanogenic hydrocarbon biodegradation*. https://doi.org/10.5072/PRISM/25297
Trevors, J. T. (2011). Hypothesized origin of microbial life in a prebiotic gel and the transition to a living biofilm and microbial mats. In *Comptes Rendus - Biologies* (Vol. 334, Issue 4, pp. 269–272). Elsevier Masson SAS. https://doi.org/10.1016/j.crvi.2011.02.010
U.S.EPA. (2016). *Pelham Pipeline Spill*. United States Environmental Protection Agency. https://response.epa.gov/site/site_profile.aspx?site_id=11818
USEPA. (2018). Remedial Technology Fact Sheet – Activated Carbon- Based Technology for In Situ Remediation Introduction. *Epa 542-F-18-001*, *April*. https://www.epa.gov/sites/production/files/2018-04/documents/100001159.pdf
Van Der Mei, H. C., Atema-Smit, J., Jager, D., Langworthy, D. E., Collias, D. I., Mitchell, M. D., & Busscher, H. J. (2008). Influence of adhesion to activated carbon particles on the viability of waterborne pathogenic bacteria under flow. *Biotechnology and Bioengineering*, *100*(4), 810–813. https://doi.org/10.1002/bit.21820
Vanloocke, R., De Borger, R. D., Voets, J. P., & Verstraete, W. (1975). Soil and groundwater contamination by oil spills; problems and remedies. *International Journal of Environmental Studies*, *8*(1–4), 99–111. https://doi.org/10.1080/00207237508709721
Vidali, M. (2001). Bioremediation. An overview. *Pure and Applied Chemistry*, *73*(7), 1163–1172. https://doi.org/10.1351/pac200173071163
Vinitnantharat, S., Baral, A., Ishibashi, Y., & Ha, S. R. (2001). Quantitative bioregeneration

of granular activated carbon loaded with phenol and 2,4-dichlorophenol. *Environmental Technology (United Kingdom)*, *22*(3), 339–344. https://doi.org/10.1080/09593332208618288

Voice, T. C., Pak, D., Zhao, X., Shi, J., & Hickey, R. F. (1992). Biological activated carbon in fluidized bed reactors for the treatment of groundwater contaminated with volatile aromatic hydrocarbons. *Water Research*, *26*(10), 1389–1401. https://doi.org/10.1016/0043-1354(92)90132-N

Vuotto, C., & Donelli, G. (2014). Field emission scanning electron microscopy of biofilm-growing bacteria involved in nosocomial infections. *Methods in Molecular Biology*. https://doi.org/10.1007/978-1-4939-0467-9_6

Waller, S. A., Packman, A. I., & Hausner, M. (2018). Comparison of biofilm cell quantification methods for drinking water distribution systems. *Journal of Microbiological Methods*. https://doi.org/10.1016/j.mimet.2017.10.013

Washer, C. E., & Edwards, E. A. (2007). Identification and expression of benzylsuccinate synthase genes in a toluene-degrading methanogenic consortium. *Applied and Environmental Microbiology*, *73*(4), 1367–1369. https://doi.org/10.1128/AEM.01904-06

Weaver, L., Webber, J. B., Hickson, A. C., Abraham, P. M., & Close, M. E. (2015). Biofilm resilience to desiccation in groundwater aquifers: A laboratory and field study. *Science of the Total Environment*, *514*, 281–289. https://doi.org/10.1016/j.scitotenv.2014.10.031

Weelink, S. A. B., van Eekert, M. H. A., & Stams, A. J. M. (2010). Degradation of BTEX by anaerobic bacteria: Physiology and application. *Reviews in Environmental Science and Biotechnology*, *9*(4), 359–385. https://doi.org/10.1007/s11157-010-9219-2

Westall, F., Walsh, M. M., Toporski, J., & Steele, A. (2003). Fossil Biofilms and the Search for Life on Mars. In *Fossil and Recent Biofilms* (pp. 447–465). Springer Netherlands. https://doi.org/10.1007/978-94-017-0193-8_32

Whitacre, D. M. (2010). *Reviews of environmental contamination and toxicology. Vol. 203*. Springer.

WHO. (2003a). *Benzene in Drinking-water Background document for development of WHO Guidelines for Drinking-water Quality*. https://doi.org/WHO/SDE/WSH/03.04/24

WHO. (2003b). *Ethylbenzene in Drinking-water Background document for development of WHO Guidelines for Drinking-water Quality*. https://doi.org/WHO/SDE/WSH/03.04/26

WHO. (2003c). *Toluene in Drinking-water Background document for development of WHO Guidelines for Drinking-water Quality*. https://doi.org/WHO/SDE/WSH/03.04/116

WHO. (2003d). *Xylenes in drinking-water. Background document for preparation of WHO Guidelines for drinking-water quality*. https://doi.org/(WHO/SDE/WSH/03.04/25)

Wiedemeier, T. H., Swanson, M. A., Wilson, J. T., Kampbell, D. H., Miller, R. N., & Hansen, J. E. (1996). Approximation of biodegradation rate constants for monoaromatic hydrocarbons (BTEX) in ground water. *Ground Water Monitoring and Remediation*, *16*(3), 186–194. https://doi.org/10.1111/j.1745-6592.1996.tb00149.x

Wilhartitz, I. C., Kirschner, A. K. T., Stadler, H., Herndl, G. J., Dietzel, M., Latal, C., MacH, R. L., & Farnleitner, A. H. (2009). Heterotrophic prokaryotic production in

ultraoligotrophic alpine karst aquifers and ecological implications. *FEMS Microbiology Ecology*, *68*(3), 287–299. https://doi.org/10.1111/j.1574-6941.2009.00679.x

Williams, G. P., & Gold, L. W. (1976). Ground temperatures. *Canadian Building Digest*, *BRN-114*. https://doi.org/10.4224/40000712

Wilson, C., Lukowicz, R., Merchant, S., Valquier-Flynn, H., Caballero, J., Sandoval, J., Okuom, M., Huber, C., Brooks, T. D., Wilson, E., Clement, B., Wentworth, C. D., & Holmes, A. E. (2017). Quantitative and Qualitative Assessment Methods for Biofilm Growth: A Mini-review. *Research & Reviews. Journal of Engineering and Technology*.

Wittebol, J., & Dinkla, I. (2015). *The Use of Multiple Lines of Evidence to Substantiate Anaerobic BTEX Degradation in Groundwater*. https://doi.org/10.1007/8623_2015_165

Wlodkowic, D., Skommer, J., & Darzynkiewicz, Z. (2008). SYTO probes in the cytometry of tumor cell death. *Cytometry Part A*, *73A*(6), 496–507. https://doi.org/10.1002/cyto.a.20535

Worch, E. (2012). Adsorption Technology in Water Treatment: Fundamentals, Processes, and Modeling. In *Adsorption Technology in Water Treatment*. https://doi.org/10.1515/9783110240238

Wu, M., Dick, W. A., Li, W., Wang, X., Yang, Q., Wang, T., Xu, L., Zhang, M., & Chen, L. (2016). Bioaugmentation and biostimulation of hydrocarbon degradation and the microbial community in a petroleum-contaminated soil. *International Biodeterioration and Biodegradation*, *107*, 158–164. https://doi.org/10.1016/j.ibiod.2015.11.019

Yakout, S. M., & Daifullah, A. A. M. (2014). Adsorption/desorption of BTEX on activated carbon prepared from rice husk. *Desalination and Water Treatment*, *52*(22–24), 4485–4491. https://doi.org/10.1080/19443994.2013.821629

Yang, M., Yang, Y. S., Du, X., Cao, Y., & Lei, Y. (2013). Fate and transport of petroleum hydrocarbons in vadose zone: Compound-specific natural attenuation. *Water, Air, and Soil Pollution*, *224*(3). https://doi.org/10.1007/s11270-013-1439-y

Yang, X., Beyenal, H., Harkin, G., & Lewandowski, Z. (2000). Quantifying biofilm structure using image analysis. *Journal of Microbiological Methods*. https://doi.org/10.1016/S0167-7012(99)00097-4

Yonge, D. R., Kelnath, T. M., Poznanska, K., & Jiang, Z. P. (1985). Single-Solute Irreversible Adsorption on Granular Activated Carbon. *Environmental Science and Technology*, *19*(8), 690–694. https://doi.org/10.1021/es00138a006

Zamfirescu, D., & Grathwohl, P. (2001). Occurrence and attenuation of specific organic compounds in the groundwater plume at a former gasworks site. *Journal of Contaminant Hydrology*, *53*(3–4), 407–427. https://doi.org/10.1016/S0169-7722(01)00176-0

Zhang, R. Y., Neu, T. R., Bellenberg, S., Kuhlicke, U., Sand, W., & Vera, M. (2015). Use of lectins to in situ visualize glycoconjugates of extracellular polymeric substances in acidophilic archaeal biofilms. *Microbial Biotechnology*, *8*(3), 448–461. https://doi.org/10.1111/1751-7915.12188

Zhao, X., Hickey, R. F., & Voice, T. C. (1999). Long-term evaluation of adsorption capacity in a biological activated carbon fluidized bed reactor system. *Water Research*, *33*(13),

2983–2991. https://doi.org/10.1016/S0043-1354(99)00014-7

APPENDIX

APPENDIX 1 PROTOCOLS

In this section, it can be found the detailed steps followed for sample handling as well as recipes of the solutions used in the experimental work.

ARTIFICIAL GROUNDWATER RECIPE

Recipe for 1 L of AGW in Milli-Q® water, modified from (Middeldorp et al., 1998).

- Salt solution: *autoclave-sterilized*
- 0.05 g/L NH_4Cl (53.49 g/mol, 0.93 mM)
- 0.01 g/L $MgCl_2$ (203.31 g/mol, 0.05 mM)
- 0.0019 g/L $MnCl_2$ $4H_2O$ (197.91 g/mol, 0.0096 mM)
- 0.007 g/L NaCl (58.44 g/mol, 0.12 mM)
- 0.15 g/L $CaCl_2$ (147.02 g/mol, 1 mM)
- 0.0620 g/L $Na_2HPO_4 \bullet 2H_2O$ (141.96 g/mol, 0.43 mM)
- 0.0204 g/L KH_2PO_4 (136.09 g/mol, 0.14 mM)
- 0.009 g/L Na_2SO_4 (142.0 g/mol, 0.06 mM)
- 0.86 g/L $NaHCO_3$ (86.01 g/mol, 1 M).
  Measure pH, should be around 7.

  Add the following solutions inside the anaerobic chamber to salt solution after autoclaved and cooled.

- 2 mL of trace mineral stock solution: *autoclave-sterilized*
- 0.3 g/L of H_3BO_3
- 0.1 g/L of $ZnCl_2$
- 0.75 g/L of $NiCl_2$ - $6H_2O$
- 1.0 g/L of $MnCl_2$ - $4H_2O$
- 0.1 g/L of $CuCl_2$ - $2H_2O$
- 1.5 g/L of $CoCl_2$ - $6H_2O$
- 0.02 g/L of Na_2SeO_3
- 0.1 g/L of $Al_2(SO_4)_3$ - $16H_2O$
- 1 mL of H_2SO_4

- 3 mL of amorphous ferrous sulfide stock solution: *autoclave-sterilized*
- 39.2 g/L of $(NH_4)_2Fe\ (SO_4)_2$ - $6H_2O$
- 24.0 g/L of Na_2S - $9H_2O$

Washed three times with deionized water to remove free sulfide.

- 1 mL of redox indicator stock solution (for controls only):
- 1 g/L of resazurin

- 10 mL of Phosphate buffer stock solution: *autoclave-sterilized*
- 27.2 g/L KH_2PO_4
- 34.8 g/L K_2HPO_4

Mix salts from the salt solution recipe with MilliQ water (985 mL solution). Cap the bottle with a foam bung and autoclave at 121ºC for 40 minutes to remove oxygen and sterilize. Transfer the bottle to a bucket with ice while sparging N_2 gas (low pressure) through a sterile filter for 30 minutes. Once cooled cap tightly and bring to the anaerobic chamber.

Add 2 mL of anaerobic trace mineral solution and 3 mL of amorphous ferrous sulfide solution and 10 mL of phosphate buffer solution. Add 1 mL of redox indicator solution (for AGW used in controls only). Mix well and let stand in the anaerobic chamber for a week.

ARTIFICIAL GROUNDWATER SALT SOLUTION RECIPE

Recipe for 1 L of AGW salt solution in Milli-Q® water.

- 0.05 g/L NH_4Cl (53.49 g/mol, 0.93 mM)
- 0.01 g/L $MgCl_2$ (203.31 g/mol, 0.05 mM)
- 0.0019 g/L $MnCl_2\ 4H_2O$ (197.91 g/mol, 0.0096 mM)
- 0.007 g/L NaCl (58.44 g/mol, 0.12 mM)
- 0.15 g/L $CaCl_2$ (147.02 g/mol, 1 mM)
- 0.0620 g/L $Na_2HPO_4 \bullet 2H_2O$ (141.96 g/mol, 0.43 mM)
- 0.0204 g/L KH_2PO_4 (136.09 g/mol, 0.14 mM)
- 0.009 g/L Na_2SO_4 (142.0 g/mol, 0.06 mM)
- 0.86 g/L $NaHCO_3$ (86.01 g/mol, 1 M).
  Measure pH, should be around 7.

TOLUENE STOCK SOLUTION

Recipe for 4.5 L of toluene amended – AGW salt solution.

1. Place 4.5 L of AGW salt solution in a dispensing bottle with a Teflon coated magnetic stirrer.
2. Place the bottle on top of the stirrer at speed 8.
3. Add 250 µL of neat toluene and cap immediately, securing the cap with tape, this volume gives a final concentration of ~ 30 mg/L.
4. Leave for at least 12 h to allow toluene to dissolve completely.

TOLUENE SERIAL DILUTIONS

The next table summarize the ratio between toluene stock solution and fresh AGW salt solution needed to obtain the seven initial concentrations used for the sorption/desorption experiments.

Concentration (mg/L)	Toluene stock solution (mL)	Fresh AGW salt solution (mL)
1	40	1160
5	200	1000
10	400	800
15	600	600
20	800	400
25	1000	200
30	1200	0

BATCH SORPTION/DESORPTION EXPERIMENT PROTOCOL

1. Fill six 160 mL serum bottles containing 10 mg PAC and three 160 mL serum bottles without PAC (controls) per initial concentration without headspace and crimp with aluminum seal- Teflon silicon septa.
2. Transfer to a platform shaker and agitate at 100 rpm for 24 h.
3. Stop agitation.
4. Leave undisturbed for 24 h to allow the PAC to precipitate from the aqueous phase.

Sorption Assay and Controls (12-14)

5. Perform aqueous phase extraction for each sample.
6. Remove the remaining aqueous phase from the sorption assay bottles leaving the PAC inside.
7. Perform PAC sorbent extraction as in for each sorption assay bottle.

Desorption Assay (15-23)

8. Remove the aqueous phase from the bottles leaving the PAC inside.
9. Fill with fresh AGW salt solution and seal tightly.
10. Transfer to a platform shaker and agitate at 100 rpm for 24 h.
11. Stop agitation.
12. Leave undisturbed for 24 h to allow the PAC and the aqueous phase to separate.
13. Perform aqueous phase extraction for each sample.
14. Remove the remaining aqueous phase from the desorption assay bottles leaving the PAC inside.
15. Perform PAC sorbent extraction for each desorption assay bottle.
16. Transfer dichloromethane phase to 2 mL autosampler vials.
17. Having all extracted samples analyze in the GC-FID.

STAINING PROTOCOL

Dilutions for PAC-biofilm staining

SYTO 9

i. Store stock solution in single-use aliquots (3 µL) at -20 ºC. Avoid refreezing and thawing, store protected from light.

ii. For staining PAC samples prepare a 30 µM dilution using the 5 mM SYTO9 stock solution as provided by the manufactured (3 µL in 500 µL filter sterilized saline solution). Use 2 mL plastic Eppendorf tubes (diluted stain adheres to glass).

Concanavalin A, Alexa Fluor 633 (ConA)

i. Prepare a 5 mg/mL stock solution in 0.1 M sodium bicarbonate solution using filter sterilized water (pH 8.3), as suggested by the manufacturer. Add 1 mL of $NaHCO_3$ (0.1 M) to the lot.

iii. Store stock solution in single-use aliquots (8 µL) at -20 ºC. Avoid refreezing and thawing, store protected from light.

ii. For staining PAC samples prepare a 200 µg/mL dilution from ConA stock solution (8 µL of stock in 200 µL filter sterilized saline solution).

*Before diluting freeze stock solutions, allow solution to warm to room temperature.

Staining of PAC-biofilms

1. Remove half volume of aqueous phase from microcosms.
2. Gently swirl the remaining water plus PAC.
3. Take an aliquot of 1 mL and place it in plastic Eppendorf tubes.
4. Allow PAC to precipitate.
5. Remove the aqueous phase avoiding carry over of PAC.

6. Gently add 1 mL of filter sterilized saline solution (150 mM NaCl), allow the water to run down the tube walls to avoid strong “vortex” effect, as it might detach adhered cells.

7. Cap the tube and perform slow rotatory movements for a gentle mixing.

8. Leave undisturbed for 10 minutes as PAC precipitate.

9. Remove the aqueous phase avoiding carry over of PAC.

10. Add 500 µL of 30 µM SYTO9 solution (allow the water to run down the tube walls to avoid strong “vortex” effect).

11. Cap tube and store undisturbed in the dark.

12. Every 5 minutes gently rotate the tube to allow stain to mix with PAC.

13. After 30 min remove aqueous phase.

14. Gently add 1 mL of filter sterilized saline solution (150 mM NaCl), as in step 6.

15. Repeat steps 7,8 and 9.

16. Add 200 µL of a 200 µg/mL ConA solution.

17. Cap tube and store undisturbed in the dark.

18. Every 5 minutes gently rotate the tube to allow stain to mix with PAC.

19. After 30 min remove aqueous phase.

20. Gently add 1 mL of filter sterilized saline solution (150 mM NaCl), as in step 6.

21. Repeat steps 7,8 and 9.

22. Mount sample and observe in the microscope same day.

BIOFILM DETACHMENT PROTOCOL

1. Microcosms will be centrifuged (6000 x g, 10 min), and then the aqueous phase will be removed.
2. The PAC will be washed using 10 mL of sterile 1X phosphate-buffered saline solution (PBS) added to the microcosms and gently agitating to suspend loosely adhered cells from the biofilm.
3. Microcosms will be allowed to sit and PAC to settle.
4. Then 9 mL of the aqueous phase will be removed, and Steps 2 to 4 will be performed and additional four times.
5. The remaining 1 mL (+ PAC) will be transferred to a 2 mL centrifuge.
6. The tube will be continuously vortexed for 30 sec at full speed.
7. The sample will be sonicated at low energy (170 W, 35 kHz) for 4 min and at the end of the sonication cycle, the bulk liquid will be transferred to a clean 2 mL centrifuge tube (bulk liquid-centrifuge tube),
8. The PAC- centrifuge tube will be refilled with 1 mL PBS, and Steps 7 and will be performed an additional four times.
9. The bulk liquid-centrifuge tube will be centrifuged (6000 x g, 15 min); the supernatant will be discarded, and the cell pellet will be resuspended in 1 mL washing solution and homogenized in the vortex for 15 seconds.

APPENDIX 2 SUPPLEMENTARY MATERIAL

Table A2.1. Isotherm experimental data

Fresh PAC - Sorption								
C_0	**C_e**	**SD**	**V**	**m**	**q_e**	**SD**	**M_{PAC}**	**SD**
mg/L	mg/L	mg/L	L	g	mg/g	mg/g	mg	mg
0.876	0.038	0.007	0.160	0.010	13.415	0.107	0.127	0.003
5.185	0.812	0.075	0.160	0.010	69.270	1.191	0.686	0.028
10.380	2.977	0.046	0.160	0.010	116.120	0.721	1.189	0.034
15.510	5.584	0.132	0.160	0.010	158.816	2.114	1.491	0.050
20.571	9.164	0.499	0.160	0.010	184.356	8.065	1.815	0.059
25.610	12.917	0.309	0.160	0.010	201.083	4.894	1.941	0.054
30.788	17.649	0.380	0.160	0.010	208.143	6.022	1.962	0.084
Fresh PAC - Desorption								
C_0	**C_e**	**SD**	**V**	**m**	**q_e**	**SD**	**M_{PAC}**	**SD**
mg/L	mg/L	mg/L	L	g	mg/g	mg/g	mg	mg
0.876	0.000	0.000	0.160	0.010	12.444	0.293	0.089	0.009
5.185	0.410	0.028	0.160	0.010	62.064	2.380	0.574	0.006
10.380	1.341	0.031	0.160	0.010	98.475	3.856	0.855	0.007
15.510	2.138	0.035	0.160	0.010	119.111	5.045	1.052	0.042
20.571	2.718	0.220	0.160	0.010	136.600	2.707	1.165	0.077
25.610	3.359	0.114	0.160	0.010	137.532	3.476	1.215	0.030
30.788	3.523	0.102	0.160	0.010	141.292	6.940	1.227	0.016
80-Day bio-coated PAC - Sorption								
C_0	**C_e**	**SD**	**V**	**m**	**q_e**	**SD**	**M_{PAC}**	**SD**
mg/L	mg/L	mg/L	L	g	mg/g	mg/g	mg	mg
0.848	0.221	0.063	0.160	0.010	29.505	0.780	0.003	0.067
4.424	1.853	0.373	0.160	0.010	60.199	6.691	0.535	0.013
9.874	4.673	0.202	0.160	0.010	101.751	3.470	1.030	0.059
19.399	11.896	0.924	0.160	0.010	137.512	14.489	1.401	0.198
29.577	19.499	0.357	0.160	0.010	178.473	4.100	1.876	0.083
180-Day bio-coated PAC - Sorption								
C_0	**C_e**	**SD**	**V**	**m**	**q_e**	**SD**	**M_{PAC}**	**SD**
mg/L	mg/L	mg/L	L	g	mg/g	mg/g	mg	mg
1.135	0.208	0.023	0.160	0.0102	20.192	0.665	0.234	0.038
5.270	2.173	0.119	0.160	0.0101	54.717	2.346	0.559	0.017
10.336	4.606	0.342	0.160	0.0103	94.856	5.843	1.091	0.072

14.073	6.822	0.072	0.160	0.0102	119.322	2.088	1.295	0.039
19.748	10.982	0.037	0.160	0.0103	142.146	5.196	1.545	0.105
23.091	14.367	1.047	0.160	0.0101	144.328	6.400	1.642	0.136
33.629	17.960	0.395	0.160	0.0102	154.958	14.050	1.576	0.147

Table A2.2. Cumulative toluene loss and methane production

Active	**Cumulative AT**				**Cumulative AC**			
Time	**Toluene**	**SD**	**Methane**	**SD**	**Toluene**	**SD**	**Methane**	**SD**
days	µmoles	µmoles	µmoles	µmoles	µmoles	µmoles	µmoles	µmoles
1	0.021	0.027	0.090	0.117	0.000	0.000	0.111	0.109
14	0.715	0.499	3.087	2.158	0.703	0.540	2.087	2.111
28	1.113	0.347	4.807	1.500	2.011	0.646	5.884	2.776
47	2.142	0.563	9.254	2.434	5.782	0.556	10.463	4.396
62	4.524	0.691	19.542	2.985	10.996	0.248	26.402	5.444
78	7.848	1.239	33.903	5.351	11.752	0.683	28.379	8.396
111	14.197	1.443	61.331	6.233	20.276	1.298	61.139	12.682
126	-	-	-	-	22.283	1.121	62.729	8.393
140	18.752	4.065	81.006	17.560	26.243	0.319	74.042	12.415
150	24.114	6.711	104.173	28.993	28.418	0.258	112.225	12.415
175	25.497	9.068	110.148	39.174	28.418	0.258	121.380	20.484

Sterile	**Cumulative KP**				**Cumulative KC**			
Time	**Toluene**	**SD**	**Methane**	**SD**	**Toluene**	**SD**	**Methane**	**SD**
days	µmoles	µmoles	µmoles	µmoles	µmoles	µmoles	µmoles	µmoles
1	0.000	0.000	0.003	0.001	0.000	0.000	0.004	0.002
14	0.012	0.011	0.003	0.001	0.316	0.345	0.003	0.001
28	0.667	0.494	0.003	0.001	1.201	0.966	0.003	0.001
47	1.343	0.447	0.004	0.002	4.279	1.876	0.004	0.002
62	1.677	0.289	0.002	0.000	5.083	1.362	0.002	0.000
78	3.187	1.552	0.003	0.001	4.208	1.701	0.003	0.001
111	0.951	0.845	0.004	0.000	7.049	1.904	0.004	0.002
114	1.535	1.083	-	-	7.827	2.053	-	-
150	0.620	1.325	0.006	0.001	8.995	1.665	0.006	0.002
175	1.206	1.288	0.008	0.002	8.755	1.487	0.005	0.002

Table A2.3. Microcosms physicochemical parameters

Day	pH	SD	ORP (mV)	SD	DO (mg/L)	SD
0	7.055	0.021	-237.800	27.294	0.030	0.014
50	6.897	0.076	-208.267	6.473	0.030	0.010
80	6.810	0.085	-197.933	18.799	0.527	0.012
140	6.597	0.153	-280.900	5.524	0.020	0.000
175	6.500	*	-286.950	7.566	0.120	0.028

Table A2.4. Biofilm parameters: descriptive statistics

Thickness (µm)	Day	N	Mean	SD	Minimum	Q1	Median	Q3	Maximum
Cells	50	50	4.495	1.426	1.999	3.497	4.197	5.274	9.319
EPS	50	50	3.645	0.894	0.702	3.002	3.665	4.081	5.840
Cells	80	50	4.267	1.308	1.607	3.360	4.298	5.202	6.812
EPS	80	50	3.269	1.467	0.903	1.932	3.467	4.430	6.031
Cells	140	50	4.269	2.637	1.095	2.158	3.145	6.480	9.513
EPS	140	50	5.854	1.882	2.081	4.721	5.621	7.016	11.185
Cells	180	50	7.391	3.901	2.508	4.055	6.346	9.850	18.723
EPS	180	50	6.411	3.417	1.118	4.073	5.521	7.875	19.500
Biovolume (μm^3)	**Day**	**N**	**Mean**	**SD**	**Minimum**	**Q1**	**Median**	**Q3**	**Maximum**
Cells	50	50	15.554	17.256	0.204	2.848	5.657	25.305	59.670
EPS	50	50	22.829	59.220	0.050	2.066	3.987	19.969	389.438
Cells	80	50	28.822	34.898	1.756	6.672	12.578	31.510	140.130
EPS	80	50	25.473	32.631	1.695	5.711	15.092	28.271	176.638
Cells	140	50	43.152	31.463	1.399	15.109	40.287	59.942	147.179
EPS	140	50	41.862	40.308	0.788	11.421	31.589	65.093	214.001
Cells	180	50	99.453	129.820	6.166	43.413	59.248	116.412	811.364
EPS	180	50	88.965	154.662	0.433	12.745	32.751	71.565	762.213
Rougness (-)	**Day**	**N**	**Mean**	**SD**	**Minimum**	**Q1**	**Median**	**Q3**	**Maximum**
Cells	50	50	1.765	0.266	0.832	1.676	1.871	1.946	1.992
EPS	50	50	1.664	0.568	0.167	1.308	1.826	1.968	4.095
Cells	80	50	1.566	0.366	0.711	1.243	1.719	1.879	1.994
EPS	80	50	1.579	0.271	1.088	1.306	1.621	1.829	1.969
Cells	140	50	1.782	0.137	1.471	1.676	1.796	1.889	1.997
EPS	140	50	1.635	0.222	1.011	1.528	1.647	1.817	1.933
Cells	180	50	1.637	0.195	0.838	1.571	1.668	1.760	1.946
EPS	180	50	1.600	0.323	0.679	1.486	1.710	1.855	1.974

Biomass ($\mu m^3/\mu m^2$)	Day	N	Mean	SD	Minimum	Q1	Median	Q3	Maximum
Cells	50	50	0.108	0.133	0.003	0.018	0.054	0.168	0.725
EPS	50	50	0.097	0.012	0.000	0.008	0.042	0.154	0.467
Cells	80	50	0.215	0.283	0.006	0.040	0.122	0.257	0.748
EPS	80	50	0.130	0.133	0.017	0.051	0.100	0.154	0.768
Cells	140	50	0.213	0.136	0.023	0.105	0.189	0.286	0.558
EPS	140	50	0.222	0.245	0.010	0.075	0.134	0.248	0.745
Cells	180	50	0.291	0.231	0.064	0.128	0.237	0.364	0.997
EPS	180	50	0.212	0.277	0.012	0.057	0.109	0.247	0.794

Table A2.5. Biofilm parameters: p- values

Biovolume (μm^3)				
Days	**Cells**	**Significance**	**EPS**	**Significance**
50-80	0.00578	+	0.00231	+
50-140	5.26E-08	+	1.64E-06	+
50-180	8.88E-16	+	1.20E-07	+
80-140	0.00187	+	0.00472	+
80-180	3.00E-09	+	0.00108	+
140-180	3.71E-04	+	0.56527	-
Thickness (µm)				
Days	**Cells**	**Significance**	**EPS**	**Significance**
50-80	0.86511	-	0.31981	-
50-140	0.0758	+	6.08E-11	+
50-180	3.02E-05	+	6.63E-09	+
80-140	0.27207	-	3.38E-11	+
80-180	4.50E-06	+	4.47E-09	+
140-180	4.20E-06	+	0.94117	-
Roughness (-)				
Days	**Cells**	**Significance**	**EPS**	**Significance**
50-80	0.00246	+	0.34269	-
50-140	0.68905	-	0.7383	-
50-180	0.00759	+	0.49242	-
80-140	2.26E-04	+	0.26159	-
80-180	0.22663	-	0.72149	-
140-180	4.98E-05	-	0.53174	-
Biomass ($\mu m^3/ \mu m^2$)				
Days	**Cells**	**Significance**	**EPS**	**Significance**
50-80	0.01131	+	5.96832E-5	+
50-140	2.81074E-6	+	4.66732E-7	+
50-180	3.52778E-9	+	7.78252E-6	+
80-140	0.065	-	0.02622	-
80-180	0.00183	+	0.42356	-
140-180	0.10921	-	0.24099	-

(+) indicates significant difference.
(-) indicates not significant difference.

Table A2.6. Freundlich Parameter and fit statistics.

PAC type	Freundlich Parameter	Value	Standard Error	Reduced Chi-sqr	R^2	Residual Sum of Squares
Fresh PAC	K_f	79.8	6.34	112.24	0.98	561.21
	n_f	0.35	0.03			
80-day PAC	K_f	50.1	3.58	32.60	0.99	97.81
	n_f	0.42	0.02			
180- day PAC	K_f	47.7	5.83	94.65	0.96	94.65
	n_f	0.42	0.05			

Table A2.7. Freundlich model parameter comparison between PACs - F-test.

PAC type comparison	F	Numer.DF	Denom.DF	Prob > F
Fresh PAC – 80-day PAC	30.47	2	8	1.81E-4
Fresh PAC -180-day PAC	37.50	2	10	2.25E-5
80-day PAC -180-Day PAC	0.46	2	8	0.64

FORMULAS

Mass (mg)
Volume (L)
Concentration (mg/L)
Molecular weight (toluene) = MW = 92.14
Henry's constant (toluene) = H = 0.21 @20ºC

$$Mass\ aqueous\ before\ sampling = M_w = C_w \times V_w$$

$$mass\ removed\ aqueous = M_{rw} = C_w \times V_{rw}$$

$$Mass\ aqueous\ after\ sampling = M'_w = M_w - M_{rw}$$

$$Mass\ gas\ before\ sampling = M_g = C_g \times V_g$$

$$mass\ removed\ gas = M_{rg} = C_g \times V_{rg}$$

$$Mass\ gas\ after\ sampling = M'_g = M_g - M_{r\,g}$$

$$Mass\ system\ before\ sampling = M_s = C_w \times (V_w + H \times V_g)$$

$$removed\ mass\ system = M_{r\,s} = M_{rw} + M_{rg}$$

$$Mass\ system\ after\ sampling = M'_s = M_s - M_{r\,s}$$

$$Aqueous\ volume\ after\ sampling = V'_w$$

$$Gas\ volume\ after\ sampling = V'_g$$

$$Aqueous\ concentration\ after\ sampling = C'_w = \frac{M'_s}{V'_g \times H + V'_w}$$

$$Gas\ concentration\ after\ sampling = C'_g = C'_w \times H$$

$$\mu moles\ aqueous = \mu moles_w = \frac{C'_w}{MW} \times (V'_w \times 1000000)$$

$$\mu moles\ gas = \mu moles_g = \frac{C'_g}{MW} \times (V'_g \times 1000000)$$

$$\mu moles\ system = \mu moles/bottle = \frac{M'_s}{MW} \times 1000000$$

Steps:

1. From the aqueous concentration before sampling, estimate the mass aqueous before sampling.

$$Mass\ aqueous\ before\ sampling = M_w = C_w \times V_w$$

2. Estimate the aqueous mass removed based on the aqueous concentration before sampling and volume of sample removed.

$$mass\ removed\ aqueous = M_{rw} = C_w \times V_{rw}$$

3. Subtract the aqueous mass removed from the aqueous mass before sampling to get the mass after sampling.

$$Mass\ aqueous\ after\ sampling = M'_w = M_w - M_{rw}$$

4. Estimate the concentration before sampling from the aqueous concentration before sampling and Henry's constant.

$$Gas\ concentration\ before\ sampling = C_g = C_w \times H$$

5. Estimate the gas mass before sampling

$$Mass\ gas\ before\ sampling = M_g = C_g \times V_g$$

6. Estimate the gas mass removed based on the concentration and volume of gas sample removed.

$$mass\ removed\ gas = M_{rg} = C_g \times V_{rg}$$

7. Subtract the gas mass removed from the gas mass before sampling to get the gas mass after sampling.

$$Mass\ gas\ after\ sampling = M'_g = M_g - M_{rg}$$

8. Estimate the mass in the system (bottle) before sampling using the concentration and volume before sampling and Henry's constant.

$$Mass\ system\ before\ sampling = M_s = C_w \times (V_w + H \times V_g)$$

9. Estimate the mass removed in the system by adding the mass removed in the aqueous and gas phase.

$$removed\ mass\ system = M_{rs} = M_{rw} + M_{rg}$$

10. Estimate the mass in the system after sampling by subtracting the mass removed from the mass before sampling.

$$Mass\ system\ after\ sampling = M'_s = M_s - M_{rs}$$

11. Estimate the aqueous concentration after equilibrium (after sampling) using the mass in the system and volume after sampling and the Henry's constant.

$$Aqueous\ concentration\ after\ sampling = \ C'_w = \frac{M'_s}{V'_g \times H + V'_w}$$

12. Estimate the gas concentration after equilibrium (after sampling) using the aqueous concentration after equilibrium and Henry's constant.

$$Gas\ concentration\ after\ sampling = C'_g = \ C'_w \times \ H$$

PAC barrier model

The total mass at saturation estimated by,

$$M_T = (\phi C_w + K_f C_w^{n_f}\ \rho_b f_{PAC})V$$

The contaminant mass loading to the barrier estimated by,

$$M_{in} = q\ A\ C_w^{in} = q\ (1)(1)C_w^{in}$$

To estimate the time to barrier saturation the equation was derived as follow:

$$t_{sat} = \left[\frac{\phi + \ K_f C_w^{n_{f-1}} \rho_b f_{PAC}}{q}\right] L$$

$$= \left[1 + \ K_f C_w^{n_f - 1} \rho_b\ f_{PAC}\right] (\frac{L}{q/\phi})$$

$$= \frac{[\phi C_w + \ K_f C_w^{n_f} \rho_b\ f_{PAC}]V}{q\ C_w^{in} A}$$

where,
t_{sat} is the time to barrier saturation in days,
ø is the soil porosity,
ρ_b is the soil bulk density in g/m^3,
C_w^{in} is the aqueous contaminant concentration entering the barrier in g/m^3,

K_f and n_f are the Freundlich parameters obtained from the isotherms,
f_{PAC} is the fraction of PAC in the barrier,
q is the groundwater specific flux in m/day,
V is the volume of the PAC barrier in m^3,
A is the cross-sectional area in m^2,
L is the length of the barrier in m.